



NIST  
PUBLICATIONS

REFERENCE

A11103 971797

NISTIR 4988

---

---

# Performance of Electromagnetic Covermeters for Nondestructive Assessment of Steel Reinforcement

---

---

Nicholas J. Carino

Building and Fire Research Laboratory  
Gaithersburg, Maryland 20899

**NIST**

QC

100

.U56

#4988  
1992

United States Department of Commerce  
Technology Administration  
National Institute of Standards and Technology



---

---

# Performance of Electromagnetic Covermeters for Nondestructive Assessment of Steel Reinforcement

---

---

Nicholas J. Carino

December 1992  
Building and Fire Research Laboratory  
National Institute of Standards and Technology  
Gaithersburg, MD 20899



U.S. Department of Commerce  
Barbara Hackman Franklin, *Secretary*  
Technology Administration  
Robert M. White, *Under Secretary for Technology*  
National Institute of Standards and Technology  
John W. Lyons, *Director*



## ABSTRACT

*Covermeters* are electromagnetic devices for locating steel reinforcing bars in concrete structures. An experimental study was carried out to compare the basic characteristics of two types of commercial covermeters (magnetic reluctance and eddy current). Experiments were carried out using single bars and multiple bars with various configurations. One group of single-bar tests studied the relationships between meter reading and cover thickness. Empirical equations were fitted to the data, and the values of the equation parameters were found to be relatively insensitive to the bar size. The other group of single-bar tests examined the relationship between meter reading and horizontal distance between the meter probe and the bar axis (offset). Data were fitted with a bell shaped, quadratic exponential function. The parameter characterizing the decay of the meter reading with offset was found to depend on the cover in a well-defined manner. This parameter was used to characterize the differences in the influence zones of the probes. Tests with multiple, parallel bars were conducted to determine the critical spacings below which the location of the individual bars could not be discerned and below which the meter amplitude exceeded the single-bar value. A simple summation model was used to predict the response based on the individual-bar response. Criteria were proposed to estimate these critical spacings based upon the single-bar responses. Other tests showed that the meters cannot discern a bar located directly below another bar. The ability of the meters to locate the ends of bars was also investigated, and the eddy-current meter appeared superior for this purpose. The final series of tests examined the ability of the meters to measure the length of a lap splice, and the meter based upon magnetic reluctance appeared superior for this purpose. Recommendations for developing a standard test method and for improvements in meter performance are provided.

**Keywords:** Building technology, concrete, covermeter, eddy current, electromagnetic device, magnetic reluctance, nondestructive testing, reinforcing bars.

# TABLE OF CONTENTS

ABSTRACT .....	iii
1. INTRODUCTION .....	1
1.1 <u>Background</u> .....	1
1.2. <u>Objectives</u> .....	1
1.3 <u>Organization of report</u> .....	2
1.4 <u>Acknowledgements</u> .....	2
2. PRINCIPLES OF OPERATION .....	3
2.1 <u>Introduction</u> .....	3
2.2 <u>Electromagnetic induction</u> .....	3
2.3 <u>Magnetic circuit</u> .....	4
2.4 <u>Covermeters based on reluctance</u> .....	5
2.5 <u>Eddy current meters</u> .....	6
2.6 <u>Comparison of reluctance and eddy-current meters</u> .....	7
2.7 <u>Calibration of meters</u> .....	7
2.8 <u>Spacer technique</u> .....	8
2.9 <u>Interfering factors</u> .....	9
2.10 <u>Summary</u> .....	10
3. TEST RESULTS .....	19
3.1 <u>Introduction</u> .....	19
3.2 <u>Amplitude versus cover</u> .....	19
3.2.1 <i>M-R meter</i> .....	20
3.2.2 <i>E-C meter</i> .....	21
3.2.3 <i>Summary</i> .....	22
3.3 <u>Amplitude versus horizontal offset</u> .....	35
3.3.1 <i>Mathematical modeling</i> .....	35
3.3.2 <i>Summary</i> .....	36
3.4 <u>Multiple bars</u> .....	43
3.4.1 <i>Theoretical analysis</i> .....	43
3.4.2 <i>Experimental results</i> .....	45
3.4.3 <i>Corrections to model</i> .....	47
3.4.4 <i>Summary</i> .....	48
3.5 <u>Bars in two layers</u> .....	71
3.6 <u>Locating ends of bars</u> .....	77
3.7 <u>Measurement of splice length</u> .....	85
3.7.1 <i>Side-by-Side (SbS) configuration</i> .....	85
3.7.2 <i>Over-Under (OU) configuration</i> .....	87
3.7.3 <i>Presence of parallel bars</i> .....	87
3.7.4 <i>Summary</i> .....	89
4. SUMMARY AND RECOMMENDATIONS .....	113
4.1 <u>Summary</u> .....	113
4.1.1 <i>Amplitude versus cover</i> .....	113
4.1.2 <i>Amplitude versus horizontal offset</i> .....	113
4.1.3 <i>Multiple bars</i> .....	113

4.1.4	<i>Bars in two layers</i> .....	114
4.1.5	<i>Locating ends of bars</i> .....	115
4.1.6	<i>Lap splices</i> .....	115
4.2	<u>Recommendations</u> .....	115
4.2.1	<i>Standards development</i> .....	115
4.2.2	<i>Enhancements to existing devices</i> .....	116
4.2.3	<i>Development of new covermeters</i> .....	116
5.	REFERENCES .....	119
	APPENDIX 1 — Notation .....	121
	APPENDIX 2 — Annotated bibliography .....	122



# 1. INTRODUCTION

## 1.1 Background

One of the most important steps in evaluating the load carrying capacity of an existing reinforced concrete structure is to determine the quantity and configuration of the reinforcing steel. This is especially critical when evaluating earthquake resistance, because the energy absorption capacity of a concrete structure is affected strongly by the details of the reinforcement configuration. As reported by Malhotra (1976), electromagnetic devices to measure the cover of reinforcing steel became available in the 1950's. These nondestructive testing devices are known generically as *covermeters*. Today there are many commercially available which claim to be able to measure the cover and the size of steel reinforcing bars. Some of these newer instruments are presented in the textbook by Bungey (1989), and the Appendix of this report reviews some of the research to evaluate their capabilities.

Presently (1992), the United Kingdom is the only country known to the author which has developed a standard on the use of covermeters (BS 1881). There is no ASTM standard on the use of covermeters and no activities are currently underway to develop such a standard. This lack of standardization and the importance of the need to measure the reinforcement configuration in concrete structures were the motivating factors for undertaking the study summarized in this report.

## 1.2. Objectives

The objectives of this study were:

- (1) To summarize the operating principles of commercial covermeters.
- (2) To investigate procedures to describe the operating characteristics of a covermeter.
- (3) To investigate the performance of covermeters in the presence of multiple reinforcing bars.

The operating principles of electromagnetic covermeters are well-known to physicists and electrical engineers, but they are not well understood by the concrete technologists who are the users of these devices. Knowledge of the underlying principles is important to use the instrument correctly and to properly interpret the results. Existing textbooks that deal with covermeters (Malhotra 1976, Bungey 1989, Lauer 1991) offer cursory explanations of their operation. Hence, the first objective of this study is to provide the potential users of these devices with explanations of the underlying physics that govern their operation.

As was mentioned, there are many covermeters available on the market. It would be desirable to have procedures to characterize a covermeter so that the user could understand how it would perform on actual structures. The current procedures given in textbooks, manufacturers' literature, and the British Standard (BS 1881) deal only with establishing the amplitude of the meter reading as a function of the cover of individual bars. This provides insufficient information on what can be expected when the covermeter is used on a structure with closely-spaced bars. Thus the second objective is to develop a procedure to determine the operating characteristics of a covermeter, which could be used to predict the performance of the meter in the field.

Most of the published research literature on covermeters deals with their ability to measure the depth of cover and bar diameter. While these are certainly very important, other information about the reinforcement layout is often needed. For example, it may be necessary to determine the

location of the end of a bar to establish whether there is sufficient embedment to fully develop its capacity. Thus the third objective is to examine other capabilities of covermeters besides measurement of cover.

### 1.3 Organization of report

Chapter 2 discusses the operating principles of the two main classes of covermeters: those based on magnetic reluctance and those based upon eddy currents. Simple illustrations are provided to aid in these explanations. The techniques that are currently used to "calibrate" covermeters are reviewed. This is followed by an explanation of the *spacer technique* that is commonly recommended to determine the diameter and cover of reinforcing bars.

Chapter 3 summarizes the results of the experiments performed in this study to meet the second and third objectives stated above. Two commercially available covermeters were used. One of them is based on the magnetic reluctance principle and has been used for many years. The other is based on the eddy current principle and has been introduced recently to the market. An attempt is made to use mathematical models to summarize the performance characteristics of the covermeters. The ability of the devices to detect the presence of a second layer of steel, the ends of bars, and the length of a lap splice were investigated.

Chapter 4 summarizes the major findings of this study and offers recommendations for future research and development.

Appendix 1 defines the notation used in the report and Appendix 2 is an annotated bibliography of selected articles dealing with the performance of covermeters.

### 1.4 Acknowledgements

The experimental data were obtained by Mr. Milton Rodriguez under the direction of the author. Mr. Rodriguez worked at NIST as co-op student from the Department of Civil Engineering, University of Puerto Rico, Mayaguez. His diligence in recording the data, transferring data to computer files, making summary plots, and preparing drawings is greatly appreciated. His contributions were paramount to the success of the project. The author also acknowledges Prof. Benjamin Colucci, the co-op course coordinator at the University of Puerto Rico, Mayaguez. Finally, the contributions of Dr. Lawrence I. Knab of the Building Materials Division at NIST are recognized. Dr. Knab performed a comprehensive literature search on covermeters, prepared summaries which are included in the Appendix, and obtained technical literature from covermeter manufacturers.

## 2. PRINCIPLES OF OPERATION

### 2.1 Introduction

As is common with other nondestructive test methods used to infer conditions within concrete, covermeters "measure" the depth of cover by monitoring the interaction of the reinforcing bars with some other process. In this case, the interaction is between the bars and a relatively low frequency, electromagnetic field. The key to understanding the operation of covermeters lies in understanding the basic relationships between electricity and magnetism. Two fundamental concepts are involved: (1) the motion of electric charges in a conductor, i.e., a current, gives rise to a magnetic field and (2) the motion of a magnetic field gives rise to current within a conductor.

### 2.2 Electromagnetic induction

To begin the explanation of the operation of commercial covermeters, it is helpful to review briefly some of the terminology associated with a magnetic field and its interaction with electrical conductors. As stated, a magnetic field arises whenever an electrical current flows through a conductor. Figure 2.1(a) shows a coil carrying a direct current and the magnetic field that is created. The coil is surrounded by continuous loops of magnetic flux lines. The needle of a compass would align itself parallel to the direction of these magnetic lines. Depending on the direction of the current, one end of the coil acts as a north pole and the opposite end acts as a south pole. The total *magnetic flux*,  $\Phi$ , is the entire group of magnetic lines flowing between the poles of the coil. The magnetic field strength is expressed in terms of flux lines per unit area, that is, the *flux density*,  $B$ . Flux density is a vector quantity (has a magnitude and a direction).

If the coil in Fig. 2.1(a) is energized by an alternating current, the magnetic field will also be alternating. At any point near the coil, the magnetic flux will vary with time. If a conducting circuit is placed near the coil as shown in Fig. 2.1(b), an electric potential is induced in the circuit causing an induced current. This phenomenon, known as *electromagnetic induction*, is described by Faraday's law, which, in simple terms, states that the induced electric potential in a circuit is proportional to rate of change of the magnetic flux through the circuit.

If the circuit in Fig. 2.1(b) is replaced by a conducting material, as shown in Fig. 2.1(c), the same principle of electromagnetic induction is operative. The changing magnetic field induces circulating currents in the object, which are known as *eddy currents*. Because current flow gives rise to a magnetic field, eddy currents produce a secondary magnetic field which opposes the field producing the currents. The direction of the eddy currents is governed by Lenz's law, which states that the induced current is in the direction which prevents a change in the net number of lines which pass through the cross-sectional area bounded by the circuit. Thus if the applied magnetic field is changing by reducing the number of flux lines passing through the cross-sectional area of the circuit, the eddy currents flow in a direction so that the secondary magnetic field adds flux to the cross section. The magnitude of the eddy currents is affected by the following factors (see, e.g., Halmshaw 1987):

- electrical conductivity of the object
- distance between coil and object
- magnetic permeability if the object is ferromagnetic
- frequency of the alternating magnetic field
- dimensions of the object
- coil configuration

### 2.3 Magnetic circuit

The final principle to be considered is that of a *magnetic circuit* (Fitzgerald, et al. 1967). Figure 2.2(a) shows a coil of  $N$  turns around a ring of a ferromagnetic material, i.e., one which becomes magnetized in the presence of a magnetic field. When current passes through the coil, most of the magnetic field that is created is confined within the ring. Thus one can imagine a *flow* of concentric flux lines analogous to the flow of electricity in a circuit. The product of the current,  $I$ , and the number of turns in the coil defines the *magnetomotive force*,  $\mathcal{F}$ , which analogous to the electromotive force (voltage) in an electric circuit. The magnetic flux,  $\Phi$ , *flowing* through the ring can be related to  $\mathcal{F}$  in a manner analogous to Ohm's law for an electrical circuit:

$$\Phi = \frac{\mathcal{F}}{\mathbf{R}} \quad (1)$$

where  $\mathbf{R}$  is called the *reluctance* of the magnetic circuit. The reluctance, which is analogous to the resistance in an electrical circuit, is determined by the *magnetic permeability*<sup>a</sup> and geometry of the material in the magnetic circuit. For a material with a uniform cross section,

$$\mathbf{R} = \frac{L}{\mu A_m} \quad (2)$$

where  $\mu$  = the magnetic permeability,  
 $L$  = the length of the circuit, and  
 $A_m$  = the cross-sectional area.

The analogy between the quantities associated with magnetic and electrical circuits is summarized in the following table (Fitzgerald et al. 1967):

Magnetic Circuit	Electrical Circuit
Magnetomotive force, $\mathcal{F}$	Electromotive force, $\mathcal{E}$
Flux, $\Phi$	Current, $I$
Reluctance, $\mathbf{R}$	Resistance, $R$
Flux density, $B$	Current density, $J$
Magnetic permeability, $\mu$	Conductivity, $\sigma$

The principles used to analyze currents and voltages in electrical circuits may also be applied to magnetic circuits (Fitzgerald et al. 1967). For example, for a magnetic circuit composed of elements connected in series, the same total magnetic flux must exist in each element. The net excitation (ampere-turns) required to produce a given flux is the sum of the magnetomotive forces required to force that flux through each element.

---

<sup>a</sup>The magnetic permeability measures the ability of a material to concentrate magnetic lines of force when placed within a magnetic field. If the relative magnetic permeability of air, or free space, is taken to equal 1, the relative permeability of iron is on the order of 5000 (Serway 1983).

As an example of a magnetic circuit, consider the U-shaped iron core and straight steel bar shown in Fig. 2.2(b). For a given coil excitation (ampere-turns), what would be the flux through the circuit? The arrangement is a series circuit made of three components: the path through the U-shaped core, the path through two air gaps, and the path through the bar. The product of flux and reluctance for each element must add up to the applied magnetomotive force. Thus the resultant flux equals the applied coil excitation divided by the sum of the three reluctances.

In summary, the discussion up to this point has reviewed some of the basic principles underlying the operation of commercial covermeters. One of these principles is electromagnetic induction, whereby an alternating magnetic field induces a current in an electric circuit which intersects the magnetic flux. When the electrical circuit is established in a solid conducting material, the induced current is known as eddy current. The induced current results in a secondary magnetic field which acts to oppose the flux change that produced the current (Lenz's law). Another key principle is the reluctance of a magnetic circuit. Reluctance is analogous to resistance in an electrical circuit. The following sections explain how these principles have been incorporated into commercial covermeters to measure the depth and size of reinforcing bars in concrete.

#### 2.4 Covermeters based on reluctance

As was shown in Fig. 2.2(b), a U-shaped core of magnetic material can be used to establish a magnetic circuit in which the flux passes through the core and through a bar located some distance from the free ends of the core. For a given excitation and core configuration, the magnetic flux would depend on the distance between the bar and the faces of the core, the size of the bar, and the magnetic permeability of the bar material. Thus if the flux in the circuit were measured, it should be possible to infer some information about the bar. This is the underlying principle of one class of covermeters (Shirley 1971).

Figure 2.3(a) is a schematic of a covermeter based upon measuring changes in magnetic reluctance due to the presence or absence of a bar within the vicinity of the search head. The search head is composed of a ferromagnetic U-shaped core (yoke), an excitation coil, and a sensing coil. When current is applied to the excitation coil, a magnetic field is created. In the absence of a bar, the magnetic circuit composed of the yoke and the gap between ends of the yoke will have a high reluctance and the magnetic flux will be small. The excitation coil is powered by a low frequency (less than 100 Hz) alternating current. As a result, the flux flowing through the magnetic circuit will also be alternating. A small secondary current is induced in the sensing coil because of the changing flux. If a bar of ferromagnetic material is introduced, as shown in Fig. 2.3(b), the reluctance of the magnetic circuit decreases and the amplitude of the magnetic flux increases. As a consequence, the secondary current in the sensing coil increases. Thus the presence of the bar is inferred by the change in the output from the sensing coil. The circuitry used to measure the small changes in induced currents varies among different manufacturers.

For a given bar, the reluctance of the magnetic circuit in Fig. 2.3(b) would depend on the distance between the bar and the faces (poles) of the yoke. If the meter output were plotted as function of the cover distance, the relationship would be similar to that shown in Fig. 2.3(c). Since the size of the bar affects the reluctance of the portion of the magnetic circuit through the bar, there would be a separate relationship for each bar size.

The operation of any covermeter involves establishing the calibration relationships between cover and meter reading, and using those relationships to infer cover based on measurements on a structure. Up to this point in the discussion, there has been no mention of the concrete between the

search head and the reinforcing bar. If the concrete does not contain iron-bearing aggregates, the magnetic permeability of the concrete will be similar to that of air, and the concrete will not effect the meter output. On the other hand, if the concrete contains significant amount of iron, the relationship between cover and meter reading will be affected.

In summary, covermeters based upon the principle of magnetic reluctance employ a low frequency alternating current to establish a magnetic circuit that includes the reinforcing bar. A change in the cover of the bar results in a change in the amplitude of the flux through the circuit. By measuring the change in flux and by using a suitable calibration relationship, the cover can be estimated. The size of the bar and the magnetic permeability of the steel affect the calibration relationship for a given meter design.

## 2.5 Eddy current meters

As was explained in section 2.2, a coil carrying alternating current will induce eddy currents in an electrically conductive material located within the magnetic field of the coil (see Fig. 2.1(c)). The eddy currents will, in turn, produce a secondary field that interacts with the field of the coil. The second class of covermeters is based on monitoring the effects of the eddy currents induced in a reinforcing bar. There are two categories of eddy-current meters: one is based on the *continuous* excitation of the coil by an alternating current and the other is based upon *pulsed* excitation.

Figure 2.4(a) shows the search coil of a continuous eddy-current covermeter in the absence of a reinforcing bar. When an alternating voltage (usually at about 1 KHz) is applied to the coil, there will be an alternating current in the coil whose magnitude depends on the impedance<sup>b</sup> of the coil. If the coil is brought near an electrically conductive object, eddy currents are established within the surface "skin" of the object. Because the eddy currents are also alternating, they give rise to an alternating secondary magnetic field which induces a secondary current in the coil. In accordance with Lenz's law, the secondary current opposes the primary current. As a result, the net current flowing through the coil is reduced, and the apparent impedance of the coil increases (Hagemaijer 1990). Thus the presence of the metal object is inferred by monitoring the change in the impedance of the coil. This is the basic principle of eddy-current covermeters with continuously excited search coils.

Another type of covermeter based on eddy currents uses the *pulse-induction* technique<sup>c</sup>. In this case, a repetitive current pulse is applied to the coil. The applied current is turned off as quickly as possible and is followed by a period of "dead" time with no applied current prior to the start of the next pulse. When the current pulse ceases, there is a sudden collapse in the magnetic field of the coil, which induces eddy currents within a conductive objective located within the coil's influence field. The eddy currents decay with time, and the decaying magnetic field induces a secondary current

---

<sup>b</sup>When direct current is applied to a circuit, the current magnitude equals the voltage divided by the electrical resistance of the circuit. When alternating current is applied to the coil, the current amplitude is governed by the value of the applied voltage, the resistance, and another quantity called *inductance*. The inductance is an added resistance to current flow. The alternating current results in a changing magnetic field that induces a secondary current in the coil which, according to Lenz's law, opposes the applied current. The vector sum of resistance and inductance defines the *impedance* of the coil.

<sup>c</sup>Explanation of this technique was provided in technical literature from Protovale Ltd., Abingdon, Oxfordshire OX13 5AS, U.K.

in the coil. Because the coil is not carrying a primary current during the "dead" time, it acts as a sensor to monitor the induced current caused by eddy current decay. Thus the presence of a conductive objective would be indicated by the presence of an induced current during the "dead" time when the coil is acting as a receiver.

The schematic of a commercial device based upon the pulse-induction technique (see footnote c) is shown in Fig. 2.4(c). The device uses two air-core coils. The magnetic fields of the two coils and a reinforcing bar lead to a magnetic circuit similar to that previously discussed for the reluctance method. When the current in the coils is turned off, circumferential eddy currents are established in the bar which try to maintain the magnetic flux that was present while the coils were energized. As the eddy currents decay, there is a decay in their accompanying magnetic field, and this decay induces a signal current in the coils. Note that by the using two coils, the search head is directional, that is, the output signal is greatest when the bar is aligned with the coils. If the search head contains a single circular coil, the search head would not be directional. The orientation of a bar is easier to establish with a covermeter having a directional search head.

## 2.6 Comparison of reluctance and eddy-current meters

From the above discussion, it should be evident that the output of covermeters based on magnetic reluctance and eddy currents are affected by different factors. Reluctance-type meters are based on the magnetic flux flowing through the effective magnetic circuit, that is, the combined path through the concrete and the reinforcing bar. For a given cover depth, the output of this type of meter would depend upon the area of the reinforcing bar and its magnetic permeability, which would depend on the alloy composition and the type of mechanical processing. Also, as was stated, the meter output would be affected by the presence of iron bearing aggregates in the concrete.

On the other hand, eddy-current meters rely on the electrical conductivity of the bar to support the induced surface currents. Thus eddy current meters will detect magnetic as well non-magnetic embedded metals. However, a ferromagnetic material produces a stronger signal because of the enhanced strength of the secondary magnetic field created by the eddy currents. This is especially important when the target is small or deeply embedded (footnote c). Finally, eddy current meters are not affected greatly by the presence of iron-bearing aggregates. Since the iron is usually in the form of non-conducting oxides or small particles, the magnitude of the eddy currents induced in iron-bearing aggregate would be much weaker than those in the bar. Additional information on the performance of various types of covermeters may be found in the references by Malhotra (1976), Bungey (1989), and Lauer (1991)

## 2.7 Calibration of meters

Figure 2.5 is a schematic showing the application of a covermeter to locate and infer other information about an embedded reinforcing bar. The *search head* emits an electromagnetic field whose shape is dependent on the specific design. For simplicity, the search zone is indicated as the white region in the figure. When a reinforcing bar is located within the search zone, the covermeter indicates the presence of the bar by a change in its display, which may be a digital or analog meter. Maximum amplitude is indicated when the center line of the search head is located directly above the long axis of the bar, i.e., the *horizontal offset* is zero. For a covermeter with a directional search head, the output is a maximum when the longitudinal axis of the search head is aligned with the longitudinal axis of the bar. Thus with any covermeter it a relatively simple matter to determine the location of embedded bars: the operator simply moves the search head over the surface of the

concrete until a maximum response is obtained. As the cover increases the signal strength decreases, and at some critical depth the bar cannot be detected.

In evaluating an existing structure, it is usually necessary to not only identify the presence of reinforcing bars but also determine their size and depth of cover. It is here where knowledge about the operation of the covermeter becomes important.

The output from a covermeter depends on the size and depth of the reinforcing bars and on the electrical circuitry that is employed. Because of the complexity of the interactions between the electromagnetic field emanating from the search head and the reinforcing bars, the most practical method for relating the output to the reinforcement configuration is by empirical correlations. These typically involve using different diameter bars at different cover depths to develop relationships of meter output versus cover, as was shown previously in Fig. 2.3(c). These relationships are typically incorporated into commercial instruments as calibrated dials for meter-type instruments or are included as part of the signal processing of digitally based devices. The user of a covermeter should verify that the internal calibration relationships will provide the expected level of accuracy for the specific materials encountered on a project.

As noted, there is no ASTM standard dealing with the use of covermeters, so the user is forced to follow the manufacturer's recommendations or use his own approach. However, the British Standards Institution has developed a standard for calibrating and using covermeters (BS 1881 Part 204, "Recommendations on the use of electromagnetic covermeters"). According to BS 1881 Part 204, the calibration of the instrument should be checked at least every six months. Three methods are suggested for performing the calibration:

Method A      Fabricate test prisms of concrete with an eccentrically placed smooth steel bar (see Fig. 2.6(a)). This permits 4 different cover measurements for that bar. Prisms would be prepared using different sizes of bars. The length of the prism should be at least 50 mm longer than the length of the search head, and the reinforcing bar should extend at least 100 mm from each end of the prism.

Method B      The search head is positioned on a table free of metallic components (nails, screws, etc.) and a smooth steel bar is moved across the table toward the search head (Fig. 2.6(b)). The bar axis is maintained parallel to the search head. Although not stated in BS 1881 Part 204, the search head and bar must be vertically aligned so that the center of the bar axis coincides with the center of the search head.

Method C      A wooden box is built with a series of vertical holes so that a smooth steel bar can be placed at different distances from the search head (Fig. 2.6(b)). The holes should be large enough to accommodate the largest diameter bar to be used in the calibration. The box is built without using metallic fasteners (nails, screws, etc.).

While BS 1881 Part 204 recommends using a smooth steel bar, deformed reinforcing bars can also be used to develop an improved calibration for bar with specific deformation patterns. The standard states that the accuracy of the indicated cover measurements should be within  $\pm 2$  mm or 5% of the actual cover, whichever is greater.

## 2.8 Spacer technique

Up to now it has been assumed that there is only one reinforcing bar within the zone of influence of the search head. If this condition is encountered in the field, the laboratory calibration curves can be used with confidence to measure the depth of a bar of known diameter. If the bar diameter is not known, the so-called *spacer technique* may be used to estimate both the bar size and the depth of cover. This method uses the calibration relationships between bar size, cover and meter reading. The procedure is described in the Appendix of BS 1881 Part 204 and is reviewed in this section.

Figure 2.7 illustrates the key aspects of the spacer technique. First, a measurement is made directly over the bar in question. In this example, assume that the reading is 55 on the arbitrary scale provided on the instrument. The calibration curves in Fig. 2.7(b) show that there are different combinations of bar diameter and cover thickness that would result in this meter reading. The objective is to establish the diameter of the bar and use its calibration curve to establish the cover. Therefore, another measurement is taken over the same bar using a nonmetallic spacer of known thickness. For this example, assume that the spacer is 25 mm thick and that the meter reading with the spacer is 27. Using these two measurements and the calibration curves, the apparent covers for different bar diameters are estimated as shown in Fig. 2.7(b). These different values of cover are shown in Fig. 2.7(c). For each bar diameter, the differences between the cover values with and without the spacer are computed and compared with the spacer thickness. The diameter of the unknown bar is the one for which the difference in cover equals to the spacer thickness. In this example, the bar is 16 mm in diameter and the cover is 39 mm.

This example also illustrates that this spacer technique may only give an approximate estimate of bar size. Suppose that the spacer thickness had been 27 mm and that the same readings of 55 and 27 had been obtained, then it would not be possible to establish whether the bar diameter is 22 or 29 mm. However, it may be possible to improve the accuracy of the spacer technique by using more than one spacer (Das Gupta and Tam 1983, Smith, et al. 1987). In this case, the bar diameter would be the one which, on average, results in the best agreement between the calculated differences in cover and thicknesses of the spacers.

Another spacer technique has been suggested for covermeters having a directional search head, i.e., one which results in different meter readings when the head is aligned parallel or perpendicular to the bar axis (Tam, et al. 1977). In this case, calibration curves are prepared with the search head aligned perpendicular and parallel to the bar axes. To establish the cover and size of an unknown bar, measurements are made parallel and perpendicular to the bar using multiple spacers, and the differences in cover based on the calibration curves are compared with the spacer thickness as explained above. It is claimed that this approach results in improved accuracy compared with using the parallel measurements alone.

The accuracy of any of these spacer techniques is limited by the applicability of the calibration relationships to the actual site conditions. Factors such as the magnetic properties of the steel and the type of deformation pattern can influence the actual calibration relationships. BS 1881 Part 204 states that under ideal conditions an accuracy of at least  $\pm 20\%$  is possible in the cover and bar diameter using spacer techniques.

## 2.9 Interfering factors

Major problems in measuring bar size and cover arise when more than one bar is located within the zone of influence of the search head. This can arise from close spacing of parallel bars, the presence of orthogonal reinforcement, and multiple layers of bars. In these cases, the meter reading will be greater than when a single bar is present, and estimates of cover and bar diameter will be in error if the single-bar calibration curves are used. Manufacturers of covermeters typically provide guidelines on the conditions for which their calibration relationships are valid. One of the main objectives of this study was to examine whether information from single-bar tests can be used to estimate the minimum spacing between bars for accurate measurement of cover using the single-bar calibration.

## 2.10 Summary

This chapter has given a brief introduction to the underlying principles of commercial electromagnetic covermeters. Basically, these devices use a search head that emits an electromagnetic field which interacts with an embedded reinforcing bar. The exact nature of the interaction depends on the design of the covermeter. For a given instrument, empirical calibration relationships can be established between the amplitude of the meter reading and the diameter and depth of cover of individual reinforcing bars. Such relationships can be used to estimate the diameter and depth of bars in the field, provided that there are no interfering effects due to congested reinforcement. For additional discussion of the theory of electromagnetic induction, eddy currents and magnetic circuits, see Serway 1983, Hagemaiier 1990 and Fitzgerald et al. 1967.

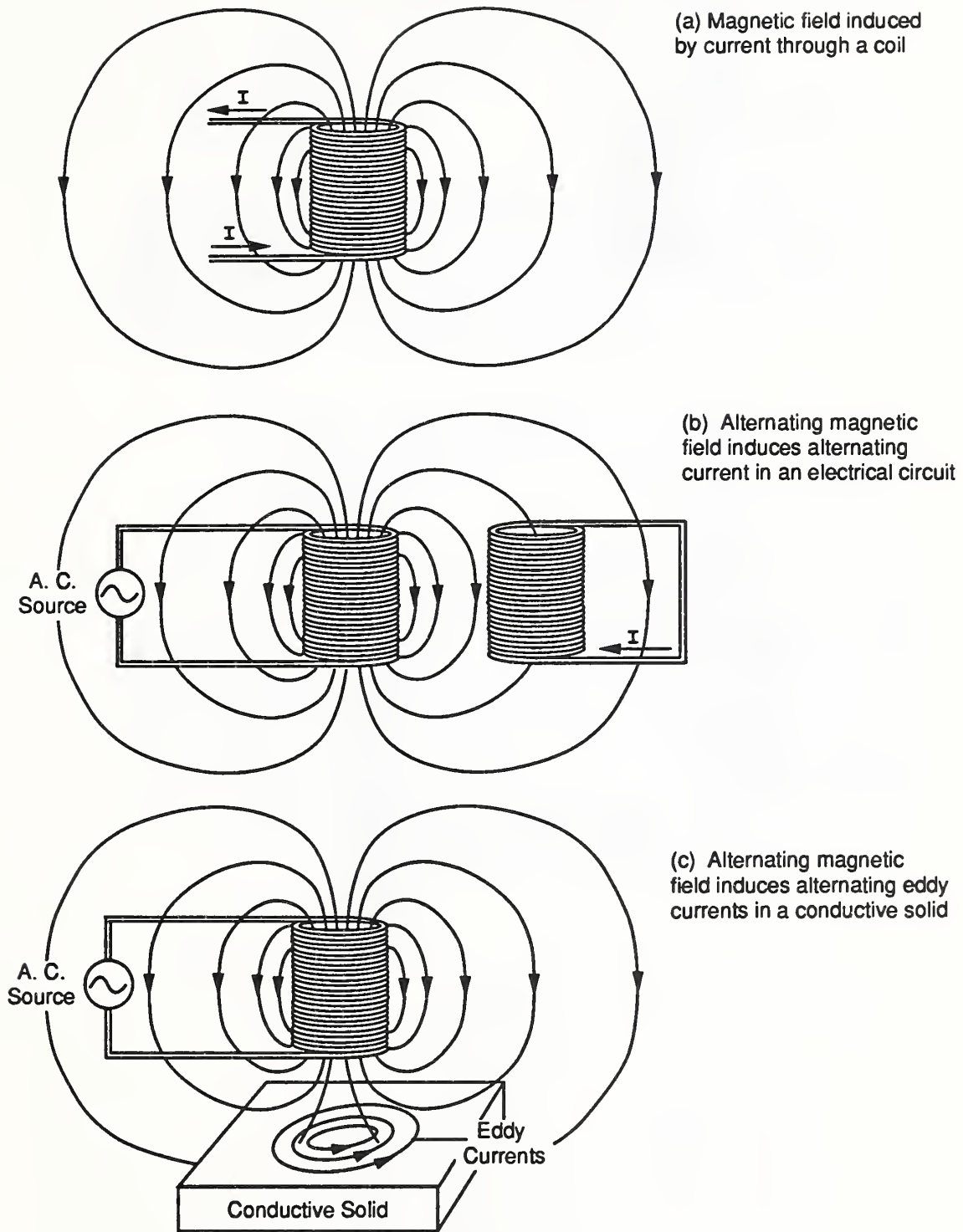
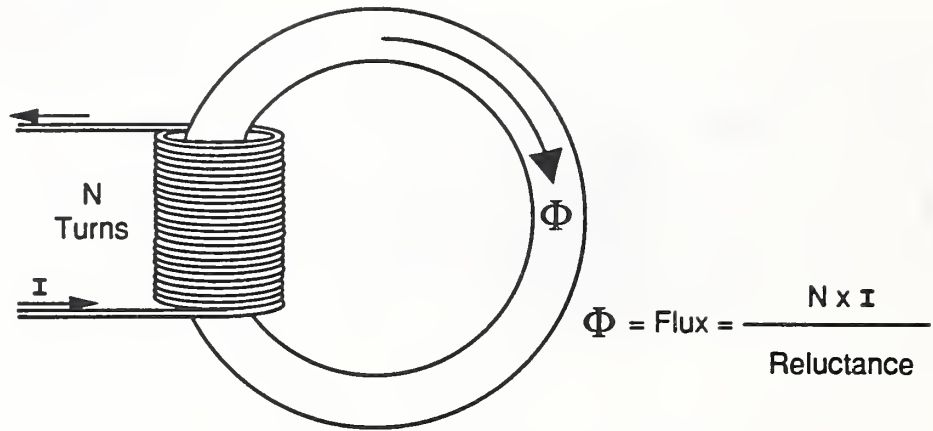


Figure 2.1 Electromagnetic principles involved in the operation of covermeters.

(a) Simple magnetic circuit



(b) Magnetic circuit example

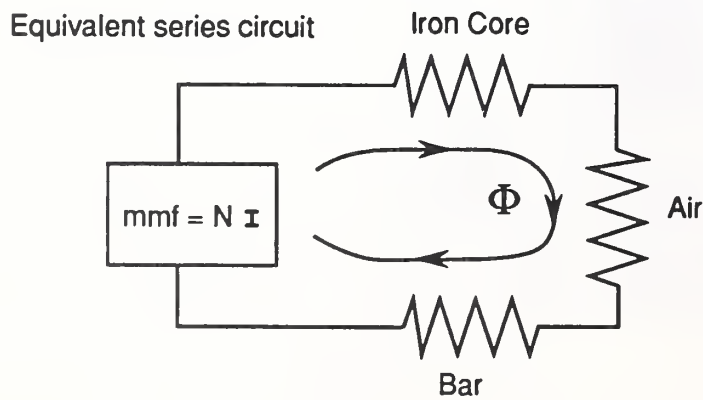
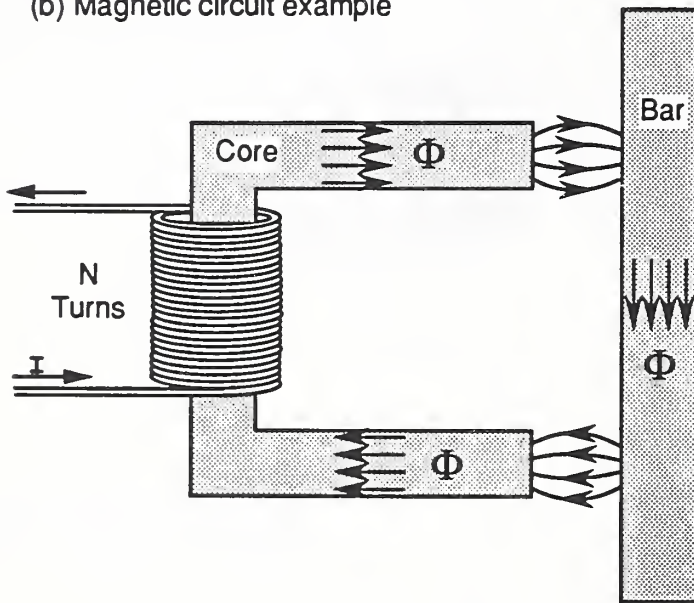
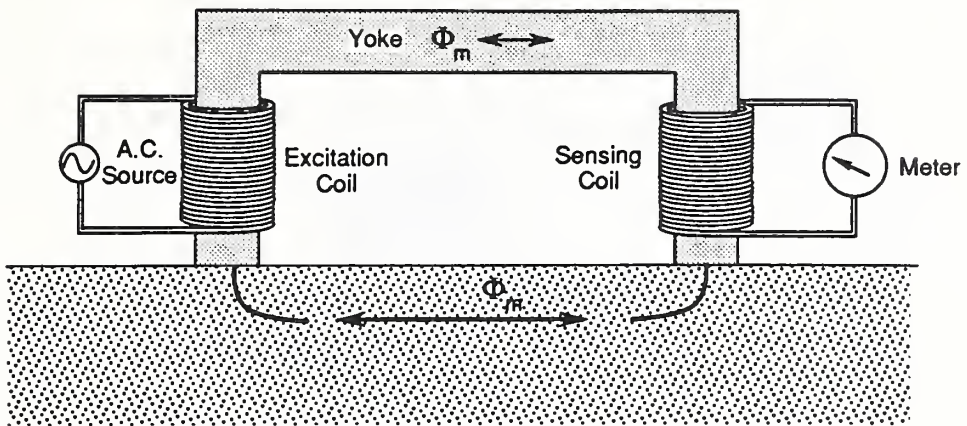
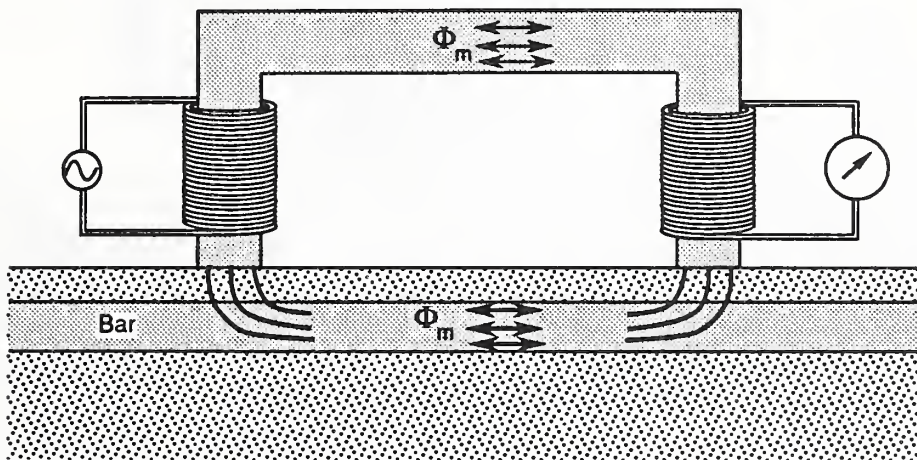


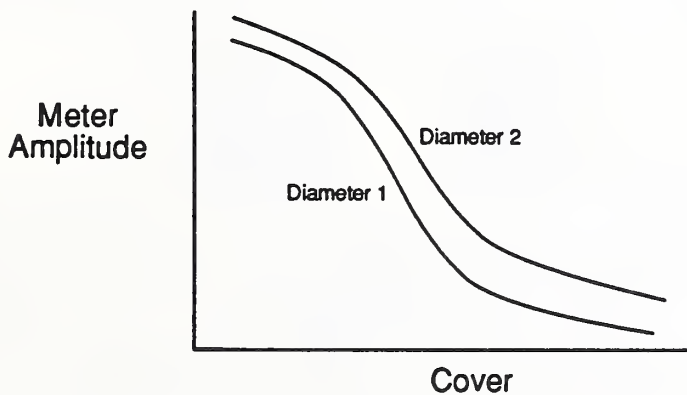
Figure 2.2 (a) Principle of a magnetic circuit and (b) illustrative example.



(a) Small current induced when no bar is present

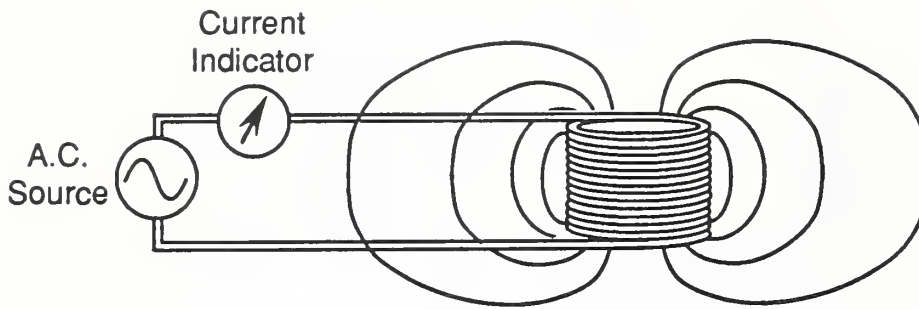


(b) Presence of bar increases flux and increases induced current

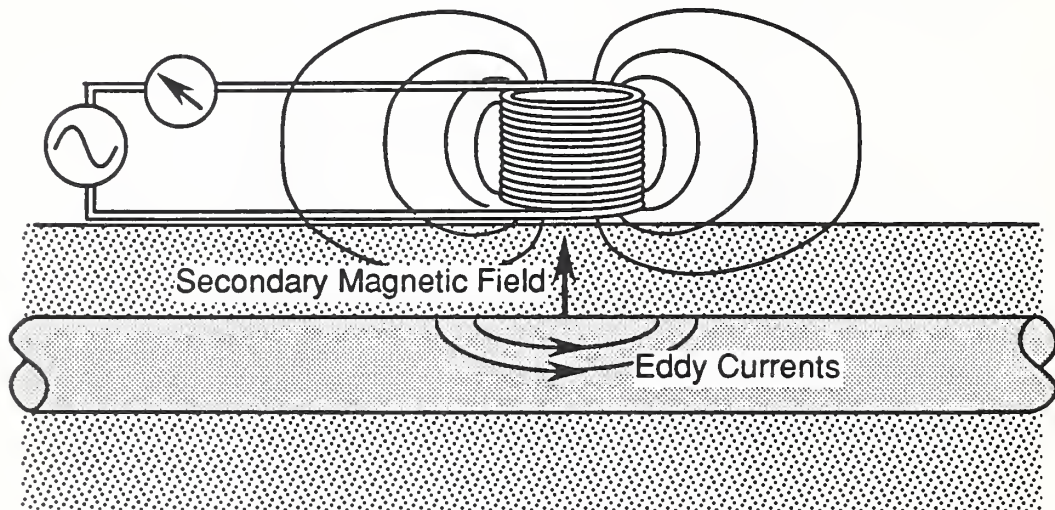


(c) Schematic of relationship between amplitude and cover

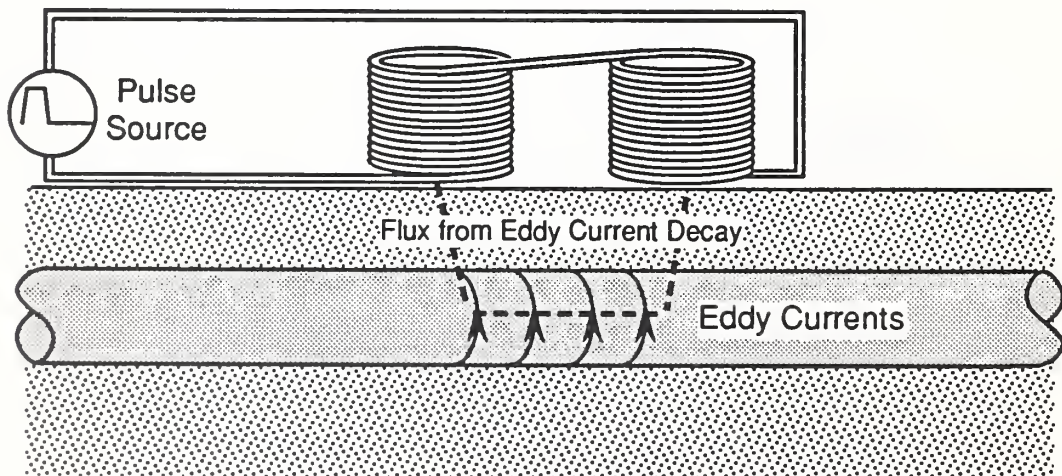
Figure 2.3 Schematics of covermeter based upon changes in the reluctance of a magnetic circuit.



(a) Coil in air results in a characteristic current amplitude



(b) Interaction with reinforcing bar causes changes in coil impedance and current amplitude



(c) Two-coil, pulse-induction system; decay of eddy currents induces current in coils

Figure 2.4 Schematics of covermeters based upon the eddy-current principle.

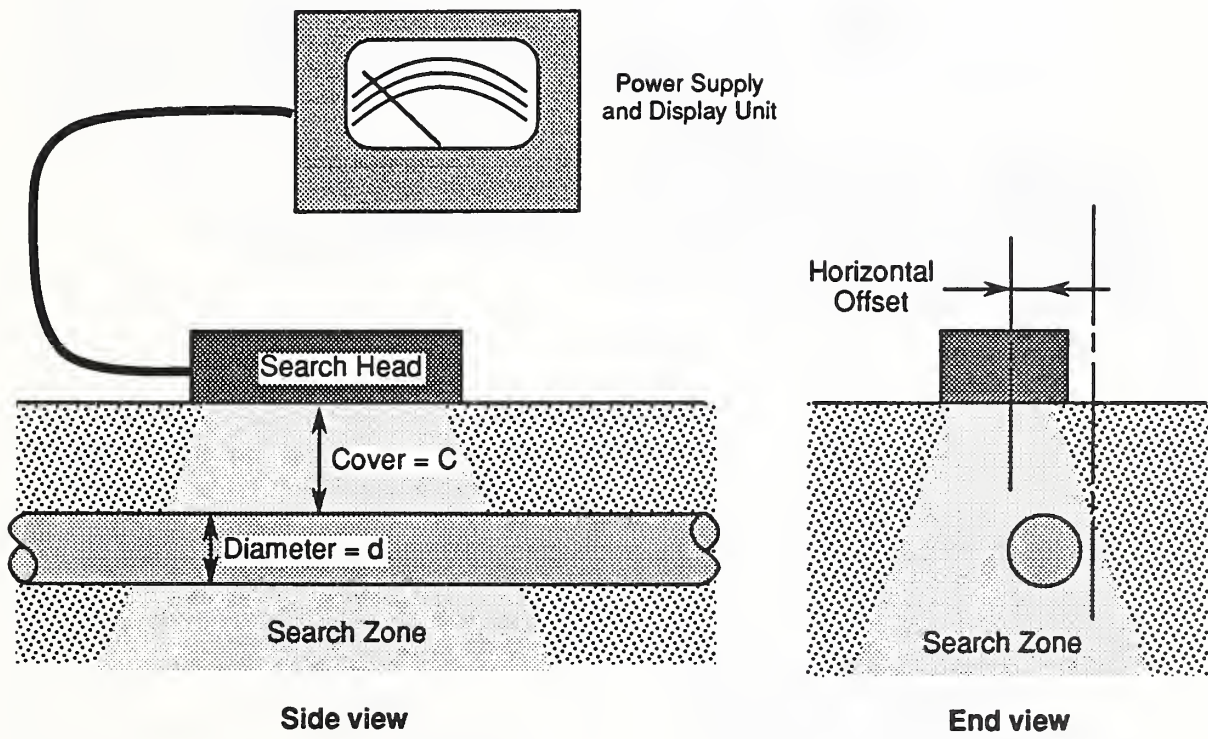
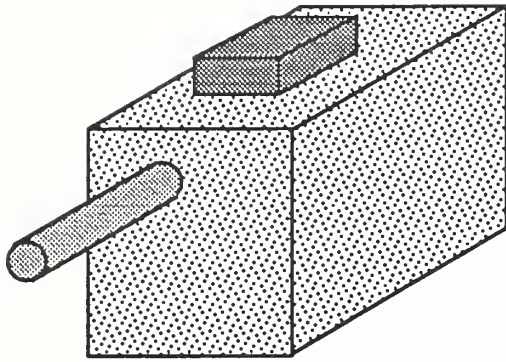
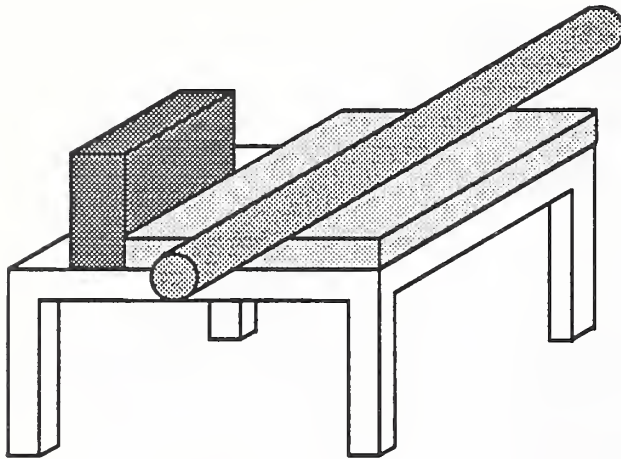


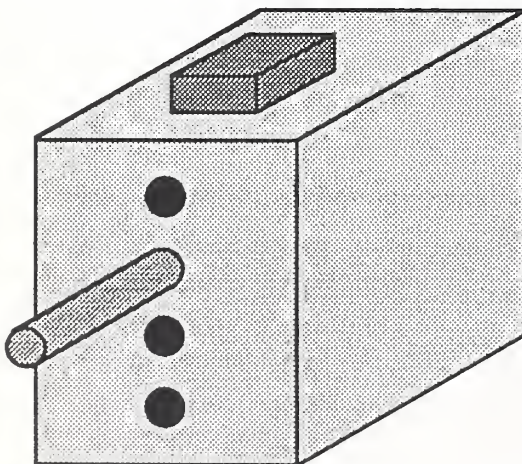
Figure 2.5 Application of covermeter to make measurement of embedded reinforcing bar.



Method A : Concrete prism with eccentric bar

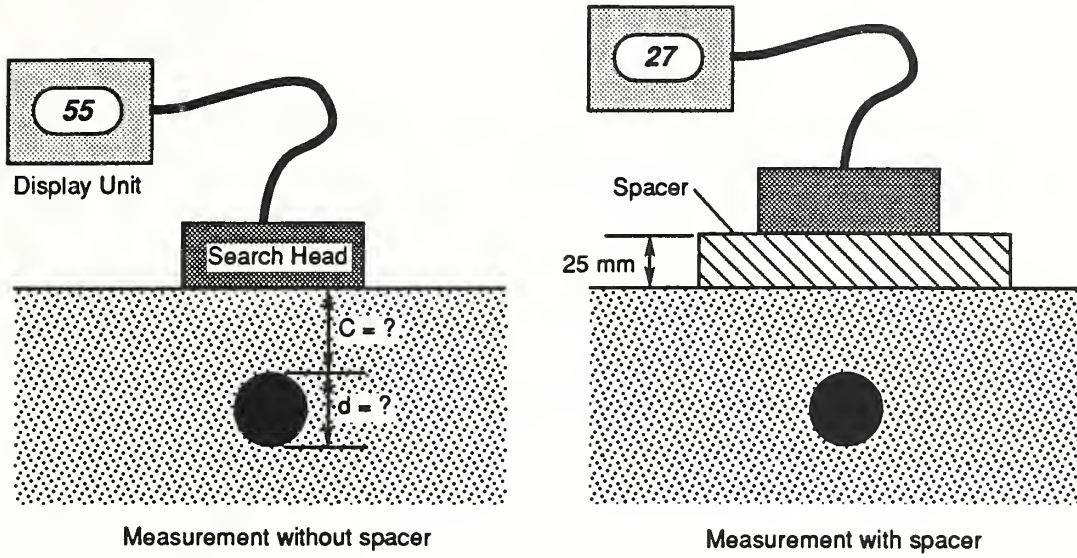


Method B: Search head and bar on table

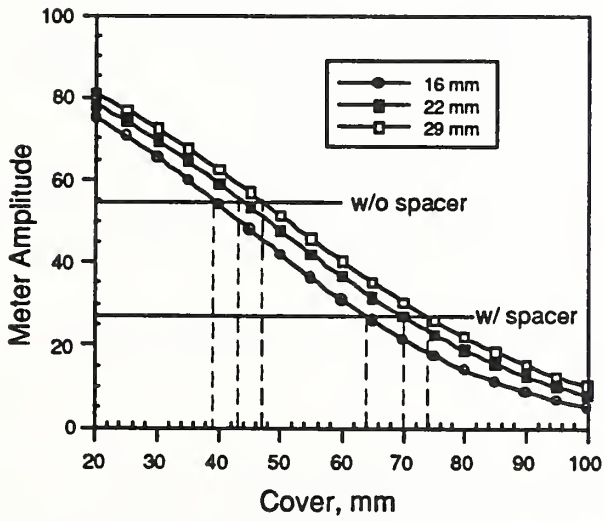


Method C: Nonmetallic box with holes at different depths

Figure 2.6 Methods for calibration of covermeters according to BS 1881 Part 204.



(a) Multiple measurement over bar



(b) Calibration curves

Diameter	Cover (mm)		Difference (mm)
	w/o Spacer	with Spacer	
16	39	64	25
22	43	70	27
29	47	74	27

(c) Estimated cover based on different bar diameter

Figure 2.7 Spacer technique to estimate cover when bar diameter is not known.



### 3. TEST RESULTS

#### 3.1 Introduction

As was mentioned in the Introduction, there are many commercially available covermeters. In this study, two meters were used. One is based on the magnetic reluctance principle and the other is based on the eddy current principle, and they will be referred to as the *M-R meter* and the *E-C meter*, respectively. These meters were chosen as representative examples of the two classes of instruments.

One objective of the experimental study was to gain an understanding of the characteristics of the two classes of instruments. To achieve this objective, measurements were made using individual bars at different cover depths. This type of testing has been performed by others using similar instruments, as indicated in the annotated bibliography at the end of this report. However, in this study an attempt was made to use mathematical models to represent the amplitude versus cover responses. This allows for a convenient way to summarize many test results by looking at the changes in the values of the model parameters as the test conditions change. In addition, the variation of signal amplitude as a function of the horizontal offset from single bars was also examined in a similar manner.

As stated in Chapter 2, the single-bar calibration relationships are useable only if the reinforcement in the structure is sufficiently sparse so that there are no interference effects. Thus another of the objectives was to understand how the single-bar response can be used to predict the response when the reinforcement is congested. A simple model is used to calculate the response in the presence of multiple, parallel bars lying in a plane parallel to the test surface. The goal was to determine the spacing above which the individual bars can be discerned and the minimum spacing that would result in accurate cover measurements based upon the single-bar calibrations. The model predictions were compared with experiments.

The final objective was to investigate the capabilities of the two types of meters to detect and locate the ends of reinforcing bars. First, the responses with individual bars was examined. This would be applicable to locating the ends of bars in lightly reinforced elements such as floor slabs. Finally, the ability to measure the length of a lap splice was investigated.

To assist the reader in following the discussion, pertinent figures and tables are placed at the end of each section rather than at the end of the chapter as was done in Chapter 2.

#### 3.2 Amplitude versus cover

The most important characteristics of a covermeter are the calibration relationships between the meter reading and the depth of cover for different reinforcing bar diameters. These relationships are necessary to measure the depth of a bar and for estimating its diameter. The development of the amplitude-cover calibration relationships is the primary objective of BS 1881 Part 204, and this type of testing has been the usual starting point of previous investigations reported in the literature. Thus the first series of experiments were performed to gain an understanding of the nature of the calibration relationships of the two different types of covermeters. The objective was to determine whether the calibration relationships could be represented by simple equations. If such equations could be developed, it would be of interest to examine the effects of bar size on the equation parameters.

The experimental approach is shown schematically in Fig. 3.1(a). A single reinforcing bar, about 500 mm long, was placed on a 0.5-m thick plain concrete slab, and pieces of 19-mm thick plywood were used to support a 10-mm thick sheet of clear plastic. The cover over the bar (not the deformations) was measured through a hole in the plastic. By adding additional pieces of plywood, the cover could be increased conveniently in 19-mm increments. Covermeter readings were taken as a function of cover until the signal amplitude was too low to be measured with confidence. The following sizes of reinforcing bars were used: #4 (12 mm), #5 (16 mm), #6 (19 mm), #8 (25 mm), #11 (36 mm) and #14 (43 mm)<sup>d</sup>. Note that the #5-bar was epoxy coated and all others were bare steel.

### 3.2.1 *M-R meter*

The covermeter based on the magnetic reluctance principle (M-R meter) has an analog meter display with a scale having 100 divisions. The search head was placed on the plastic plate above the bar and was aligned so that the maximum amplitude was attained on the scale. The scale reading was estimated to the nearest 0.1 unit. The resulting data for all the bars are shown in Fig. 3.2(a). It can be seen that the meter reading decreased approximately linearly as the cover increased to about 75 mm, and then it decreased less gradually with increasing cover up to about 150 mm. To establish an empirical equation which could describe the variation of the amplitude with cover, the data were also plotted using semi-log and log-log scales, as shown in Fig. 3(b) and 3(c). If the relationship were a simple exponential function, the data should plot as a straight line in the semi-log plot. If the data could be represented by a power function, it should plot as a straight line in the log-log plot. As can be seen neither of these conditions were observed. After trying several functions, the following quadratic exponential equation was found to provide a reasonable fit to the data:

$$A_0 = A' e^{-\left(\frac{C}{\gamma}\right)^2} \quad (3.1)$$

where  $A_0$  = amplitude with search head directly above and aligned with bar,  
 $A'$  = regression constant,  
 $\gamma$  = regression constant, mm,  
 $C$  = cover, mm.

The values of  $A'$  and  $\gamma$  were obtained by the method of least squares using commercial software. The physical significance of the parameter  $\gamma$  is discussed at the conclusion of the next sub-section. The results of the regression analyses are summarized in Table 3.1. The numbers in parentheses are the standard deviations of the estimated coefficients  $A'$  and  $\gamma$ . Figure 3.3 shows data and the best-fit curves. The quadratic exponential function fit the data well with the exception of the readings at the lowest cover (about 15 mm) and for cover above 100 mm.

It was desired to determine whether the coefficients of the best-fit equations were related to the diameter of the bars. Figure 3.4 shows values of  $A'$  and  $\gamma$  plotted as a function of the nominal bar diameter. The error bars represent two times the standard deviations of the coefficients. It is seen that the  $\gamma$ -values tended to increase with bar size. However, for some of the adjacent bar sizes there were no significant differences in these values. The coefficient  $A'$  also tended to increase with bar size, but the differences between adjacent bar sizes were also insignificant. Note the points corresponding to the #5-bar (16 mm) deviate from the pattern established by the other bar sizes. This difference is likely due to the fact that the #5 bar was epoxy-coated.

---

<sup>d</sup>These are the approximate metric equivalents of the bars. For simplicity, these metric equivalents are not repeated in the remainder of the text.

As was reviewed in Chapter 2, the spacer technique has been proposed as a means for determining size and cover of an unknown bar. The basis of this method is that each bar size possesses its own unique calibration relationship. By making multiple measurements one is able to establish which calibration curve is applicable and thereby establish the bar size. The above results for the M-R meter show that the calibration curves for adjacent bar sizes are similar, as indicated by the similarity of the values of  $A'$  and  $\gamma$ . Therefore, one should not expect to be able to distinguish reliably between adjacent bar sizes by means of the spacer technique. This observation is not new, as similar conclusions have been reached by others (e.g. Tam, et al. 1977, Smith, et al. 1987), but the above analysis shows clearly why this is so. A better covermeter would be one for which the  $A'$  values were dependent strongly on the bar size.

### 3.2.2 E-C meter

The other covermeter is based on the eddy current principle and is identified as the *E-C meter*. The instrument includes two search heads: a smaller one is known as a *spot* probe and the coil diameter is about 50 mm; the other is called a *depth* probe and the coil diameter is about 80 mm. Both probes are nondirectional, which means that the reading is not affected by orientation relative to the bar. However, for uniformity, in these tests the probes were located above the bar with the longitudinal alignment mark always parallel to the bar axis. This instrument has a digital readout of signal amplitude from values of 0 to 1999. When the probe is too close to a bar, the digital display will be "1999" which means that the range has been exceeded and the measurement is invalid.

The results for the spot and depth probes of the E-C meter are shown in Figs. 3.5 and 3.6, respectively. The penetration depth of the spot probe was about 75 mm, whereas the depth probe went to about 140 mm. The semi-log and log-log plots show that the variation of amplitude with cover is distinctly different from what was obtained with the M-R meter. In the semi-log plot, the data fall close to a straight line, which means that simple exponential functions could be used to approximate the calibration relationships. Likewise, the log-log plot shows that a power function could also be used to approximate the data. Hence the following models were investigated:

$$A_0 = \frac{A'}{C^3} \quad (3.2)$$

$$A_0 = A' e^{-\frac{C}{\gamma}}$$

where  $A_0$ ,  $C$ , and  $\gamma$  have the same meaning as in the previous Eq. (3.1). While the fit of these functions to the data was reasonably good (correlation coefficients greater than 0.99), they systematically underestimated the amplitude at high cover. It was found that the following inverse exponential function gave excellent fit to the data:

$$A_0 = A' \left( 1 - e^{-\left(\frac{\gamma}{C}\right)^{3.3}} \right) \quad (3.3)$$

The exponent value of 3.3 in Eq. (3.3) was established by first doing a least-squares fit in which the exponent was a fitted parameter. In those analyses, the best-fit value of the exponent varied between 3.2 and 3.6., so the approximate median value of 3.3 was chosen.

Figures 3.7 and 3.8 show the fit of the inverse exponential function to the data obtained using the spot and depth probe, respectively. Table 3.2 summarizes the results of the regression analyses.

It is seen that the residual standard deviations<sup>e</sup> are low, especially for the spot-probe data. Figure 3.9 shows the relationships between the regression constants  $A'$  and  $\gamma$  and the bar diameter. Again, the errors bars are twice the standard deviations for the estimated values of the constants (some of these errors are too small to be seen in the plots). In general, the following trends are noted: For the spot probe,  $A'$  tends to increase with diameter, whereas  $\gamma$  seems to be independent of bar diameter. For the depth probe, the trends are reversed:  $A'$  appears to be independent of bar diameter and  $\gamma$  seems to increase with diameter. Note that in all cases the points corresponding to the #5 bar deviate from the trends described by the other points. Again, the likely cause is the fact that this bar was epoxy coated.

A comparison of the calibration curves for the two probes (Figs. 3.7 and 3.8) shows that the differences between the curves of adjacent bar sizes are greater for the depth probe than the spot probe. The only exception is for the #11- and #14-bars, where the curves are practically identical for each type of probe. This means that the depth probe would be preferred if the spacer technique were used to estimate bar size. However, for shallow cover the depth probe would probably result in an out-of-range reading. This could be dealt with by using thicker spacers.

To conclude this section, the significance of the  $\gamma$ -parameter in Eqs. (3.1) and (3.3) is mentioned. Figure 3.10 is a plot of these two equations, which have been normalized by setting  $A' = 1$ . The relative amplitude is plotted as a function of  $C/\gamma$  instead of  $C$ , the cover. In the figure, *quadratic* refers to Eq. (3.1) used for the M-R meter, and *inverse* refers to Eq. (3.3) used for the E-C meter. For the M-R meter, when the cover equals twice the value of  $\gamma$  ( $C/\gamma = 2$ ), the amplitude drops to 2% of the maximum amplitude. While for the E-C meter, the relative amplitude drops to 10% of the maximum value when  $C/\gamma = 2$ . Thus the value of  $\gamma$  defines how the signal amplitude decays with increasing cover and is, therefore, an indicator of the depth of penetration of the covermeters. A larger value of  $\gamma$  is preferred as this signifies the ability to detect more deeply embedded bars. A review of the  $\gamma$ -values in Figs. 3.4(a) and 3.9(a) shows how the penetration depth is affected by bar size. The penetration increases with bar size for the M-R meter and the E-C meter with the depth probe, but is not affected significantly by bar size when the spot probe is used with the E-C meter.

### 3.2.3 Summary

In summary, these initial sets of tests were conducted to establish the nature of the amplitude versus cover relationships for the two type of covermeters. Empirical models were fitted to the data to permit a systematic analysis of the effect of bar size on the calibration curves. The models used to represent the data for the two covermeters were different in form, but they both involve two parameters,  $A'$  and  $\gamma$ . Examination of these parameters as a function of bar size showed that some trends existed, but, in general, the values of the parameters for adjacent bar sizes were not very different. This means that, for adjacent bar sizes, the curves of amplitude versus cover are similar. This shows the inherent limitations of electromagnetic covermeters in discriminating between different bar sizes. It was also observed that the parameters obtained for the #5 epoxy-coated bar deviated from the trends defined by bare steel bars. It is not known whether the anomalous behavior is due to the epoxy-coating or to a difference in the metallurgical characteristics of the coated bar. This aspect merits further study in view of the widespread use of epoxy-coated bars in highway construction.

---

<sup>e</sup>The residual standard deviation (RSD) is a measure of the difference between the best-fit curve and the data.

Table 3.1 Results of regression analysis of amplitude versus cover for M-R meter

$$\text{Model: } A_0 = A' e^{-\left(\frac{C}{\gamma}\right)^2}$$

Bar (mm)	A' †	γ, mm†	n	RSD	r
#4 (12)	80.4 (1.7)	57.1 (1.2)	11	1.8	0.9978
#5 (16)	83.9 (1.8)	56.9 (1.3)	12	2.2	0.9972
#6 (19)	82.6 (1.4)	62.3 (1.1)	12	1.8	0.9982
#8 (25)	83.6 (1.3)	64.9 (1.0)	11	1.6	0.9960
#11 (36)	87.7 (2.0)	69.5 (1.7)	11	2.6	0.9967
#14 (43)	87.3 (2.2)	67.3 (1.8)	12	2.6	0.9958

† Values in parentheses are the standard deviations of the estimated regression coefficients  
 n = number of data points  
 RSD = residual standard deviation  
 r = correlation coefficient

Table 3.2 Results of regression analysis of amplitude versus cover for E-C meter

$$\text{Model: } A_0 = A' \left(1 - e^{-\left(\frac{\gamma}{C}\right)^{2.3}}\right)$$

Bar (mm)	A' †	γ, mm†	n	RSD	r
Spot Probe					
#4 (12)	1015 (28)	15.8 (0.2)	6	3.2	0.99995
#5 (16)	2590 (42)	12.3 (0.1)	6	2.1	0.99999
#6 (19)	1368 (31)	15.8 (0.2)	7	3.3	0.99995
#8 (25)	1620 (56)	15.6 (0.3)	6	4.0	0.99995
#11 (36)	1661 (6)	17.2 (0.1)	8	1.9	0.99999
#14 (43)	1870 (432)	16.4 (1.3)	6	2.9	0.99986

† Values in parentheses are the standard deviations of the estimated regression coefficients  
 n = number of data points  
 RSD = residual standard deviation  
 r = correlation coefficient

Table 3.2 (Continued) Results of regression analysis of amplitude versus cover for E-C meter

$$\text{Model: } A_0 = A' \left( 1 - e^{-\left(\frac{\gamma}{c}\right)^{3.3}} \right)$$

Bar (mm)	$A'$ †	$\gamma$ , mm†	n	RSD	r
Depth Probe					
#4 (12)	1889 (36)	29.3 (0.3)	10	5.6	0.99991
#5 (16)	1446 (62)	34.6 (0.6)	9	6.5	0.99975
#6 (19)	2086 (73)	32.8 (0.5)	9	6.5	0.99987
#8 (25)	1912 (156)	36.2 (1.2)	8	9.8	0.99956
#11 (36)	2478 (134)	38.8 (0.9)	9	17.7	0.9946
#14 (43)	2085 (65)	40.8 (0.7)	10	16.1	0.99951

† Values in parentheses are the standard deviations of the estimated regression coefficients

n = number of data points

RSD = residual standard deviation

r = correlation coefficient

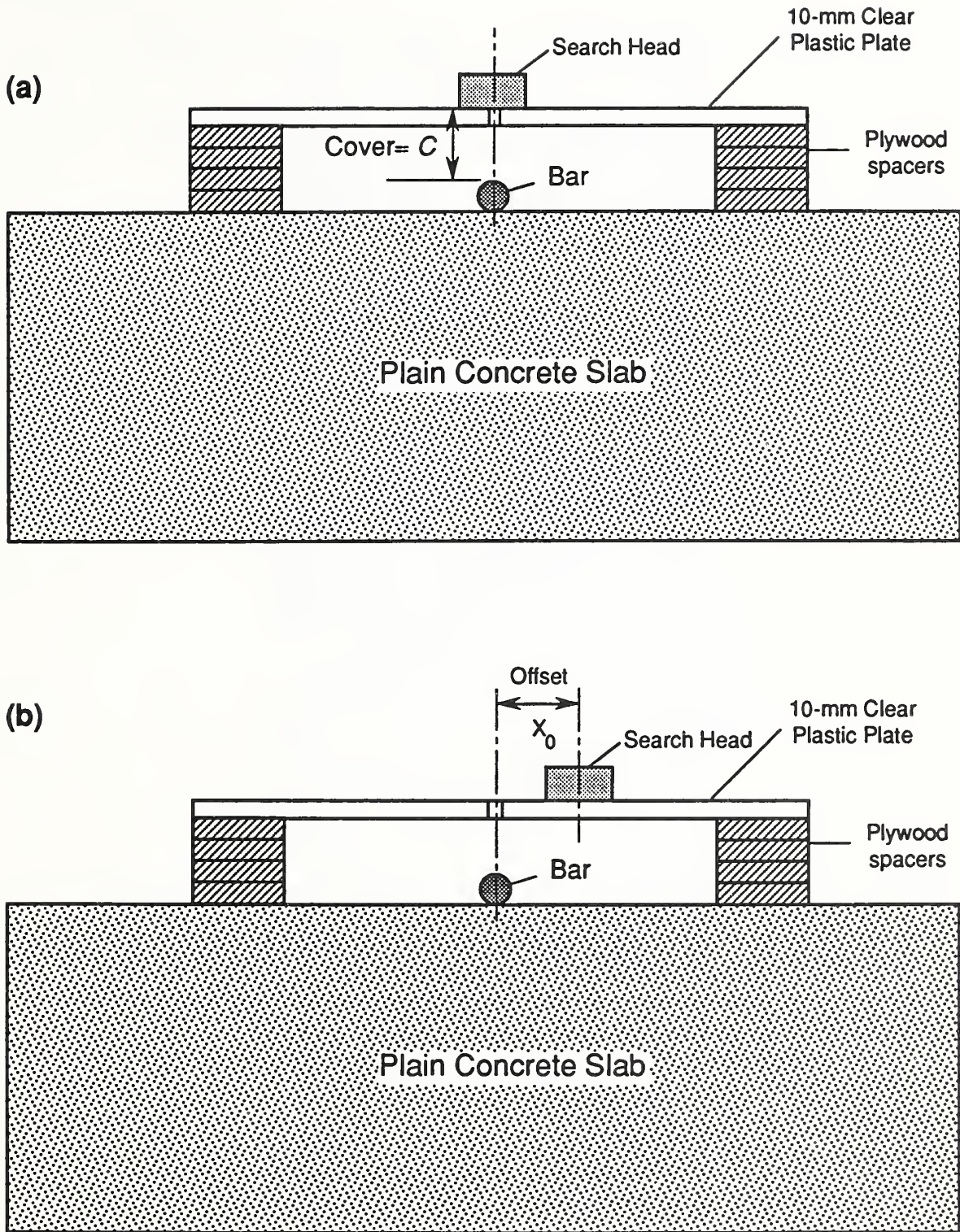


Figure 3.1 Schematics of testing procedures: (a) for amplitude versus cover measurements and (b) for amplitude versus horizontal offset for different covers.

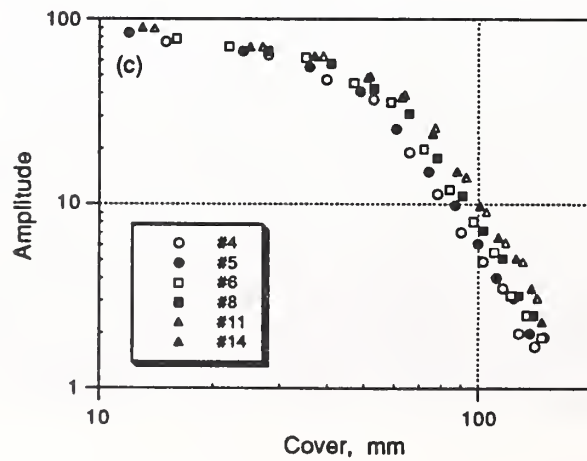
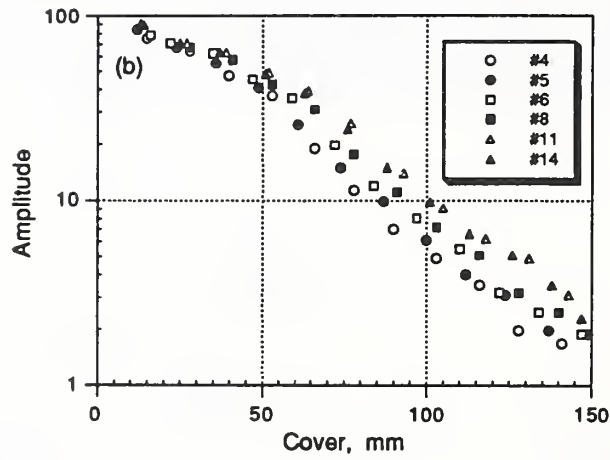
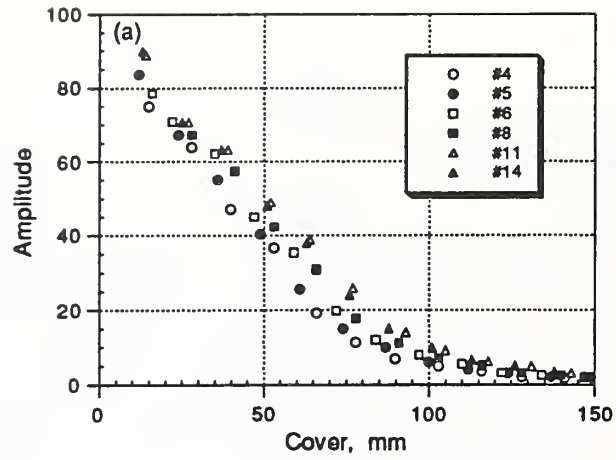


Figure 3.2 Amplitude versus cover data for M-R meter: (a) ordinary plot, (b) semi-log plot, and (c) log-log plot.

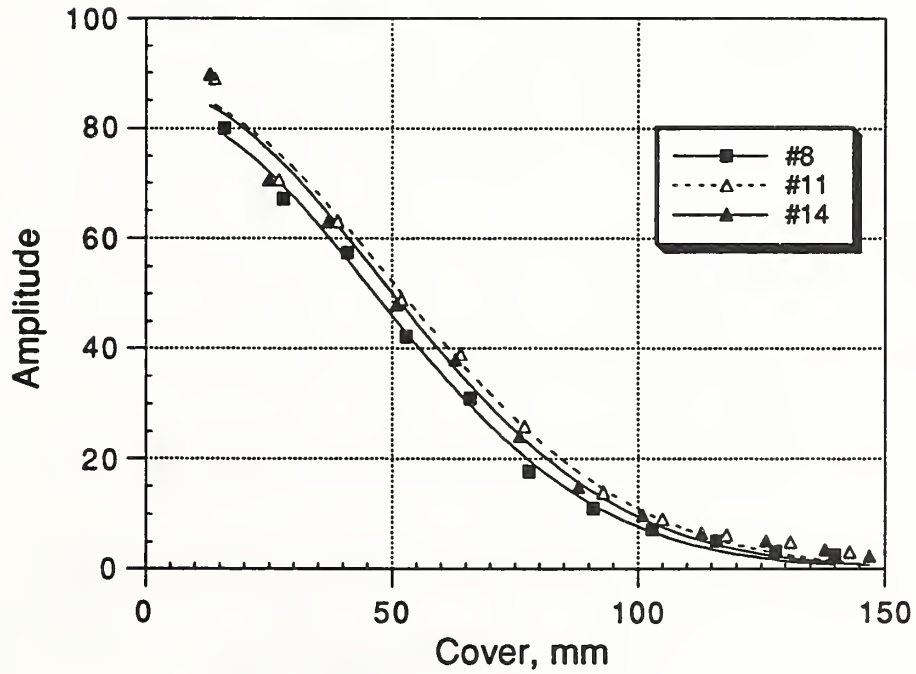
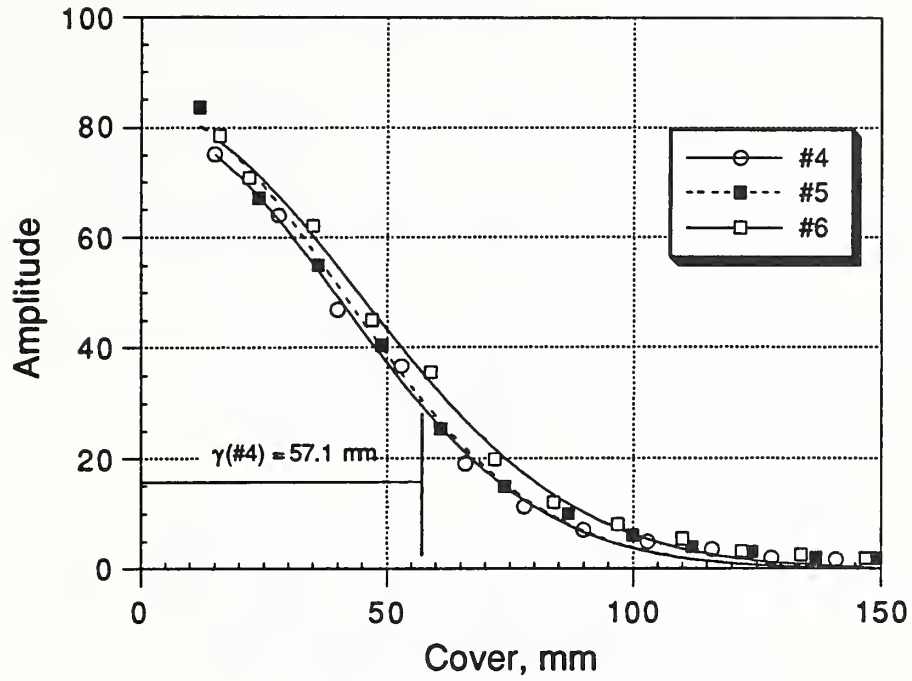


Figure 3.3 Amplitude versus cover for M-R meter: data and best fit quadratic exponential function, Eq. (3.1).

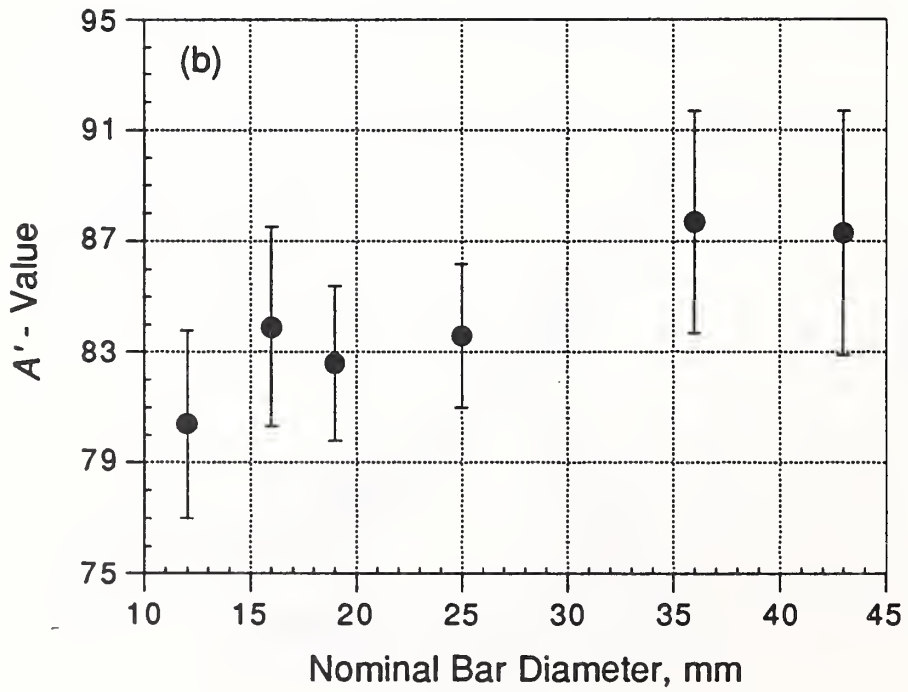
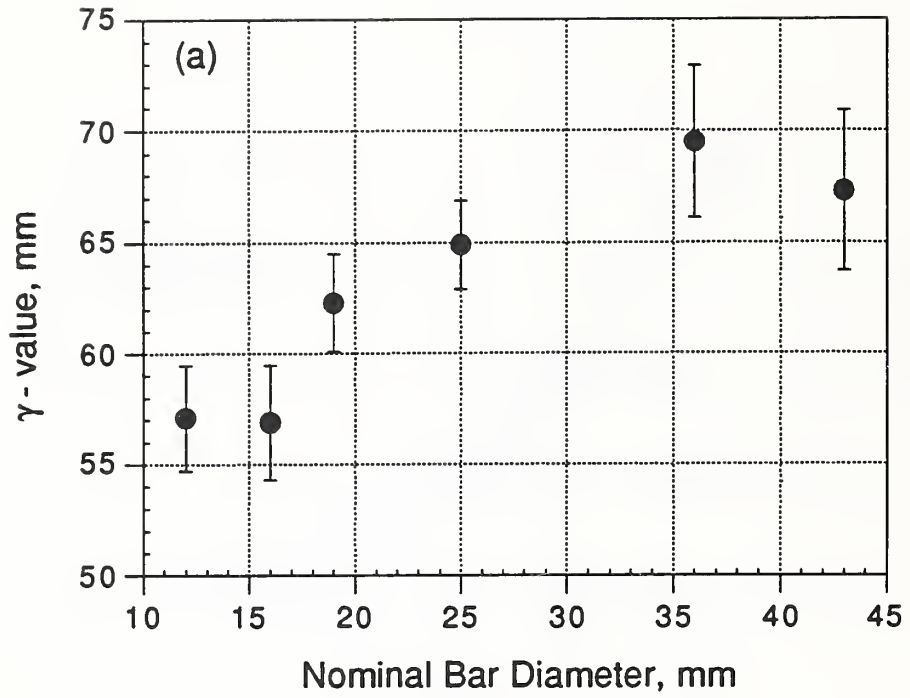


Figure 3.4 Values of regression constants for Eq. (3.1) as a function of nominal bar diameter for M-R meter.

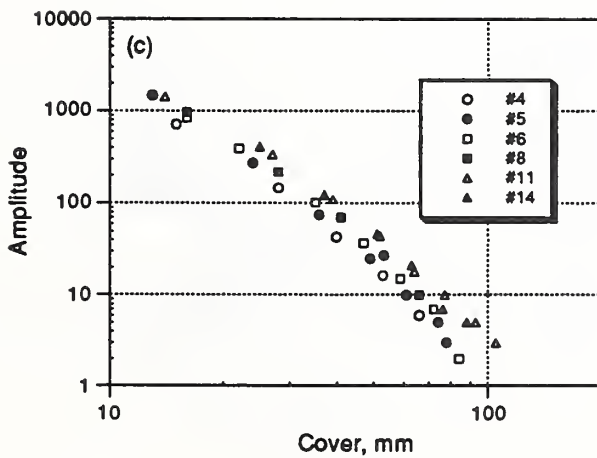
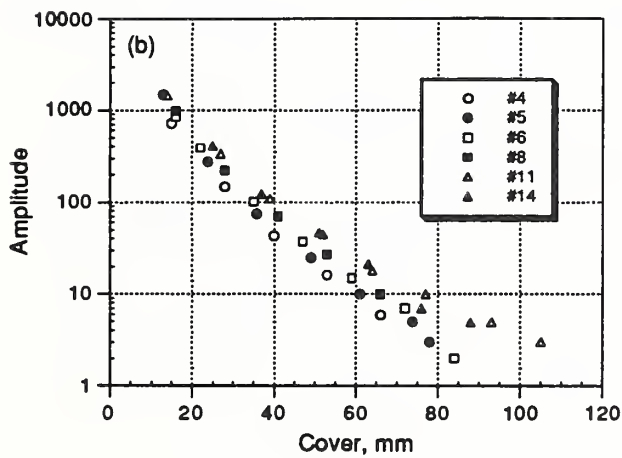
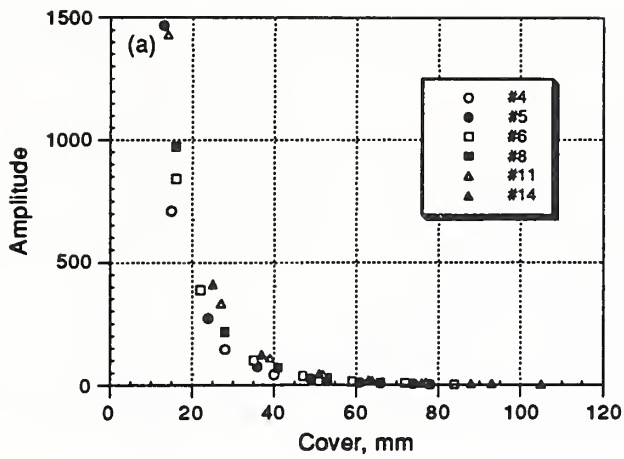


Figure 3.5 Amplitude versus cover data for E-C meter with spot probe: (a) ordinary plot, (b) semi-log plot, and (c) log-log plot.

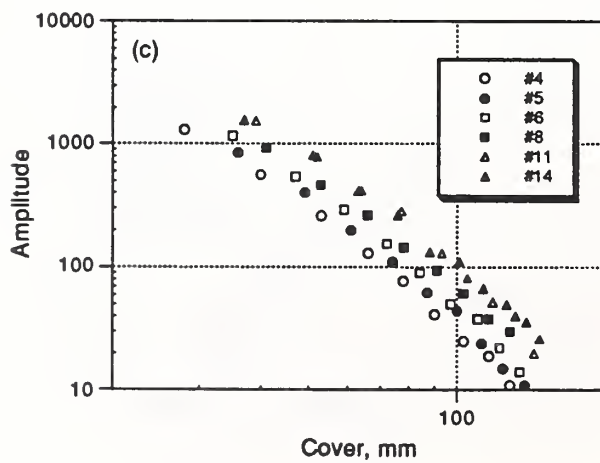
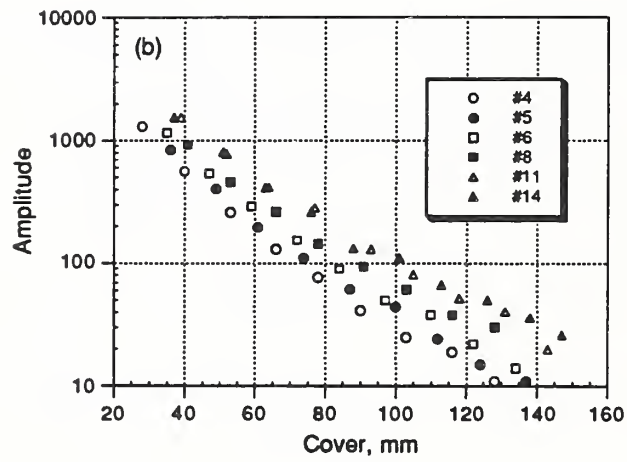
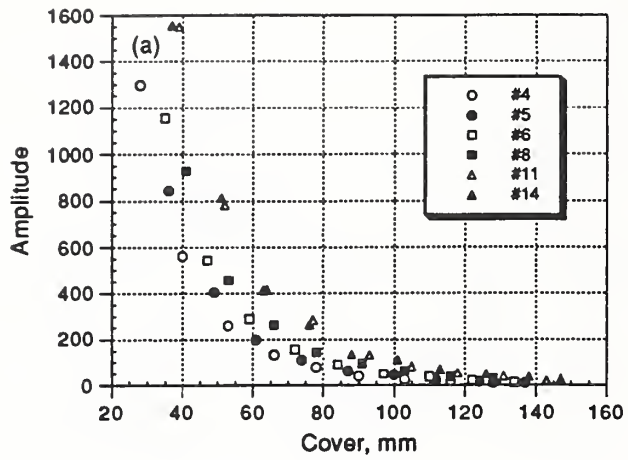


Figure 3.6 Amplitude versus cover data for E-C meter with depth probe: (a) ordinary plot, (b) semi-log plot, and (c) log-log plot.

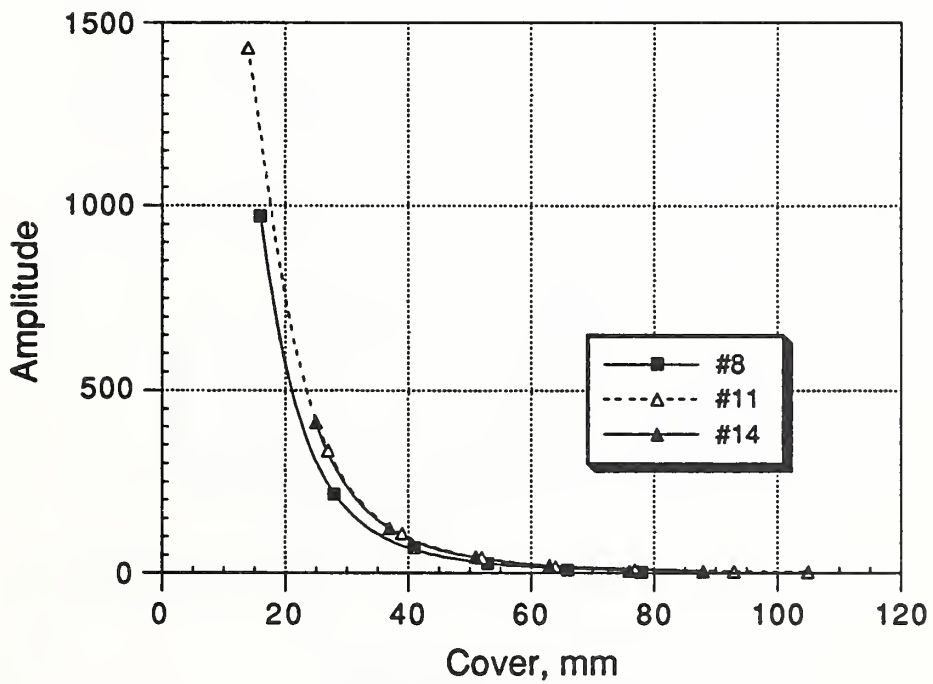
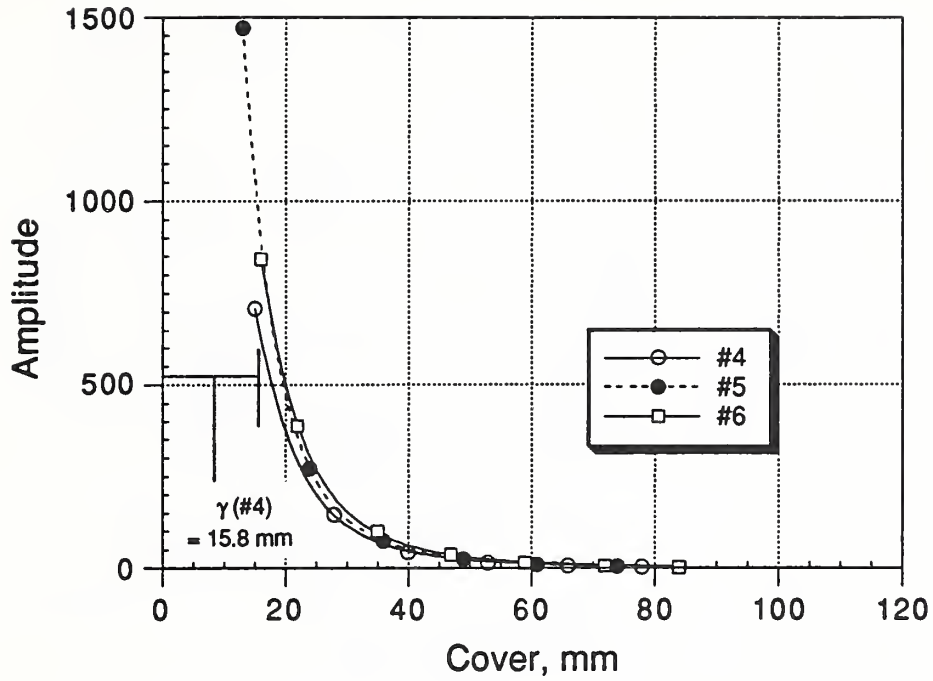


Figure 3.7 Amplitude versus cover for E-C meter with spot probe: data and best fit inverse exponential function, Eq. (3.3).

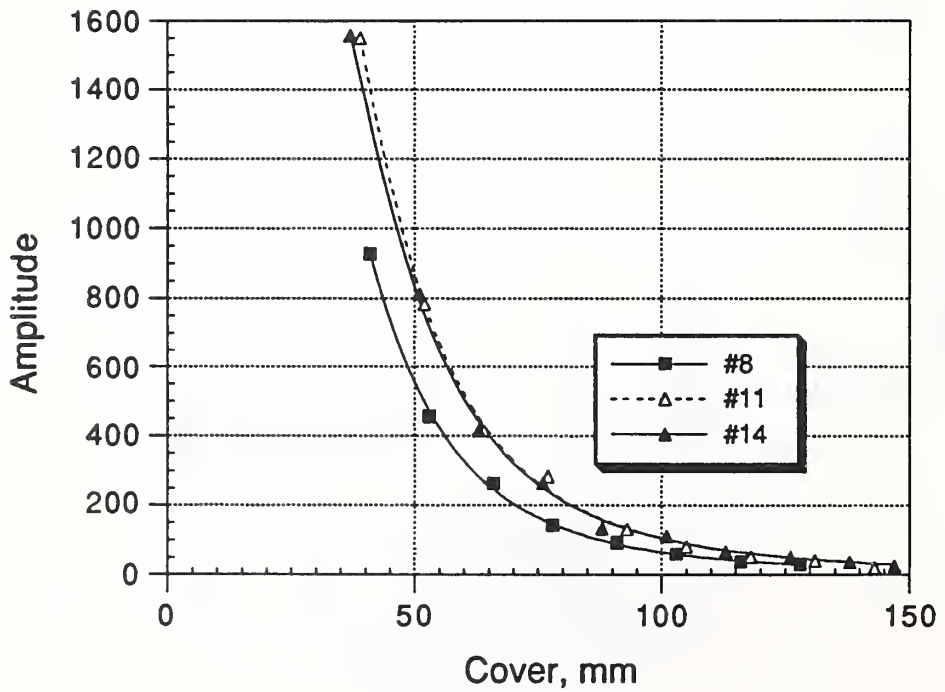
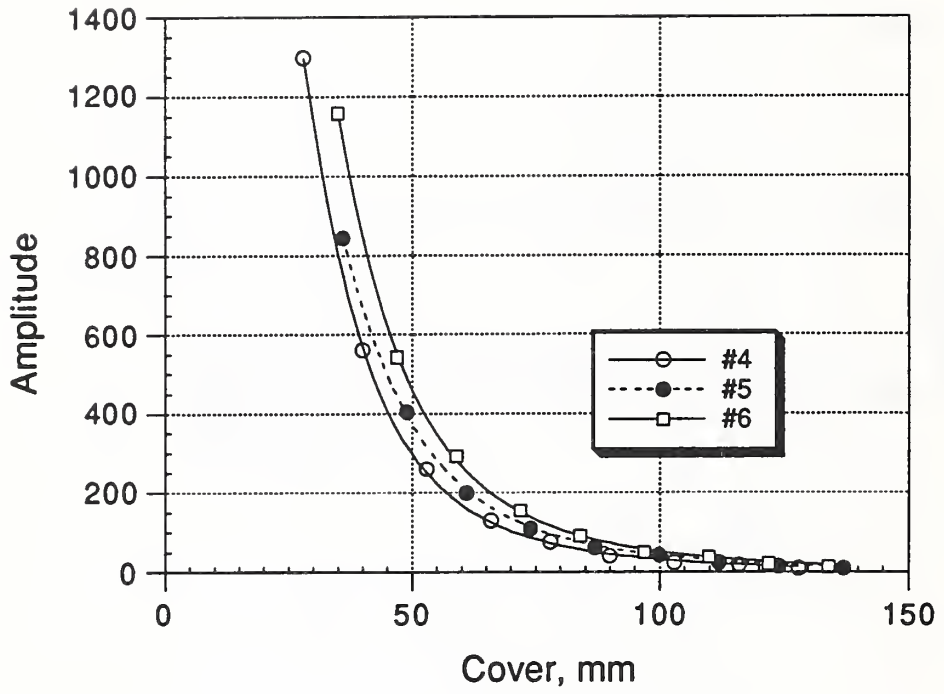


Figure 3.8 Amplitude versus cover for E-C meter with depth probe: data and best fit inverse exponential function, Eq. (3.3).

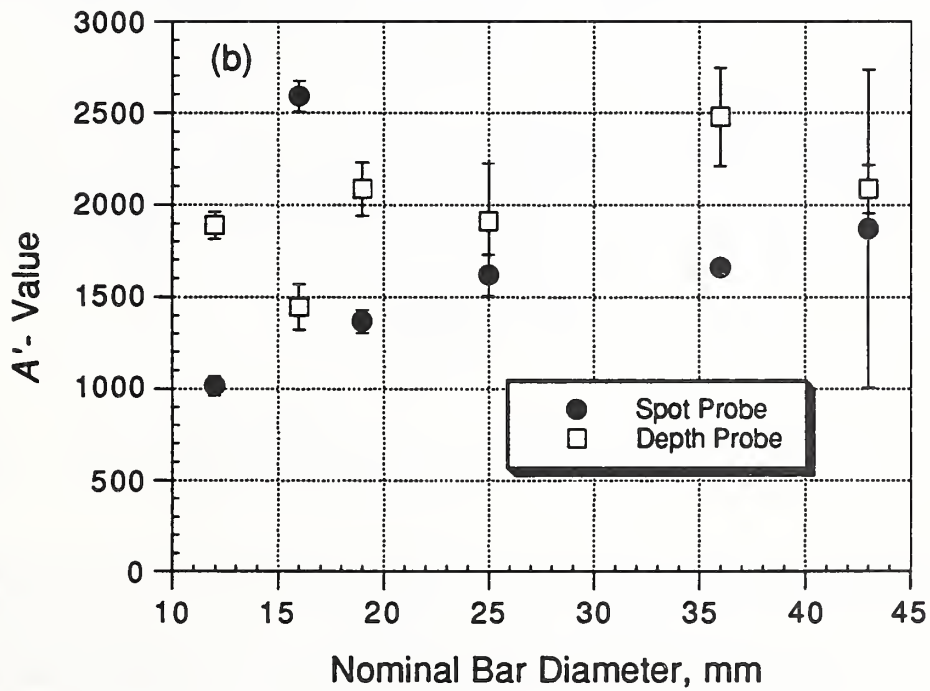
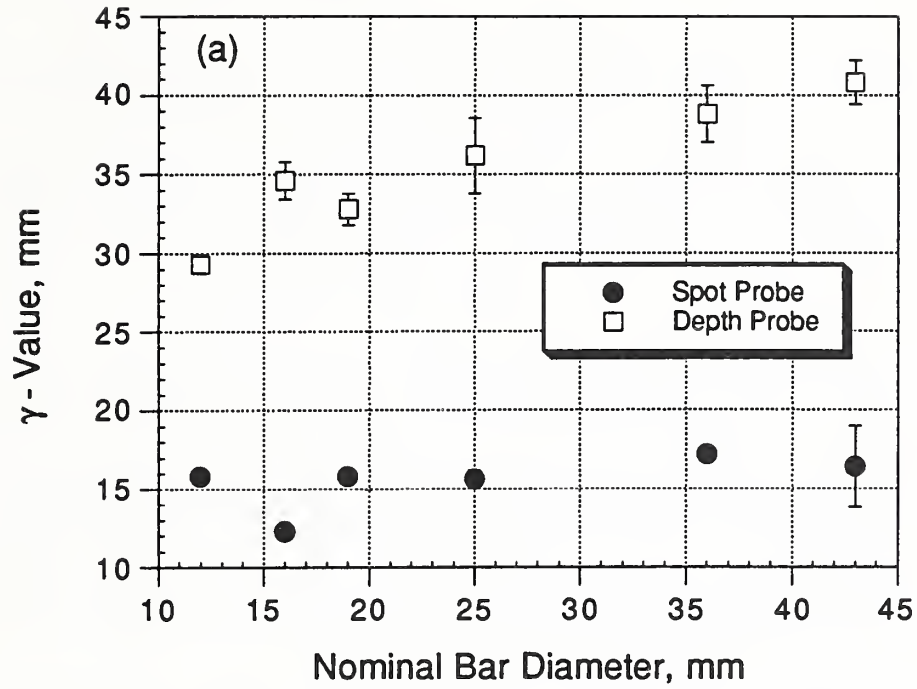


Figure 3.9

Values of regression constants for Eq. (3.3) as a function of nominal bar diameter for E-C meter.

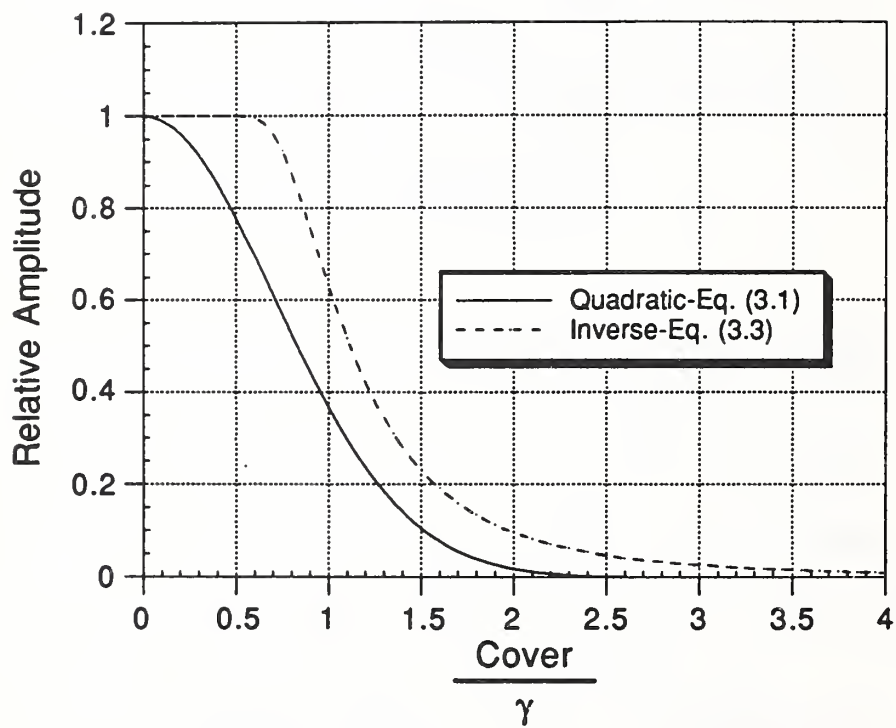


Figure 3.10 Relative amplitude as function of cover/ $\gamma$  for quadratic and inverse exponential functions, where  $\gamma$  is a parameter obtained from regression analysis of amplitude versus cover data.

### 3.3 Amplitude versus horizontal offset

The amplitude versus cover calibration relationships for a covermeter can be used in the field provided that the field conditions are similar to those used to develop the relationships. Thus if the calibrations are performed using individual bars, they will be applicable only if the bars in the structure are far enough apart to avoid interference effects. Manufacturers of covermeters typically provide guidance on the limits of their calibration curves. For example, the manufacturer of the M-R meter used in this study recommends a minimum clear distance of 100 mm between adjacent bars. The manufacturer of the E-C meter provides a graph showing that the allowable clear spacing increases with cover and also depends on the bar size.

The reading of a covermeter is affected by adjacent parallel bars that lie within the zone of influence of the search head. Thus one of the important characteristics of a covermeter is the nature of the field pattern of the probe. This was the motivation for the second set of experiments. The experimental procedure was similar to that used for the amplitude versus cover study, except that meter readings were recorded as the search head was moved horizontally away from the vertical plane passing through the center of the bar (see Fig. 3.1(b)). Readings were taken at 10-mm intervals, beginning with the search head directly above the bar, i.e., at  $X_0 = 0$ . These measurements were made for different values of cover and for three bar sizes, namely, #4, #6, and #11. The data were fitted with an equation that permitted an understanding of the performance of the two covermeters.

Popovics and Popovics (1992) have reported on similar measurements of amplitude versus horizontal offset for a covermeter similar to the M-R meter used in this study. They suggested that the information from such measurements may be useful for estimating bar diameter with more reliability than the traditional spacer technique. However, the equations used to represent the relationship of amplitude versus offset were not given.

#### 3.3.1 *Mathematical modeling*

Figure 3.11 shows the data for the #6 bar. It is seen that for both types of covermeters, the variation of meter reading with horizontal offset appears to be *bell-shaped*. Thus the data were fitted with the following quadratic exponential equation which is similar to that used to represent the amplitude-cover relationship for the M-R meter:

$$A = A_0' e^{-\left(\frac{X_0}{\delta}\right)^2} \quad (3.4)$$

where  $A$  = meter reading,  
 $X_0$  = horizontal offset, mm  
 $A_0'$  = regression constant, and  
 $\delta$  = regression constant, mm.

Tables 3.3 and 3.4 summarize the values of the regression constants, their standard deviations, and the residual standard deviation of the fitted curves. Additional data were obtained as part of the bar spacing study discussed in the next section, and the results from these tests are also shown. Figure 3.12 shows data and fitted curves for three cases (the M-R meter and the E-C meter with the two probes) using a #6 bar. The quadratic exponential functional provides a good fit to the data, but there are some systematic errors. The curve tends to underestimate the amplitude of the meter reading for large values of the offset distance. In addition, the value of  $A_0'$ , which represents the amplitude when the search head is directly above the bar, does not always agree with the actual measured value. This latter discrepancy is summarized in Fig. 3.13, which is a plot of the ratio of the

calculated value of the amplitude at  $X_0 = 0$  (i.e.,  $A_0'$ ) to the measured value. In general, the best-fit curves tend to underestimate the measured value, but the difference is smaller for higher amplitudes, i.e., smaller cover. For the MR-meter, the calculated value exceeded the measured value for amplitudes greater than 40.

An examination of Fig. 3.12 reveals that the *widths* of the bell-shaped curves are different for each case. The widths of the curves characterize the *zone of influence* of each search head, and the regression constant  $\delta$  is a convenient parameter to quantify the extent of this zone. Equation (3.4) is identical to the quadratic exponential function plotted previously in Fig. 3.10. When the horizontal offset,  $X_0$ , equals  $1.5 \delta$ , the amplitude drops to about 10% of its maximum value at  $X_0 = 0$ , and when the horizontal offset equals  $1.75 \delta$  it drops to 5% of the maximum value. A smaller value of  $\delta$  indicates that the zone of influence of the search head is more focused, and would be desirable for minimizing the interfering effects of adjacent bars.

The effects of cover and bar size on the zone of influence of the search head can be summarized by plotting the values of  $\delta$ , listed in Tables 3.3 and 3.4, as a function of cover. Such plots are shown in Figs. 3.14. The error intervals were obtained by adding and subtracting twice the standard deviations of the estimated values of  $\delta$ , which are shown within parentheses in the fourth columns in Tables 3.3 and 3.4. As can be seen, the zones of influence of the M-R and E-C covermeters are affected by cover in different ways. For the M-R meter, the value of  $\delta$  remains essentially constant up to a cover of about 60 to 70 mm; for deeper cover,  $\delta$  increases with cover in an approximately linear fashion. On the other hand, for the E-C meter, the value of  $\delta$  increases linearly with cover, and the rate of increase is similar for the spot and depth probes. Note that in all cases the uncertainties in the computed value of  $\delta$  are higher for deeper cover. For the M-R meter, the value of  $\delta$  appears to increase with bar size, whereas  $\delta$  is affected little by bar diameter for the E-C meter.

### 3.3.2 Summary

In summary, these experiments were carried out to understand the size of zones of influence of the search heads of the two covermeters. This characteristic is vital for predicting the minimum distances between multiple parallel bars to avoid interference effects that would invalidate the single bar, amplitude-cover relationships. The results showed that the variation of meter reading with horizontal offset could be described by the bell-shaped, quadratic-exponential function that was used previously to represent the amplitude-cover relationship for the M-R meter. By fitting this function to the data, the values of the parameter  $\delta$  were estimated. The value of  $\delta$  defines how the signal amplitude decays with the horizontal offset. For example, when the horizontal offset equals  $1.75\delta$ , the amplitude drops to 5% of the maximum value when the search head is directly above a bar. For the M-R meter, the value of  $\delta$  was essentially independent of cover up to a cover of 60 to 70 mm and it increased approximately linearly with cover above these values. Larger bars resulted in larger values of  $\delta$ . For the E-C meter,  $\delta$  increased approximately linearly with cover and was less affected by bar size.

These results can now be used to estimate the minimum bar spacing to avoid inference when multiple parallel bars are present. If it is assumed that interference effects are negligible when the amplitude drops to less than 5% of the reading when the bar is directly below the search head, the minimum bar spacing should be about  $1.75 \delta$ . The series of experiments discussed in the next section, examined the effects of multiple bars in more detail.

Table 3.3 Results of regression analysis of amplitude versus horizontal offset for M-R meter

Bar (mm)	Cover,mm	$A_0^\dagger$	$\delta$ , mm†	n	RSD
#4 (12)	16	74.9 (1.0)	61.9 (1.0)	17	1.7
	35	55.8 (0.7)	63.1 (1.0)	16	1.3
	54	34.5 (0.8)	58.1 (1.6)	15	1.3
	72	13.9 (0.2)	71.9 (1.1)	13	0.3
	91	7.1 (0.1)	78.0 (0.9)	10	0.1
	109	3.6 (0.1)	90.9 (4.2)	11	0.2
	128	1.9 (0.1)	100.0 (13.4)	7	0.2
#6 (19)	21	74.0 (1.0)	69.2 (1.1)	17	1.8
	40	53.9 (0.9)	70.1 (1.5)	17	1.7
	59	34.3 (0.9)	64.3 (2.0)	17	1.5
	75	16.0 (0.2)	80.0 (1.4)	15	0.5
	94	7.6 (0.2)	92.0 (2.8)	14	0.4
	113	4.7 (0.1)	101.5 (3.6)	14	0.3
	131	2.6 (0.1)	105.3 (8.0)	10	0.2
	19*	79.0 (1.4)	72.5 (1.5)	19	2.5
	38*	62.0 (0.7)	70.8 (0.9)	21	1.2
	57*	39.9 (0.8)	68.8 (1.7)	17	1.4
#11 (36)	21	78.5 (1.0)	81.5 (1.2)	16	1.9
	39	64.1 (0.6)	78.9 (0.9)	16	1.2
	52	49.7 (0.7)	79.0 (1.4)	16	1.4
	68	36.7 (0.7)	77.0 (1.8)	16	1.4
	87	16.7 (0.2)	88.6 (1.6)	16	0.5
	105	9.1 (0.2)	102.6 (2.5)	16	0.4
	124	4.9 (0.1)	119.8 (1.8)	16	0.1
	19*	81.3 (0.8)	86.6 (0.9)	31	2.0
	76*	28.0 (0.5)	78.5 (1.8)	11	3.6
	97*	12.8 (0.1)	95.0 (0.9)	11	3.4

† Values in parentheses are the standard deviations of the estimated regression coefficients

\* Results from multiple bar study discussed in 3.4

Table 3.4 Results of regression analysis of amplitude versus horizontal offset for E-C meter

Bar (mm)	Cover,mm	$A_0'$ †	$\delta$ , mm†	n	RSD
#4 (12) Spot Probe	16	628 (17.6)	17.7 (0.7)	6	19.5
	35	72 (0.7)	29.5 (0.4)	5	0.9
	54	15 (0.8)	37.7 (2.9)	6	1.4
Depth Probe	16	3043 (86)	34.0 (0.5)	10	17.7
	35	826 (7.5)	42.6 (0.5)	14	11.3
	54	256 (4.3)	52.9 (1.1)	12	7.1
	72	104 (1.4)	62.9 (1.1)	11	2.4
	91	44 (1.1)	72.5 (2.0)	11	1.8
	109	22 (0.9)	88.4 (5.6)	10	1.7
#6 (19) Spot Probe	21	428 (7.8)	23.2 (0.6)	8	9.4
	40	62 (1.0)	33.4 (0.7)	7	1.3
	59	14 (0.7)	44.2 (3.3)	6	1.0
	19*	512 (8.0)	22.2 (0.3)	12	10.9
	20*	496 (5.8)	22.9 (0.3)	13	8.1
	39*	69 (1.1)	31.9 (0.6)	14	1.8
	56*	20 (0.7)	38.4 (1.6)	11	1.1
Depth Probe	59	284 (3.4)	56.7 (0.8)	15	5.7
	75	125 (2.0)	64.1 (1.2)	16	3.6
	94	56 (0.9)	76.1 (1.4)	16	1.6
	113	26 (1.1)	90.5 (4.4)	15	2.1
	131	16 (0.6)	93.1 (5.1)	12	1.3
	39*	897 (7.5)	46.2 (0.4)	29	2.3
	56*	353 (2.8)	54.0 (0.5)	29	6.0
	77*	129 (1.3)	64.9 (0.8)	25	3.1
#11 (36) Spot Probe	21	656 (12.5)	25.9 (0.6)	9	14.7
	39	108 (2.8)	38.2 (1.3)	9	4.1
	52	45 (1.2)	40.0 (1.3)	8	1.8
	68	16 (0.5)	55.7 (2.2)	9	0.8
	19*	830 (11.3)	26.7 (0.4)	20	17.4
	38*	127 (4.4)	38.0 (1.5)	10	5.6
Depth Probe	21	3869 (131)	49.9 (0.7)	12	28.9
	39	1537 (16.8)	49.9 (0.7)	16	27.0
	87	761 (10.8)	55.8 (1.0)	16	18.1
	68	355 (3.9)	67.3 (0.9)	16	7.1
	87	158 (2.1)	75.6 (1.2)	16	3.9
	105	77 (1.0)	87.4 (1.4)	16	2.0
	124	42 (0.7)	96.1 (1.9)	16	1.4
	38*	1717 (28)	50.3 (1.0)	11	41.3
	97*	105 (1.5)	82.0 (1.4)	13	2.8

† Values in parentheses are the standard deviations of the estimated regression coefficients

\* Results from multiple bar study discussed in 3.4

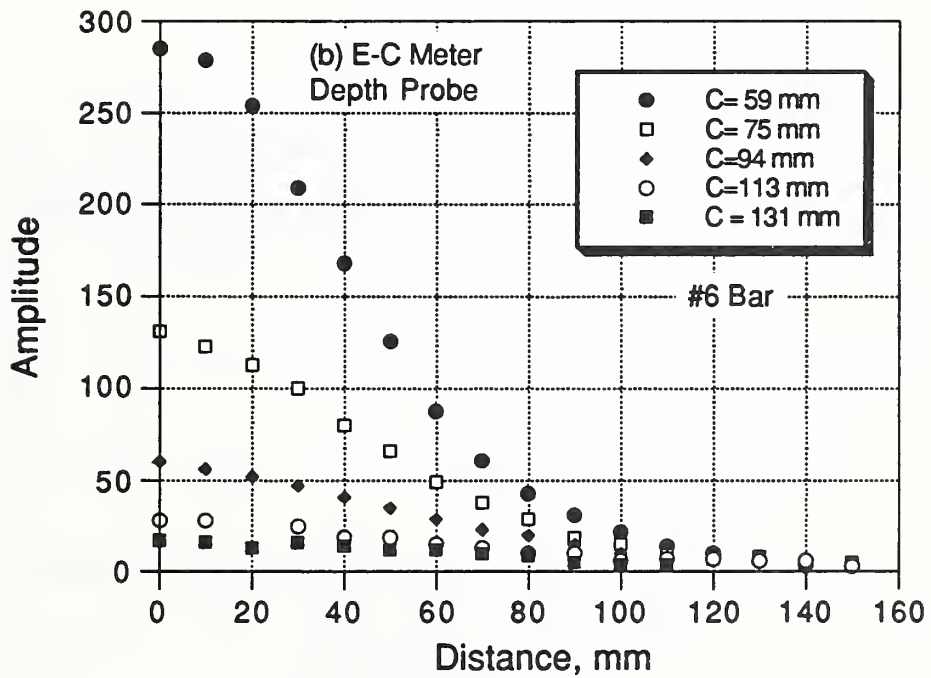
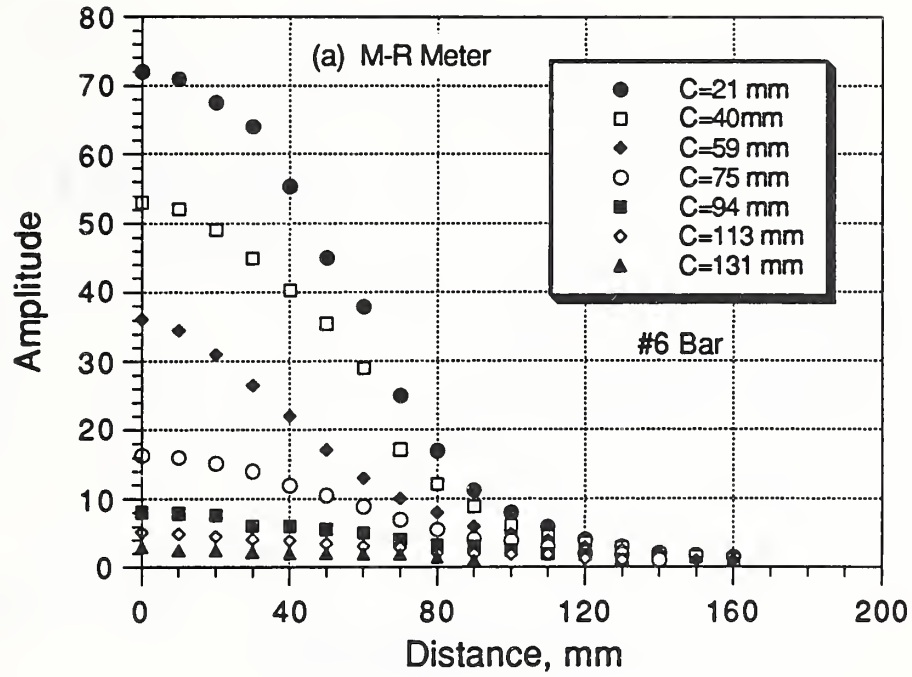


Figure 3.11 Amplitude versus horizontal offset for #6 (19 mm) bar: (a) M-R meter and (b) E-C meter.

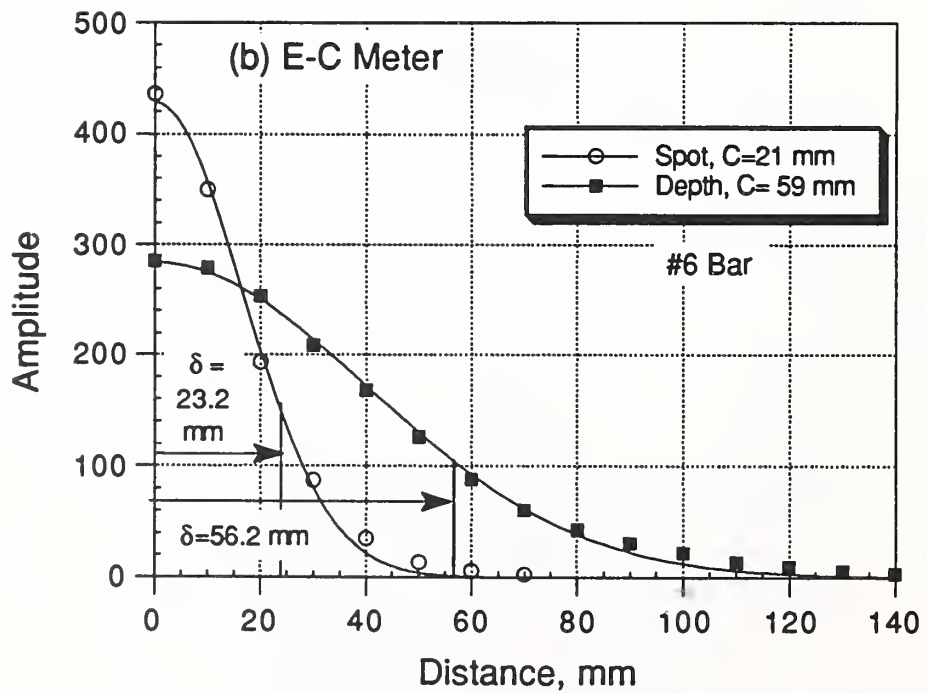
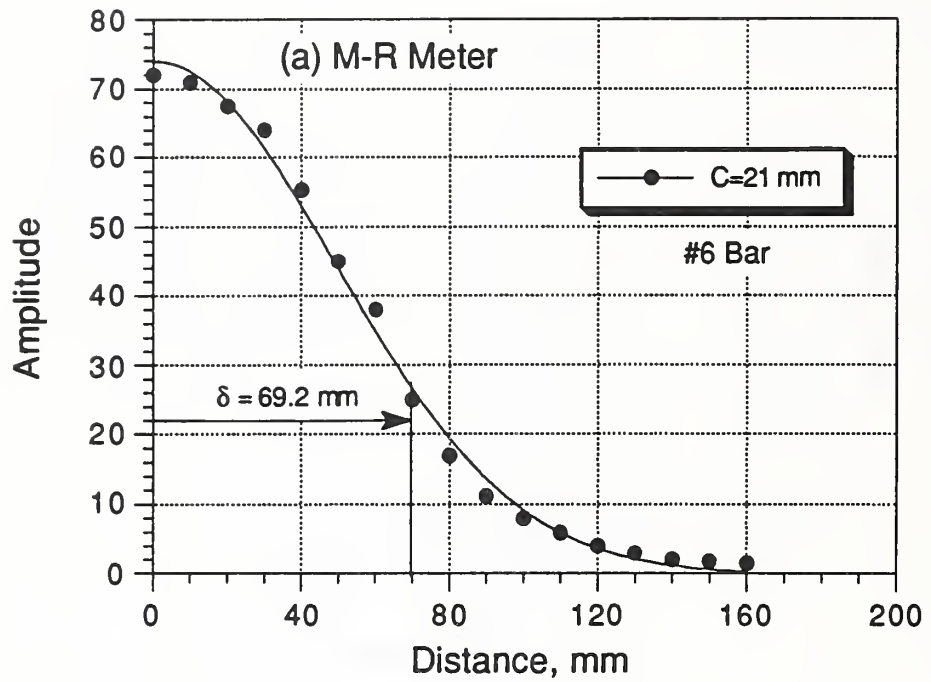


Figure 3.12 Amplitude versus horizontal offset showing fit of quadratic exponential function.



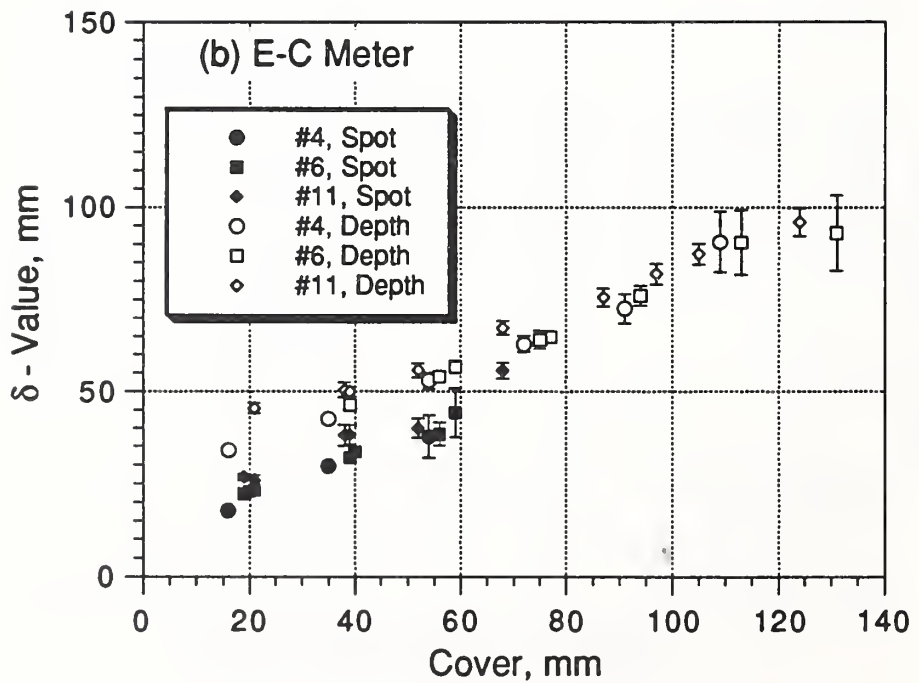
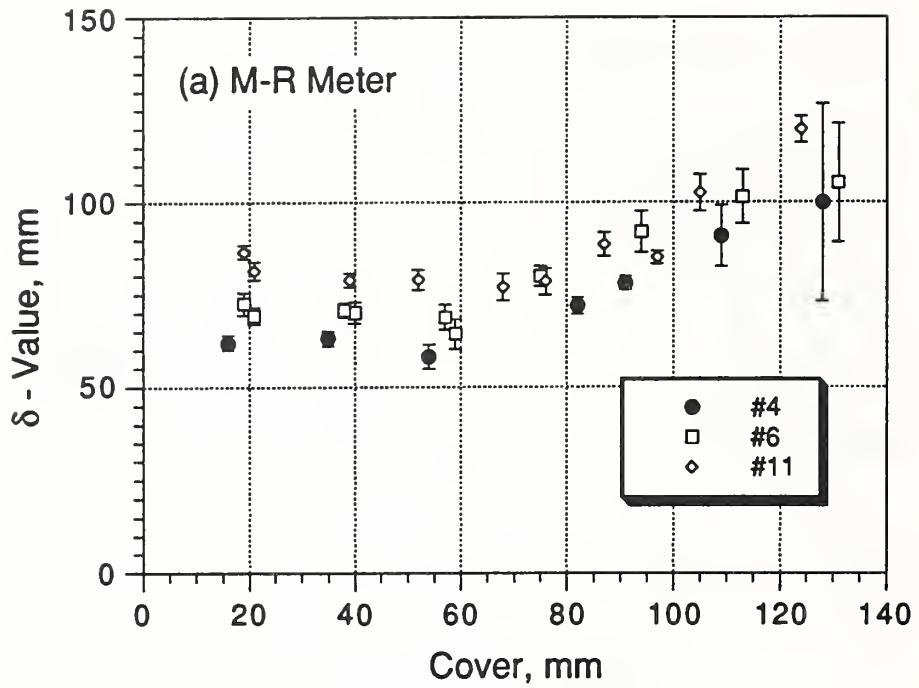


Figure 3.14 Value of  $\delta$  obtained by fitting Eq. (3.4) as a function of the cover: (a) M-R meter and (b) E-C meter.

### 3.4 Multiple bars

The study of amplitude versus horizontal offset revealed that amplitude varied in a well-defined manner with the offset, and that parameter  $\delta$  could be used as an indicator of the size of the influence zone for a single bar. It was postulated that a multiple of  $\delta$ , such as  $1.75 \delta$ , could also be used to estimate the minimum spacing between reinforcing bars for which interference effects would be negligible. For bar spacing greater than this minimum values, one should be able to accurately measure cover using the single-bar calibration relationships.

The next series of tests investigated the performance of the two meters in the presence of multiple bars. The experimental set up is shown in Fig. 3.15(a). Five bars were placed on the plain concrete slab with an equal center-to-center spacing of  $S$ . Plywood spacers were used to vary the cover over the bars, and a piece of plywood laid on the spacers provided the scanning surface. Scans were begun at a distance of  $2S$  from the first bar and measurements were taken at 10-mm intervals. In addition, for each depth of cover, scans were carried out using single bars to establish the single-bar response that would serve as the basis of comparison. Even though the single-bar response had been studied previously, these tests were repeated to assure that the single- and multiple-bar tests were carried out with the same cover and under other comparable conditions. The resulting best-fit parameters when Eq. (3.4) was fitted to the results of the single-bar scans were summarized in Tables 3.3 and 3.4. To reduce the amount of testing, two bars sizes were used: #6 and #11. Cover depths varied between 19 and 97 mm, and the center-to-center spacing varied from 25 to 240 mm.

Prior to performing the experiments, a simple model was used to predict the response based on the amplitude versus horizontal offset response of a single bar. This analysis is discussed first and then the experimental results are compared with the analytic predictions.

#### 3.4.1 *Theoretical analysis*

In the previous section it was shown that variation of meter amplitude with horizontal offset could be described by a quadratic exponential equation, Eq. (3.4). As a first approximation, it was assumed that response for multiple bars could be predicted by summing the contributions from each bar within the zone of influence of the search head. The contribution from each bar was based on the values of  $A'_0$  and  $\delta$  obtained from a single-bar test. Thus the influence zone of the search was assumed to be independent of the bar spacing.

The model that was analyzed is shown in Fig. 3.15(b), and it conforms with the experimental setup shown in Fig. 3.15(a). The single bar response, Eq. (3.4), was normalized by dividing by  $A'_0$  so that the maximum amplitude equals 1 when the search head is directly above the bar (i.e.,  $X_0 = 0$ ):

$$A_r = e^{-\left(\frac{X_0}{\delta}\right)^2} \quad (3.5)$$

where  $A_r$  = relative amplitude,  
 $X_0$  = horizontal offset from the center line of the bar.

The amplitude of the multiple-bar response was calculated as a function of  $X$ , where  $X$  is taken as 0 at a distance  $2S$  before the first bar (Fig. 3.15(b)). By superposition, the amplitude at  $X$  would be as follows:

where  $X$  = the distance from the origin shown in Fig. 3.15(b),  
 $S$  = center-to-center spacing between bars, and

$$A_r(X) = \sum_{i=1}^5 e^{-\left(\frac{X-S(i+1)}{\delta}\right)^2} \quad (3.6)$$

$i$  = an index corresponding to each of the five bars.

Fig. 3.15(c) shows an example of how the summation model works. The locations of the bars are indicated by the black circles. Above each bar is a bell-shaped curve that represents the amplitude versus horizontal offset relationship for a single bar. The thick curve represents the sum of the contributions from the individual bars and is obtained by using Eq. (3.6). For a given bar spacing  $S$ , the value of  $\delta$  determines the extent of overlap of the bell-shaped curves and, hence, the overall shape of the summation curve.

Equation (3.6) can be rewritten by dividing the top and bottom terms in the exponent by the spacing  $S$ , so that it becomes:

$$A_r(X/S) = \sum_{i=1}^5 e^{-\left[\left(\frac{X}{S} - (i+1)\right) \frac{S}{\delta}\right]^2} \quad (3.7)$$

Thus the relative amplitude can be computed as a function of  $X/S$ , for different values of  $S/\delta$ . Examples of the resulting calculations are shown in Fig. 3.16. In these examples,  $S/\delta$  values of 2.5, 2.0, 1.5 and 1.0 were used. For each case, the individual single-bar responses are shown with thin lines and the summation is shown as the thick line. Two noticeable changes occur to the computed multiple-bar response as the  $S/\delta$ -value decreases from 2.5 to 1.0:

- (1) the differences between the amplitudes of peaks and the valleys decrease, and
- (2) the maximum amplitude increases above a value of 1.0.

The presence of the peaks and valleys allows one to identify the location of individual bars when multiple bars are present, and the maximum amplitude would be used to infer the cover using the single-bar, amplitude versus cover relationship. Because the maximum amplitude increases as  $S/\delta$  decreases, the measured cover (based on the single-bar response) would be underestimated. This is because the increase in amplitude would be interpreted incorrectly as shallower cover. Also, for very low values of  $S/\delta$ , it would be difficult to identify the individual bars because of the lack of peaks and valleys in the response.

Next, we examine how the maximum amplitude and differences between the peaks and valleys is affected by  $S/\delta$ . The effects of  $S/\delta$  can be summarized by computing the amplitude when the search head is directly above the middle bar (No. 3 in Fig. 3.15(b)) and when it is halfway between the middle bar and either of the adjacent bars. Let the maximum amplitude above the middle bar be called  $A_3$  and let the amplitude of the valley adjacent to the middle bar be called  $A_{2,3}$  (see Fig. 3.15(c)). For the five-bar model, these amplitudes have the following values:

$$\begin{aligned} A_3 &= 1 + 2e^{-\left(\frac{S}{\delta}\right)^2} + 2e^{-\left(\frac{2S}{\delta}\right)^2} \\ A_{2,3} &= 2e^{-\left(\frac{0.5S}{\delta}\right)^2} + 2e^{-\left(\frac{1.5S}{\delta}\right)^2} + e^{-\left(\frac{2.5S}{\delta}\right)^2} \end{aligned} \quad (3.8)$$

Figure 3.17(a) shows the values of  $A_3$  and  $A_{2,3}$  as  $S/\delta$  varies between 1.0 and 4.0. Figure 3.17(b) shows the effect of  $S/\delta$  on the difference between  $A_3$  and  $A_{2,3}$ . The interpretation of Fig. 3.17 is as

follows: When  $A_3$  is greater than 1.0 (Fig. 3.17(a)), the cover would be under-estimated based on the single-bar calibration. When the difference between  $A_3$  and  $A_{2,3}$  equals zero (Fig. 3.17(b)), there would be no peaks and valleys in the response and individual bars could not be discerned. Based on these results, it could be concluded that individual bars could be detected if  $S/\delta$  were greater than 1.0 and that the cover could be measured correctly if  $S/\delta$  were greater than about 2.0. The theoretical results based on this simple model were used to plan the subsequent experiments and were compared with the experimental results.

### 3.4.2 Experimental results

The objective of the tests was to determine the critical center-to-center spacings at which (1) the maximum meter reading began to exceed the value obtained from the single-bar calibration test, and (2) it was no longer possible to determine the locations of the individual bars. The various combinations of cover and bar spacing that were used are summarized in Table 3.5. For the tests with #6 bars, readings were taken at 10 or 20 mm intervals, beginning at a distance from the first bar equal to twice the spacing (see Fig. 3.15 (a)). For the #11 bars, readings were taken only directly over each bar and halfway between adjacent bars. In addition, a scan over a single bar was performed to establish the single-bar response for that particular value of cover. The single bar results were analyzed using Eq. (3.4) to obtain the values of the parameters  $A'_0$  and  $\delta$ . These values were presented in Tables 3.3 and 3.4 and, for completeness, are listed again in Tables 3.6 and 3.7.

**#6 (19-mm) Bars** — The results of the scans over the #6-bars were compared with the theoretical responses obtained by using the summation model, Eq. (3.6) with the appropriate values of  $A'_0$  and  $\delta$ . Examples of the results for a cover of 38 mm are shown in Figs. 3.18, 3.19 and 3.20. The data are shown as points and the theoretical responses are shown as solid lines.

First, consider the measurements with the M-R meter shown in Fig. 3.18. For a spacing,  $S$ , of 75 mm, which corresponds to an  $S/\delta$  value of 1.06, the data show that the individual bars can barely be detected, as indicated by the presence of the minor peaks and valleys. In addition, the maximum meter reading is only slightly greater than the single-bar amplitude, which is shown as a thick horizontal line at an amplitude of 62. The predicted response using the summation model does not match the data very well. For a spacing of 100 mm ( $S/\delta = 1.44$ ), the individual bars are easily identified and the measured maximum amplitude is only slightly larger than the single bar amplitude. For the theoretical response, the amplitude is higher than the data and the individual bars are barely visible. For spacings of 160 mm ( $S/\delta=2.26$ ) and 200 mm ( $S/\delta=2.82$ ), the agreement between the data and the predictions is excellent. From these results it can be concluded that, for small values of  $S/\delta$ , the assumptions of the model are not adequate to predict the response. A possible explanation for these discrepancies is presented later in this section.

Figure 3.19 shows representative results for the E-C meter with the spot probe. For a spacing of 30 mm ( $S/\delta=0.94$ ), the location of the individual bars cannot be identified in the measured response, which is in agreement with the predicted response. However, the predicted response is greater than that measured. For the 60-mm spacing ( $S/\delta=1.88$ ), there is good agreement between data and the predicted responses. For a spacing of 80 mm ( $S/\delta=2.51$ ), the comparison between data and predictions is erratic. The predicted differences between the peaks and valleys agree with the measurements, but the values of the peak amplitudes are not in good agreement. This could have been caused by experimental inaccuracies in controlling the actual cover or positioning of the bars. For the spacing of 100 mm ( $S/\delta=3.14$ ), there is very good agreement between data and predictions.

Finally, Fig. 3.20 shows the responses for the E-C meter with the depth probe. For the 50-mm spacing ( $S/\delta=1.08$ ), the individual bars cannot be discerned, and the predicted response is greater

than the measured response. At a spacing of 70-mm ( $S/\delta=1.52$ ), the bar locations are clearly identifiable, and the predictions are in close agreement with the measurements. For spacings of 100 mm ( $S/\delta=2.17$ ) and 140 mm ( $S/\delta=3.03$ ), the predictions agree with the measurements.

From comparisons, such as those shown in Figs. 3.18 to 3.20, between the measured and predicted responses, the following patterns of behavior were noted:

- For smaller values of  $S/\delta$ , the amplitudes of the predicted response exceeded the measured amplitudes.
- For smaller values  $S/\delta$ , the predicted differences between the amplitudes of the peaks and valleys were less than the measured differences.
- Generally, the simple summation model was accurate for  $S/\delta$  values above 2.

These differences between the predicted and measured responses can be summarized in the form of two graphs. One is the normalized amplitude, i.e., the maximum amplitude,  $A_{max}$  divided by  $A'_0$ , plotted as function of  $S/\delta$ . The other is a plot of the quantity  $\alpha$  versus  $S/\delta$ , where  $\alpha$  is defined as

$$\alpha = \frac{A_{max} - A_{min}}{A'_0} \quad (3.9)$$

where  $A_{max}$  = the maximum amplitude recorded with the search head directly above the middle bar (analogous to  $A_3$  in the predicted response shown in Fig. 3.15(c)),  
 $A_{min}$  = the amplitude recorded with the search head midway between the middle bar and the adjacent bar (analogous to  $A_{2.3}$  in the predicted response shown in Fig. 3.15(c)), and  
 $A'_0$  = the maximum amplitude for the single bar response based on fitting Eq. 3.4.

Values of  $A_{max}$  and  $\alpha$  obtained from the measured data are listed in Tables 3.6 and 3.7. The parameter  $\alpha$  is analogous to the difference between  $A_3$  and  $A_{2.3}$  in the predicted response that was shown in Fig. 3.17(b). Thus an  $\alpha$ -value of 0 means that individual bars cannot be discerned due to the absence of peaks and valleys in the measured response, and larger values of  $\alpha$  indicate that the bars are discernable.

Figures 3.21(a) and (b) show the normalized amplitudes as a function of  $S/\delta$  for the M-R and E-C meters, respectively. The solid line is the maximum normalized amplitude  $A_3$  calculated using Eq. (3.8), which was previously shown in Fig. 3.17(a). The following observations are noted:

- For the M-R meter and for cover less than 77 mm, the normalized amplitude does not increase as the value of  $S/\delta$  decreases below a value of 2. The exception was at a cover of 77 mm, for which the trend of the data agreed reasonably well with the prediction. Referring to Fig. 3.14, it is noted that a cover of 77 mm is in the region where the value of  $\delta$  starts to increase with cover.
- For the E-C meter with the spot probe, the normalized amplitude tended to increase with decreasing value of  $S/\delta$ , but the increase was less than predicted by the simple summation model.
- For the E-C meter with the depth probe, there was good agreement between the results and the predictions. The agreement tended to be better for the deeper cover.

To summarize, the significance of the results shown in Fig. 3.21 is as follows. A calibration relationship to measure the cover of a given size bar is obtained typically from tests using a single bar.

When multiple bars are present and as the bar spacing decreases, the amplitude of the meter reading increases above the single-bar value. Thus the cover, based on the single-bar calibration, will be underestimated. In a plot of normalized ( or relative) amplitude versus  $S/\delta$ , the critical value of  $S/\delta$  is that for which the normalized amplitude begins to exceed 1.0. For example, the results in Fig. 3.21(a) for the M-R meter show that for cover less than about 38 mm, the normalized amplitude for the #6-bar remains close to a value of 1 even when the  $S/\delta$ -value is as low as 1. Thus the cover would be correctly measured for a spacing as low as 60 mm ( $\delta \approx 60$  mm for  $C = 38$  mm; see Fig. 3.14(a)). For cover greater than 57 mm, the critical  $S/\delta$ -value is greater than about 1.5. On the other hand, for the E-C meter (Fig. 3.21(b)), the critical  $S/\delta$ -value seems to be equal to about 2.

Figures 3.22(a) and 3.22(b) show the variation of  $\alpha$  with the value of  $S/\delta$ . The solid curves are the prediction based on difference between  $A_3$  and  $A_{2,3}$  given in Eq. (3.8), which was previously shown in Fig. 3.17(b). When  $\alpha = 0$ , there are no peaks and valleys in the measured response as the search head is scanned over the bars, and it would not be possible to "see" the individual bars. The model predicts that  $S/\delta$  should be greater than about 1.1 in order for  $\alpha$  to be greater than zero and, therefore, be able to detect the individual bars. The results in Fig. 3.22(a) for the M-R meter show that for a cover of 19 mm, the individual #6 bars can be detected at an  $S/\delta$ -value as low as 0.5. For  $S/\delta$ -values less than 2, the measured  $\alpha$ -values are greater than the predicted ones, with the exception of the case with a cover of 57 mm, which are in agreement with the predictions. For the E-C meter, the results are in better agreement with the predictions, but for  $S/\delta$  less than about 2.5 the values of  $\alpha$  exceed the predictions. In summary, for  $S/\delta$  less than about 2 to 2.5 (depending on the meter), the values of  $\alpha$  based on the tests exceeded the predictions. This means, that for a given value of  $\delta^f$ , the actual minimum spacing at which individual bars can be seen is smaller than that predicted by the summation model.

**#11 (36-mm) Bars** — As was mentioned, for the multiple-bar tests with #11-bars, data were taken only directly over the bars and halfway between them. Thus only the values of the normalized amplitudes and  $\alpha$  are available. Figures 3.23(a) and (b) show the variation of the normalized amplitude as a function of  $S/\delta$ , for the M-R and E-C meters, respectively. Figure 3.23(a) shows that for the shallow cover, the response of the M-R meter was similar to that measured with the #6 bars, i.e., the normalized amplitude remained close to 1 for an  $S/\delta$ -values as low as 1. For covers of 76 and 96 mm, the measured response was near to the predictions. This behavior is further evidence that there is a change in the performance of the M-R meter when the  $\delta$ -value begins to increase with cover (Fig. 3.14(a)). Figure 3.23(b) shows the results with the E-C meter. For the spot probe, the predicted values exceeded those measured at the two low  $S/\delta$ -values. The result for  $S/\delta = 3.16$  and  $C = 38$  mm is unusual, since the measured maximum amplitude was lower than the single-bar result, i.e., the normalized maximum amplitude was less than 1.0. For the depth probe and 96-mm cover, the amplitudes were higher than predicted for  $S/\delta$ -values greater than 1.5.

The values of  $\alpha$  for the tests with #11-bars are shown in Figs. 3.24(a) and (b). For both types of meters, the measured responses were greater than those predicted for  $S/\delta$ -values less than 2.5.

### 3.4.3 Corrections to model

Figure 3.25(a) and (b) compare the normalized amplitudes and  $\alpha$ -values obtained from all the multiple-bar tests with the predictions based upon the simple summation model described in 3.4.1.

---

<sup>f</sup>To review, the value of  $\delta$  is obtained from measurements of amplitude versus horizontal offset obtained from a single-bar test, and it is an indicator of the size of the influence zone. Generally, the value of  $\delta$  depends on the cover.

In general, the model does not accurately estimate the response when  $S/\delta$  is less than about 2. The predictions are based on the assumption that the single-bar values of  $A'_0$  and  $\delta$  are not changed by the presence of multiple bars nor are they affected by the bar spacing. A constant value of  $\delta$  means that the zone of influence of the search head is not affected by the presence of multiple bars. However, the measured response shows that this may not be a correct assumption. Further analyses were carried out to investigate the effects of multiple bars on the *apparent* zone of influence of the search heads.

Referring to Fig. 3.25(b), it is seen that the model underestimates the value of  $\alpha$  for  $S/\delta$ -values between 1 and about 2.5. This implies that the actual value of  $\delta$  that should be used in the summation model to predict  $\alpha$  is smaller than the value of  $\delta$  obtained from the single-bar test. Thus a correction factor was applied to the single-bar value of  $\delta$ . For a given experimental value of  $\alpha$ , the theoretical relationship represented by the solid curve in Fig. 3.25(b) was used to obtain an *effective*  $\delta$ -value,  $\delta_e$ , that would result in a predicted value of  $\alpha$  equal to the experimental value. Using  $\delta_e$  in the summation model results in agreement between the predicted and experimental differences between the amplitudes of the peaks and valleys. To obtain agreement between the predicted and measured amplitudes over the middle bar, a correction factor,  $\beta$ , for  $A'_0$  was determined. The resulting values of  $\delta_e$ , expressed as a fraction of  $\delta$ , and the values of  $\beta$  are listed in the last two columns of Tables 3.6 and 3.7.

Figures 3.26, 3.27 and 3.28 show examples of the predictions obtained by using these correction factors into the summation model. These figures should be compared with their counterparts in Figs. 3.18, 3.19, and 3.20. The comparison shows that the new predictions correctly describe the variation of the meter reading as the search head is scanned across the bars. Note in Figs. 3.26 to 3.28 that the agreement is poor when the search head is approaching the first bar or passing beyond the last bar. It seems that at these positions the single-bar values of  $\delta$  are applicable, as shown by the good agreement for these bars in Figs. 3.18, 3.19 and 3.20.

The next set of figures show how the values of  $\delta_e/\delta$  and  $\beta$  vary among the tests. Figure 3.29 shows the results for the two meters with #6 bars and Figure 3.30 shows the results with the #11 bars. Figure 3.31 groups all the results according to bar size. Examination of these figures shows that there is a consistent pattern to the variation of  $\delta_e/\delta$  with  $S/\delta$ , which is interpreted as follows: As the value of  $S/\delta$  decreases below about 2.5, the value of  $\delta_e/\delta$  decreases. Thus the meters behave as though the zones of influence of the search heads were smaller in the presence of multiple bars than for single bars. It is inferred that the electromagnetic field of the search head becomes more *focused* with decreasing distance between bars. Examination of the  $\beta$ -values<sup>8</sup> shows that there is no consistent variation with  $S/\delta$ . Thus other factors than those considered in the summation model are likely to be influencing the responses of the meters.

#### 3.4.4 Summary

The objective of the tests reported in this section was to investigate the performance of the covermeters when scanning over multiple parallel bars located in a plane parallel to the scan surface. Specifically, the intent was to determine the spacing below which individual bars could not be discerned and the spacing below which the measured cover would be significantly in error. A simple model was proposed to predict the response based on the single-bar measurements of amplitude

---

<sup>8</sup>To review, the value of  $\beta$  is the multiplying factor for the single-bar amplitude  $A'_0$  for agreement between the measured and predicted amplitudes over the middle bar using the summation model with the value of  $\delta_e$  that correctly predicts the range between the peaks and valleys.

versus horizontal offset (discussed in section 3.3). The model was used to predict two values: (1) the peak amplitude over the middle bar of the 5-bar layout and (2) the difference between the peak amplitude and the amplitude when the search head was located midway between the middle bar and an adjacent bar. These values were calculated as a function of  $S/\delta$ , where  $S$  is the center-to-center spacing and  $\delta$  is the parameter which describes how the amplitude decreases with horizontal offset of the search head in a single-bar test. The interfering effects of adjacent bars on the response of the covermeter are reduced as  $S/\delta$  increases.

Based on the calculated responses, it was theorized that individual bars could not be discerned for  $S/\delta$ -values less than about 1, and the measured cover would be in error for  $S/\delta$ -values less than 2. Tests were performed with #6 and #11 bars to compare with the predictions. In some cases, test results agreed with the predictions but in other cases they did not (see Figs. 3.18 to 3.20).

The following summarizes the performance of the M-R meter:

- The presence of individual bars could be discerned at values of  $S/\delta$  less than 1, especially for thinner cover and the larger bar size (Figs. 3.22(a) and 3.24(a)).
- The critical value of  $S/\delta$  above which the cover could be measured accurately using the single-bar calibration depends on the cover (Fig. 3.21(a) and Fig. 3.23(a)). For thin cover (19 and 38 mm), the critical value was about 1; for thicker cover ( $> 77$  mm), the critical value was about 2.

The performance of the E-C meter was in better agreement with the predictions than the M-R meter. In general, individual bars could be discerned when  $S/\delta$  exceeds 1 (Fig. 3.22(b) and 3.24(b)) and the cover could be accurately measured when  $S/\delta$  is greater than 2 (Fig. 3.21(b) and Fig. 3.23(b)). An exception was the case of the depth probe with 96-mm of cover, for which error in the cover measurement would occur up to  $S/\delta$  of 3 (Fig. 3.23(b)).

To explain some of the discrepancies between the predictions and the measurements, the simple model was used to calculate the effective  $\delta$ -value,  $\delta_e$ , when multiple bars are present. It was found that  $\delta_e$  decreased as  $S/\delta$  decreased below 2.5, which leads to the inference that the zone of influence of the search head decreases as the bar spacing is reduced.

It is acknowledged that the summation model may be too simple to account for the apparently complex interactions that occur when multiple bars are present. Nevertheless, its prediction of a critical  $S/\delta$ -value of about 1 is a conservative approximation that can be used to estimate the bar spacing below which the covermeters would not be able to discern individual bars. The critical  $S/\delta$ -value at which cover can be accurately measured will, apparently, depend on the specific meter, but the value of 2 predicted by the model appears to be a reasonable conservative value for the two meters used in this study.

In conclusion, single-bar tests, in which the amplitude is measured as a function of the horizontal offset for different cover depth, provides vital information to predict the limitations of a particular covermeter in the presence of multiple parallel bars.

Table 3.5 Conditions for tests with multiple parallel bars

Bar Size	Meter	Cover, mm	Center Spacing, mm
#6 (19 mm)	M-R	19	40, 50, 75, 100, 160
		38	40, 50, 75, 100, 160, 200
		57	60, 80, 100, 160, 200
		77	80, 120, 160, 200
	E-C Spot Probe	20	25, 40, 60, 80
		39	30, 40, 60, 80, 100
	E-C Depth Probe	39	50, 70, 100, 140
		56	60, 80, 120, 160
		77	70, 90, 120, 160
	#11 (36 mm)	M-R	19
76			90, 110, 180, 220
97			100, 140, 200, 240
E-C Spot Probe		19	40, 50, 70
		38	50, 90, 120
E-C Depth Probe		38	50, 90, 150
		97	90, 140, 200, 240

Table 3.6 Results of tests and analysis with multiple #6 (19 mm) bars using M-R meter

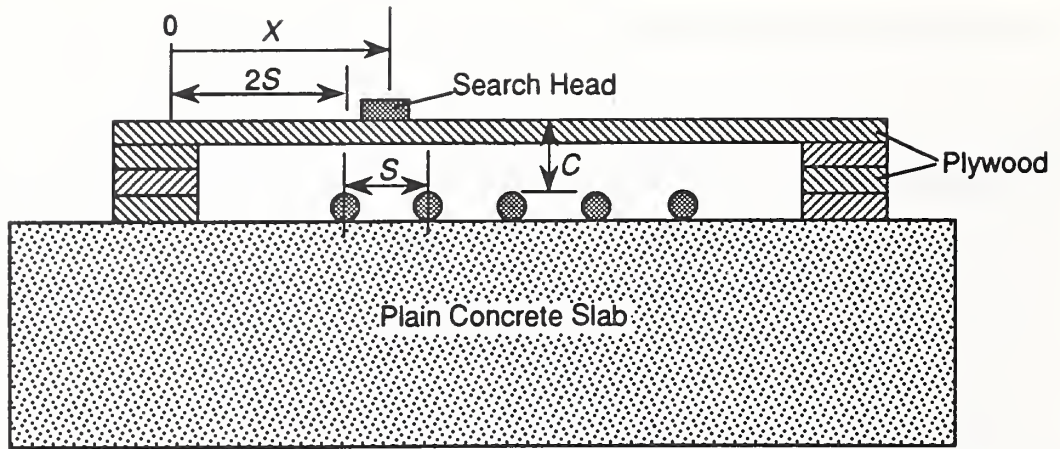
Cover, mm	$A'_0$	$\delta$ , mm	Spacing, $S$ , mm	$S/\delta$	$A_{max}$	$\alpha$	$\delta_c/\delta$	$\beta$
19	79.0	72.5	40	0.55	82.7	0.02	0.41	0.79
			50	0.69	79.5	0.03	0.49	0.78
			75	1.03	77	0.09	0.65	0.84
			100	1.38	76	0.15	0.80	0.87
			160	2.21	75	0.45	0.98	0.94
38	62.0	70.8	40	0.56	67	0	0.48	0.71
			50	0.71	66	0	0.61	0.70
			75	1.06	63.8	0.03	0.76	0.80
			100	1.41	62.5	0.18	0.80	0.93
			160	2.26	60.5	0.47	0.99	0.97
			200	2.82	60.5	0.68	1.05	0.97
57	39.9	68.8	60	0.87	48	0.01	0.70	0.85
			80	1.16	41.5	0.03	0.83	0.81
			100	1.45	41.5	0.06	0.97	0.86
			160	2.33	40	0.51	0.99	0.99
			200	2.91	41.7	0.73	1.03	1.02
77	21	82	80	0.98	31	0.02	0.72	1.10
			120	1.46	23	0.21	0.80	1.03
			160	1.95	20.5	0.42	0.89	0.96
			200	2.44	20.5	0.62	0.95	0.97

Table 3.6 (continued) Results of tests and analysis with multiple #6 (19 mm) bars using E-C meter

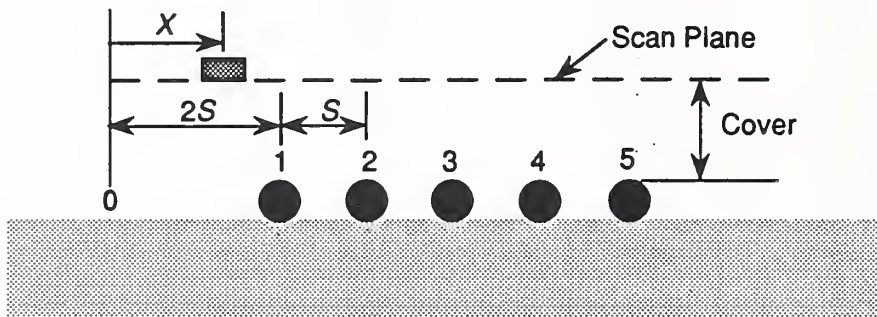
Cover, mm	$A'_0$	$\delta$ , mm	Spacing, $S$ , mm	$S/\delta$	$A_{max}$	$\alpha$	$\delta_c/\delta$	$\beta$
Spot Probe								
20	496	22.9	25	1.09	530	0.04	0.76	0.85
			40	1.75	480	0.28	0.89	0.93
			60	2.62	460	0.6	1.03	0.92
			80	3.49	460	0.78	1.16	0.93
39	69	31.9	30	0.94	88	0.02	0.71	0.95
			40	1.25	80	0.05	0.85	0.94
			60	1.88	70	0.27	0.96	0.97
			80	2.51	65	0.55	1.02	0.93
			100	3.13	67	0.75	1.08	0.97
Depth Probe								
39	897	46.2	50	1.08	1250	0.01	0.87	0.98
			70	1.52	1030	0.13	0.90	1.03
			100	2.16	920	0.46	0.95	1.01
			140	3.03	900	0.78	1.02	1.00
56	353	54.0	60	1.11	523	0.01	0.89	1.04
			80	1.48	424	0.12	0.89	1.07
			120	2.22	356	0.5	0.95	1.00
			160	2.96	350	0.76	1.02	0.99
77	129	64.9	70	1.08	192	0.02	0.81	1.11
			90	1.38	165	0.1	0.85	1.12
			120	1.85	140	0.3	0.92	1.05
			160	2.46	130	0.55	1.00	1.00

Table 3.7 Results of tests and analysis with multiple #11 (36 mm) bars

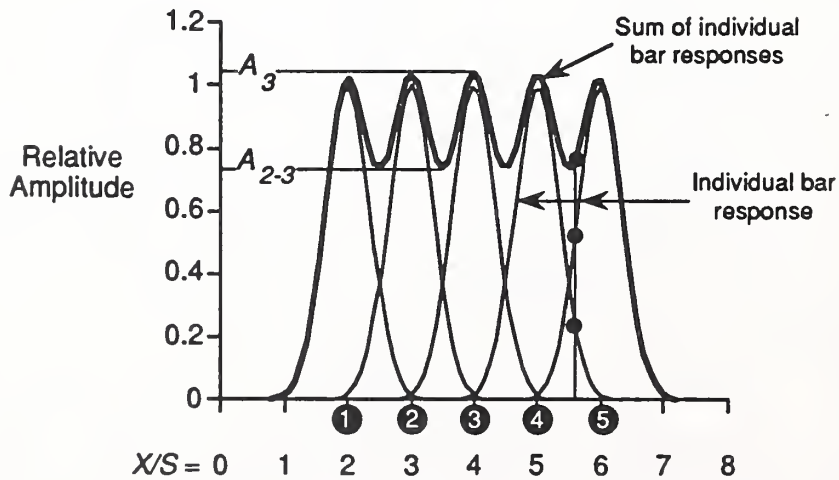
Cover, mm	$A'_o$	$\delta$ , mm	Spacing, S, mm	$S/\delta$	$A_{max}$	$\alpha$	$\delta_c/\delta$	$\beta$
R-meter								
19	81.3	86.6	90	1.04	81.0	0.13	0.61	0.89
			110	1.27	81.4	0.18	0.71	0.93
			180	2.08	80.7	0.49	0.89	0.98
			220	2.54	81.2	0.66	0.96	1.00
76	28.0	78.5	90	1.15	38.8	0.01	0.92	0.97
			110	1.40	36.7	0.1	0.86	1.14
			180	2.29	28.8	0.5	0.98	1.02
			220	2.80	29.8	0.67	1.05	1.06
97	12.8	95.0	100	1.05	20.6	0.03	0.76	1.25
			140	1.47	16.0	0.16	0.84	1.14
			200	2.11	15.0	0.44	0.94	1.16
			240	2.53	13.4	0.59	1.01	1.04
Spot Probe								
19	830	26.7	40	1.50	890	0.2	0.82	1.00
			50	1.87	825	0.37	0.88	0.97
			70	2.62	802	0.64	1.00	0.96
38	127	38.0	50	1.32	144	0.11	0.80	1.00
			90	2.37	127	0.56	0.97	1.00
			120	3.16	115	0.83	1.01	0.91
Depth Probe								
38	1717	50.3	50	0.99	over range	n.a.	n.a.	n.a
			90	1.79	1814	0.27	0.92	1.01
			140	2.78	1683	0.68	1.03	0.98
96	105	82.0	90	1.10	171	0.03	0.79	1.26
			140	1.71	127	0.28	0.87	1.16
			200	2.44	120	0.6	0.96	1.14
			240	2.93	111	0.75	1.02	1.06



(a) Test set up



(b) Bar layout used to compute theoretical response



(c) Example of theoretical response using summation model

Figure 3.15 Multiple bar study: (a) experimental set up; (b) configuration used for the summation model; and (c) example of multiple-bar response based on summation model.

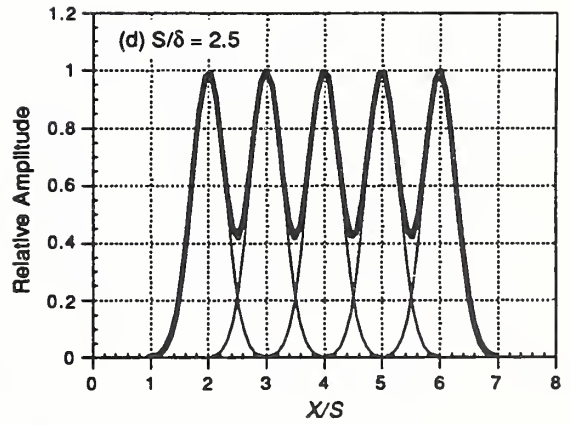
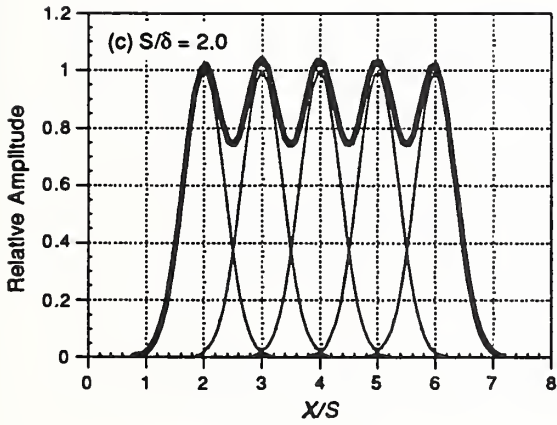
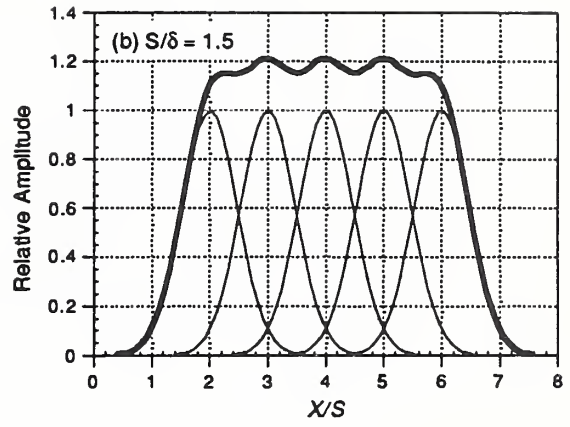
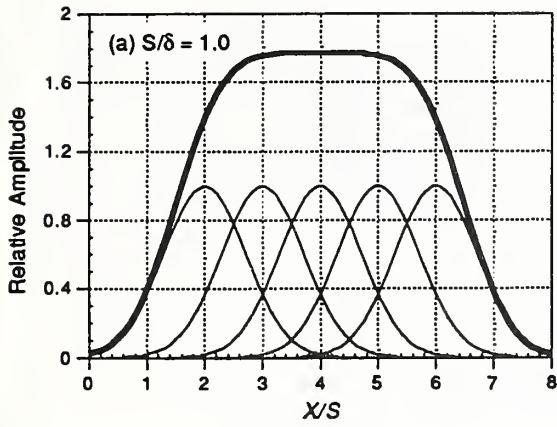


Figure 3.16 Computed multiple bar response, using summation model, as a function of the  $S/\delta$ -value (thin lines are single-bar responses, thick line is sum of single-bar responses).

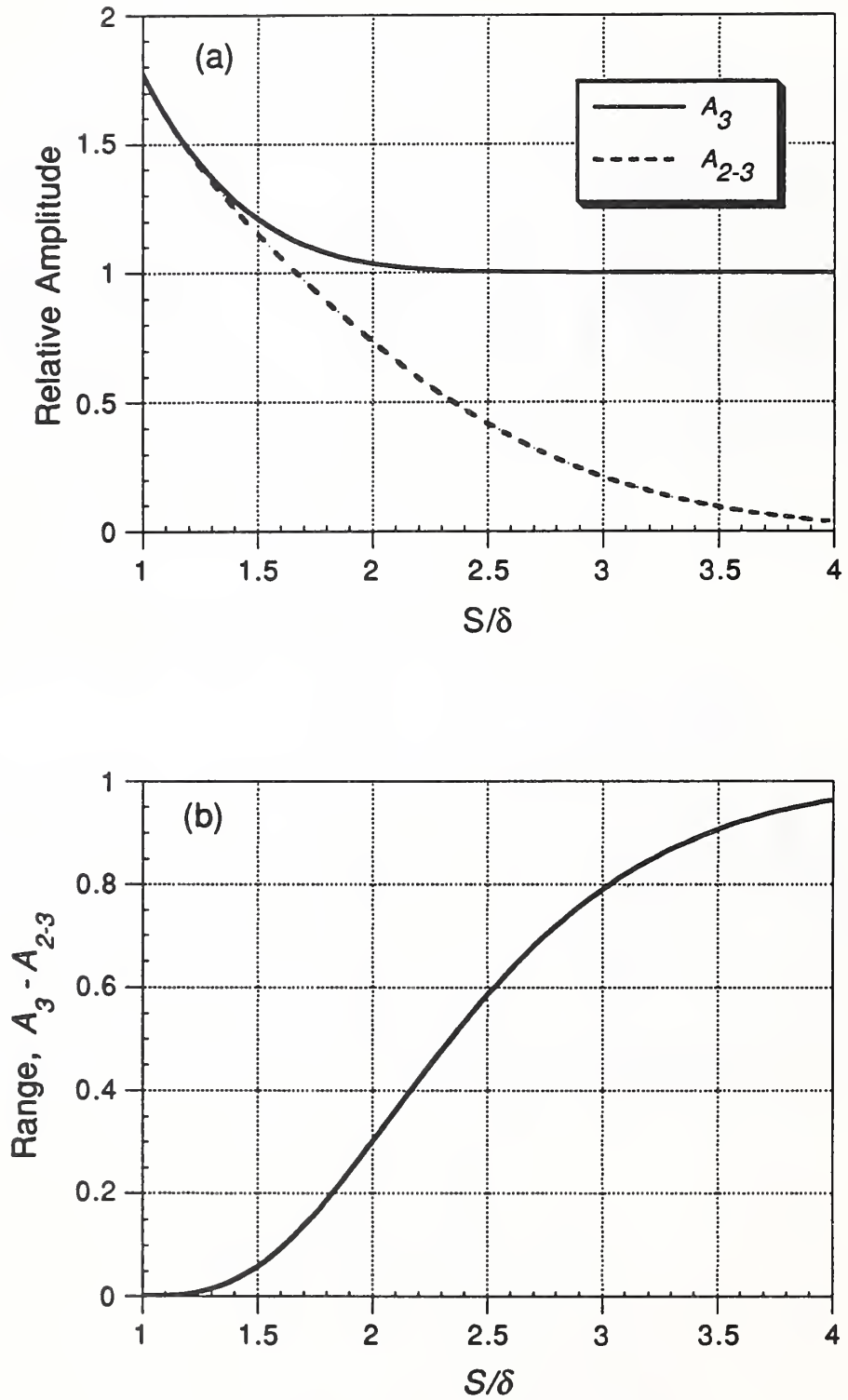


Figure 3.17 (a) Theoretical amplitude directly above middle bar ( $A_3$ ) and midway between the middle and adjacent bar ( $A_{2-3}$ ) as function of  $S/\delta$ ; (b) difference between  $A_3$  and  $A_{2-3}$  (see Fig. 3.15 for meaning of  $A_3$  and  $A_{2-3}$ ).

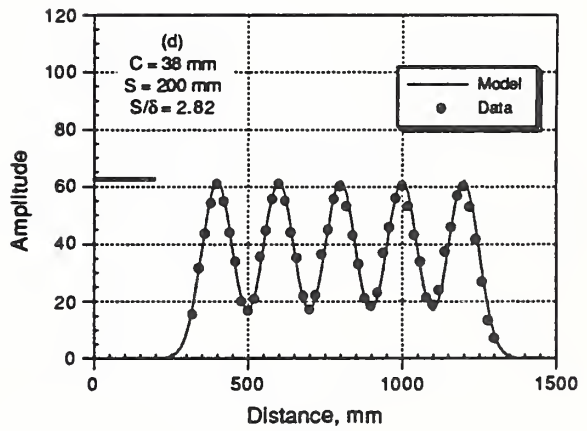
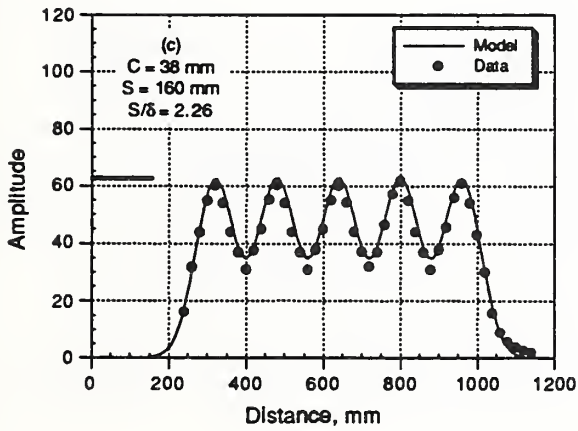
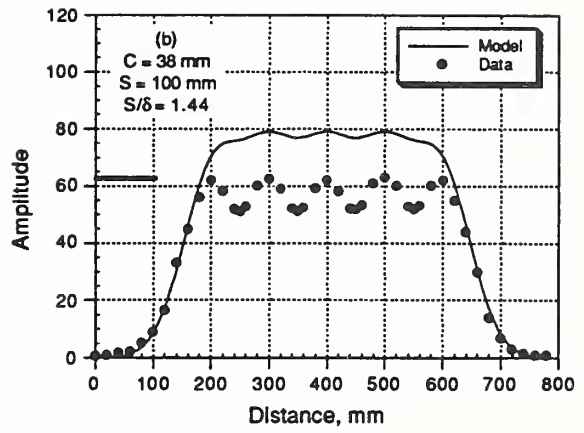
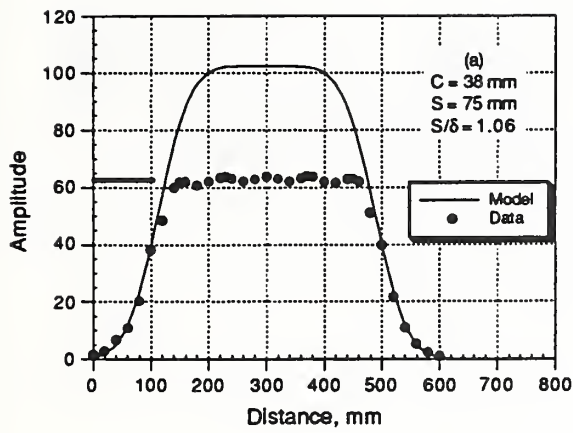


Figure 3.18 Comparison of measured and computed amplitude for scan across the five, #6 (19 mm) bars using the M-R meter, 38 mm cover and different center-to-center spacing.

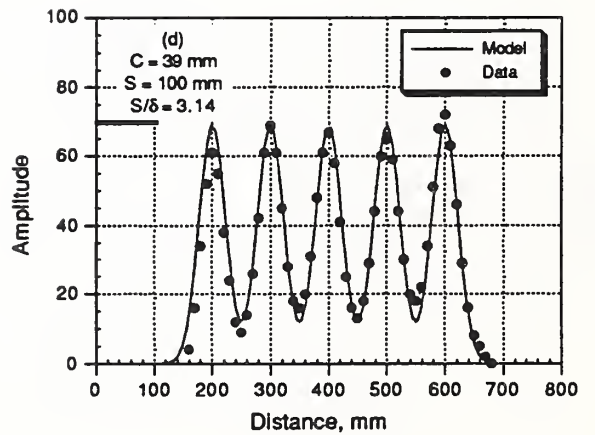
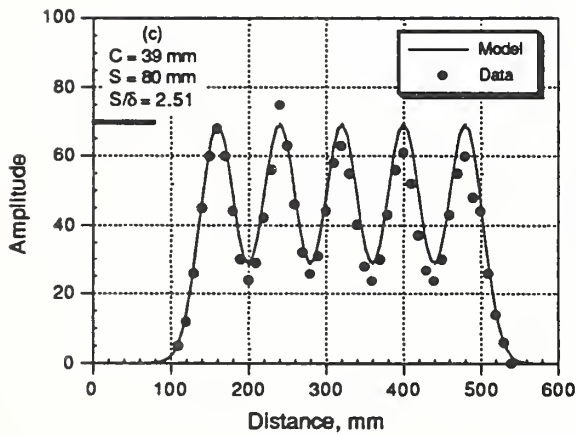
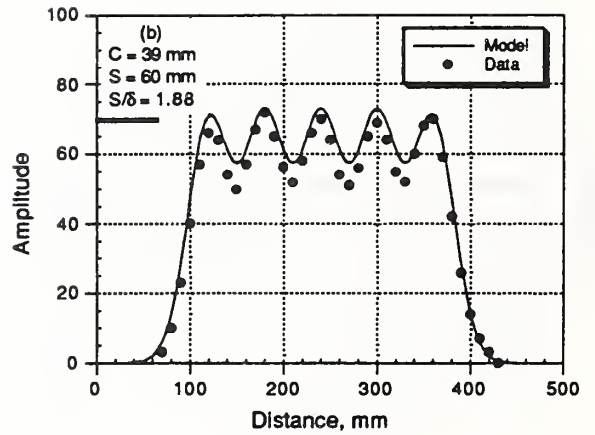
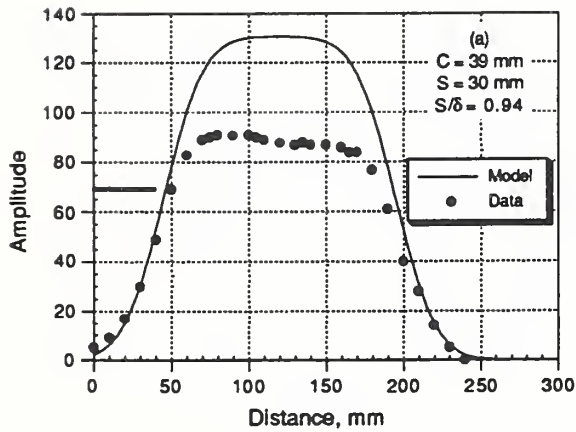


Figure 3.19 Comparison of measured and computed amplitude for scan across the five, #6 (19 mm) bars using the E-C meter with spot probe, 39 mm cover and different center-to-center spacing.

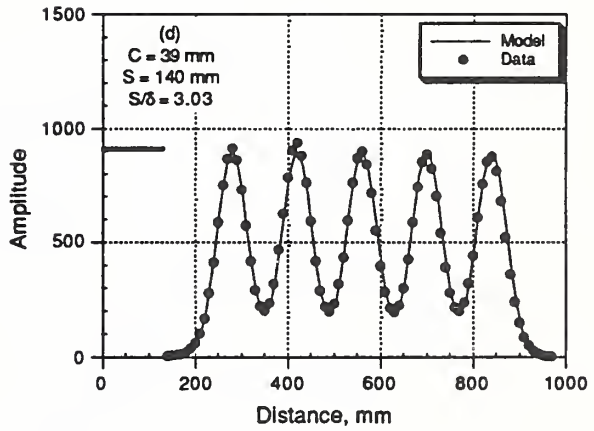
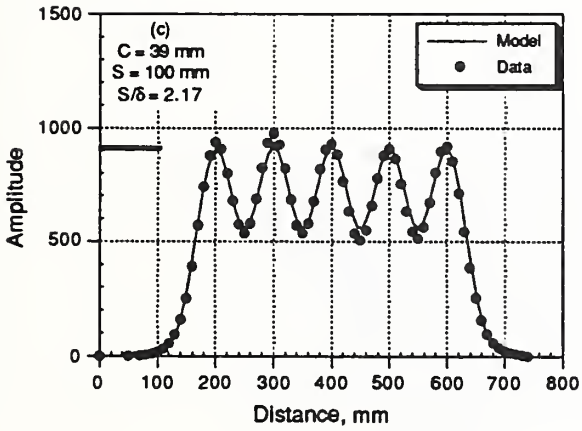
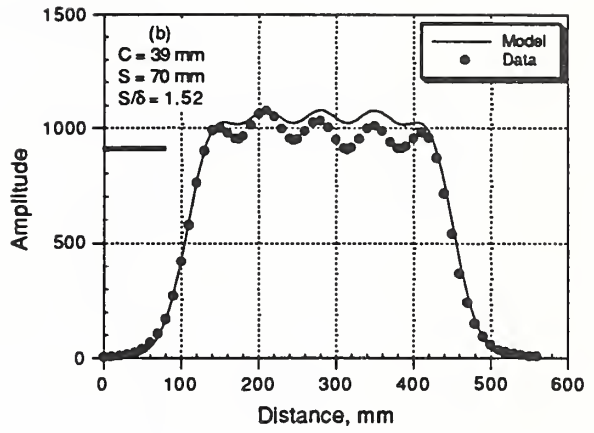
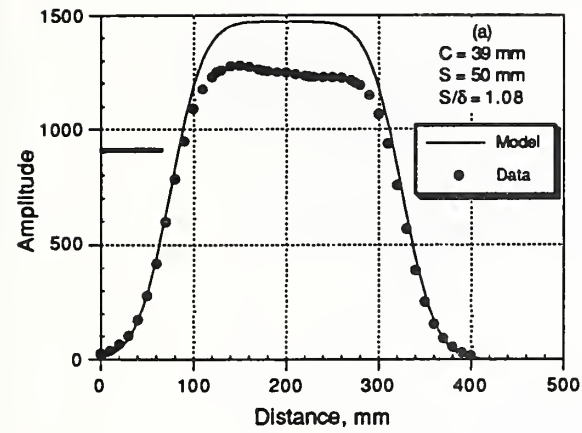


Figure 3.20 Comparison of measured and computed amplitude for scan across the five, #6 (19 mm) bars using the E-C meter with depth probe, 39 mm cover and different center-to-center spacing.

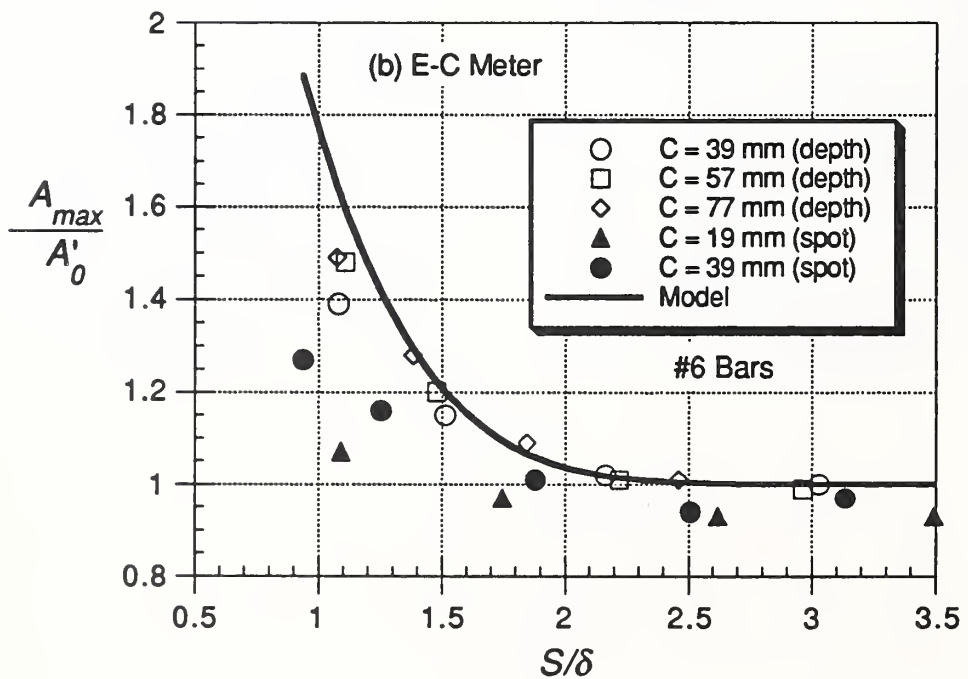
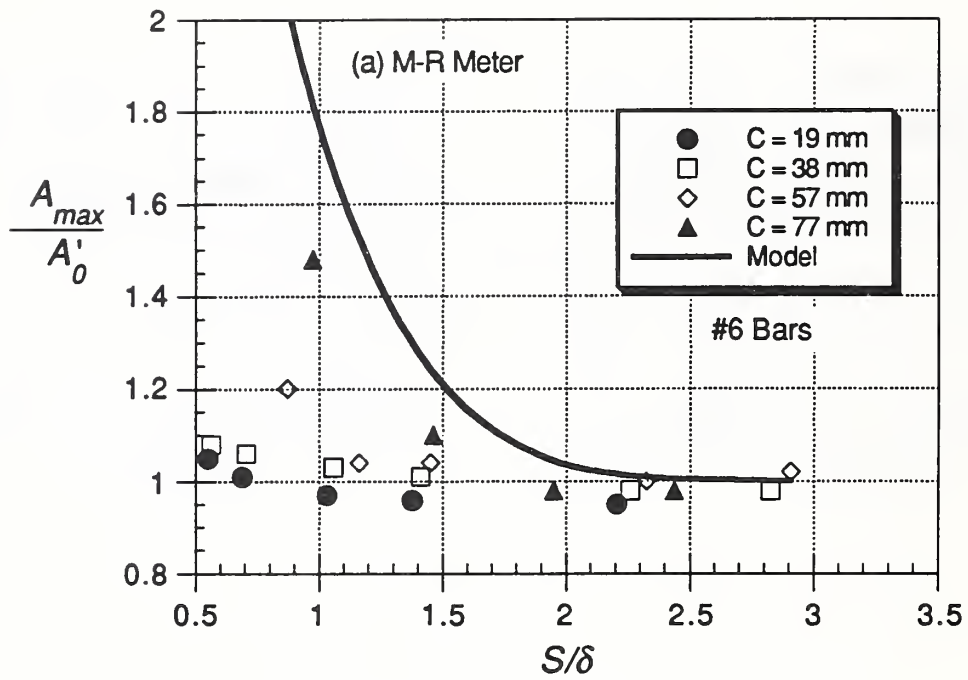


Figure 3.21 Ratio of measured maximum amplitude over middle bar to single-bar amplitude for #6 (19 mm) bars: (a) M-R meter and (b) E-C meter.

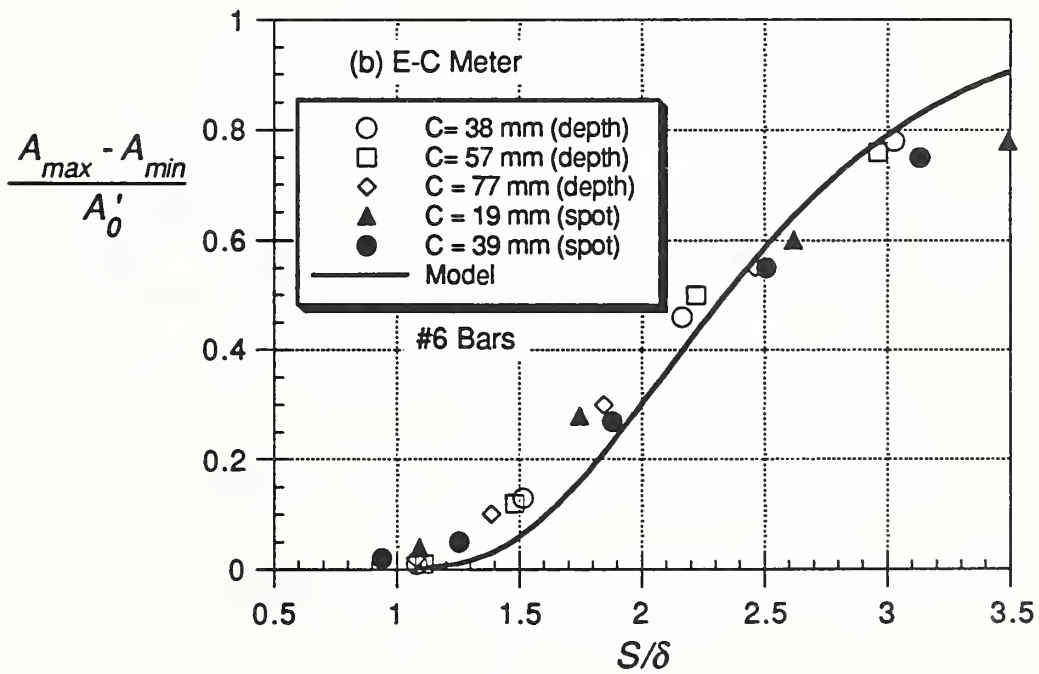
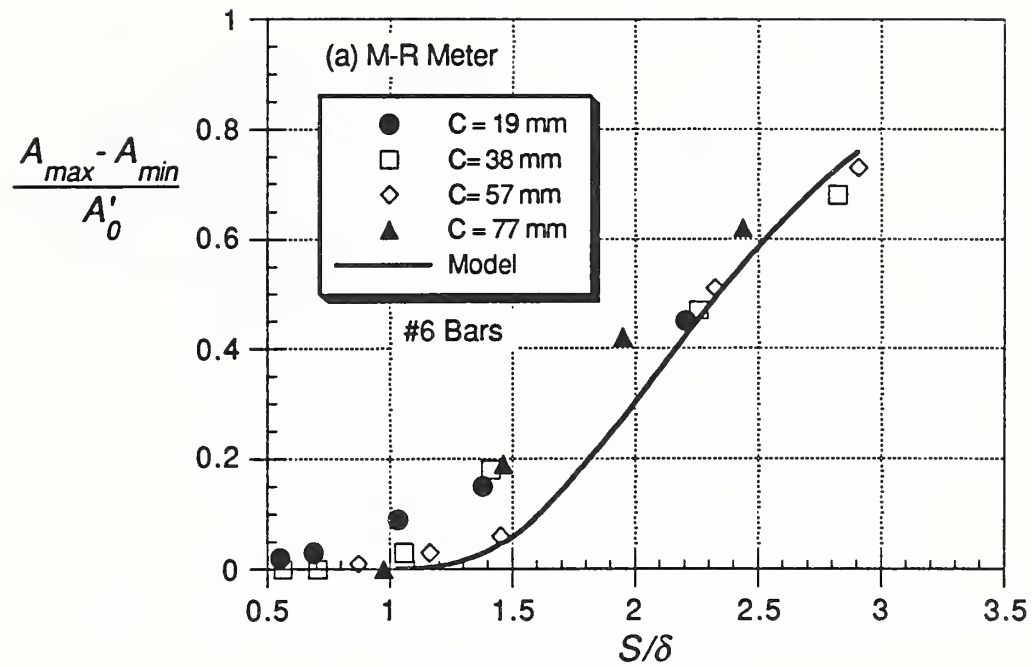


Figure 3.22 Ratio of range in measured amplitude to single-bar amplitude for #6 (19 mm) bars: (a) M-R meter and (b) E-C meter.

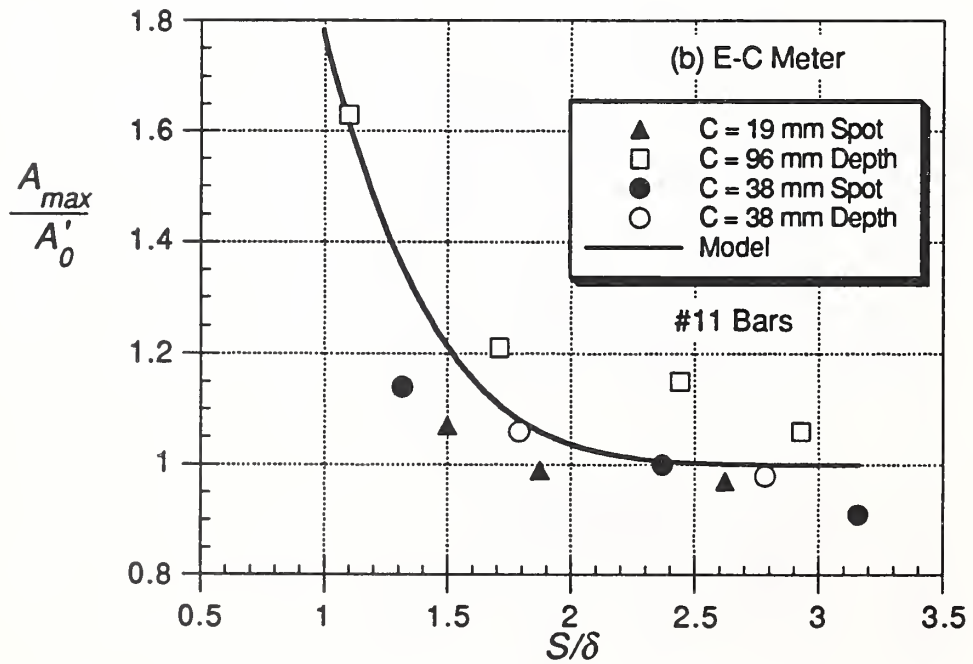
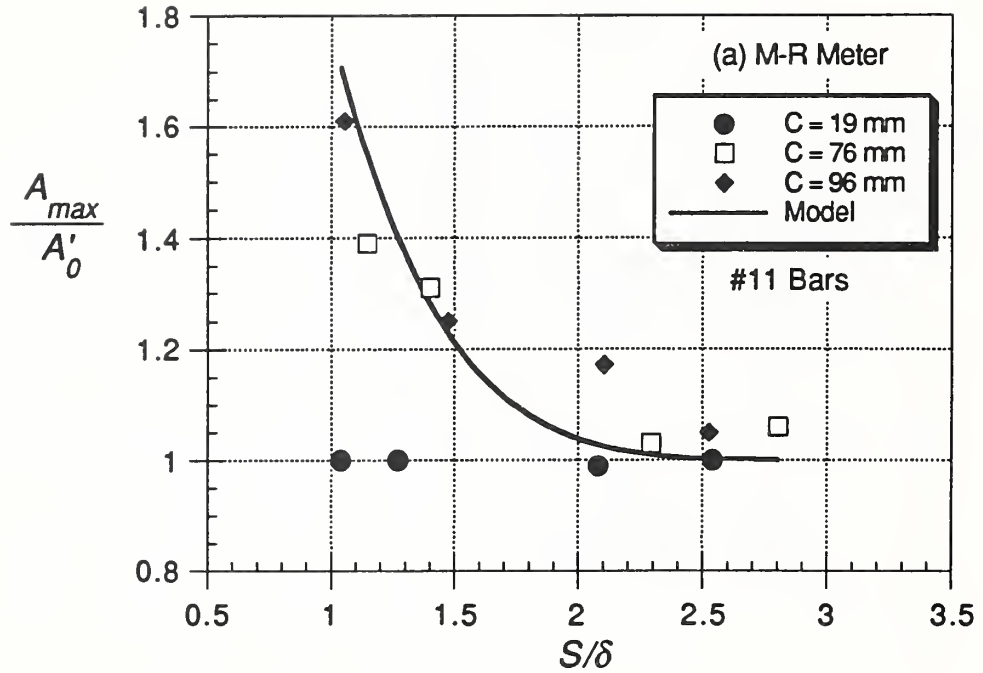


Figure 3.23 Ratio of measured maximum amplitude over middle bar to single-bar amplitude for #11 (36 mm) bars: (a) M-R meter and (b) E-C meter.

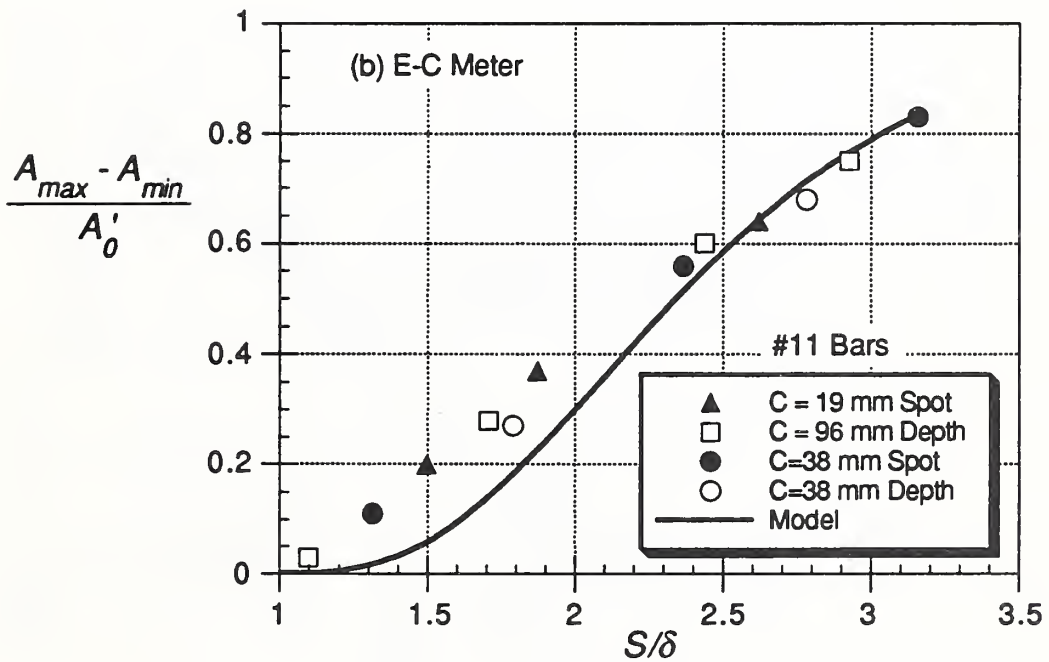
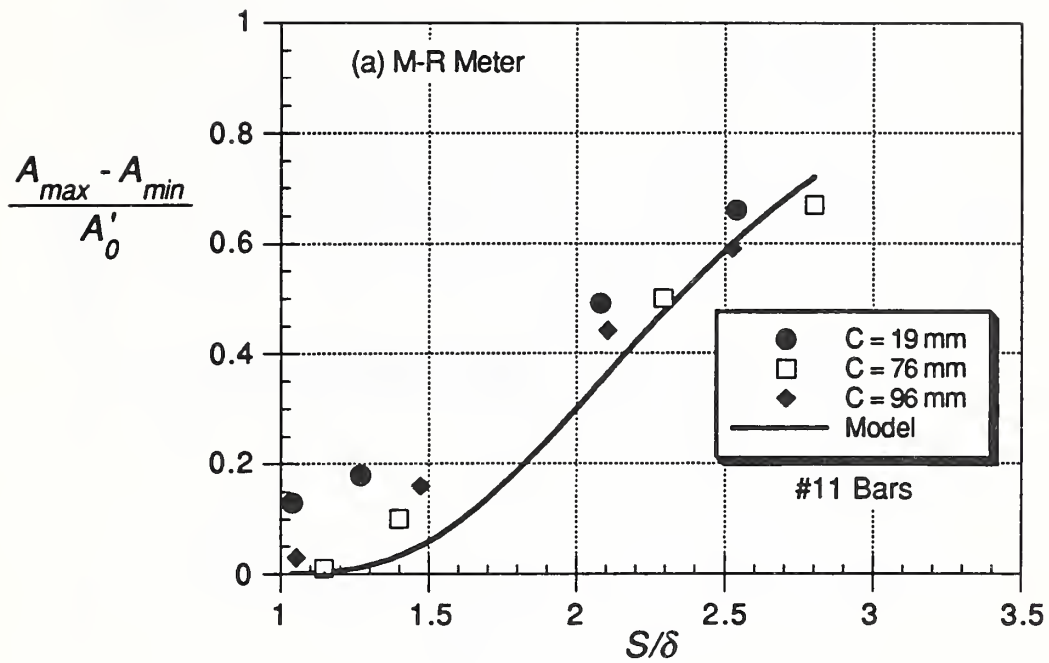


Figure 3.24 Ratio of range in measured amplitude to single-bar amplitude for #11 (36 mm) bars: (a) M-R meter and (b) E-C meter.

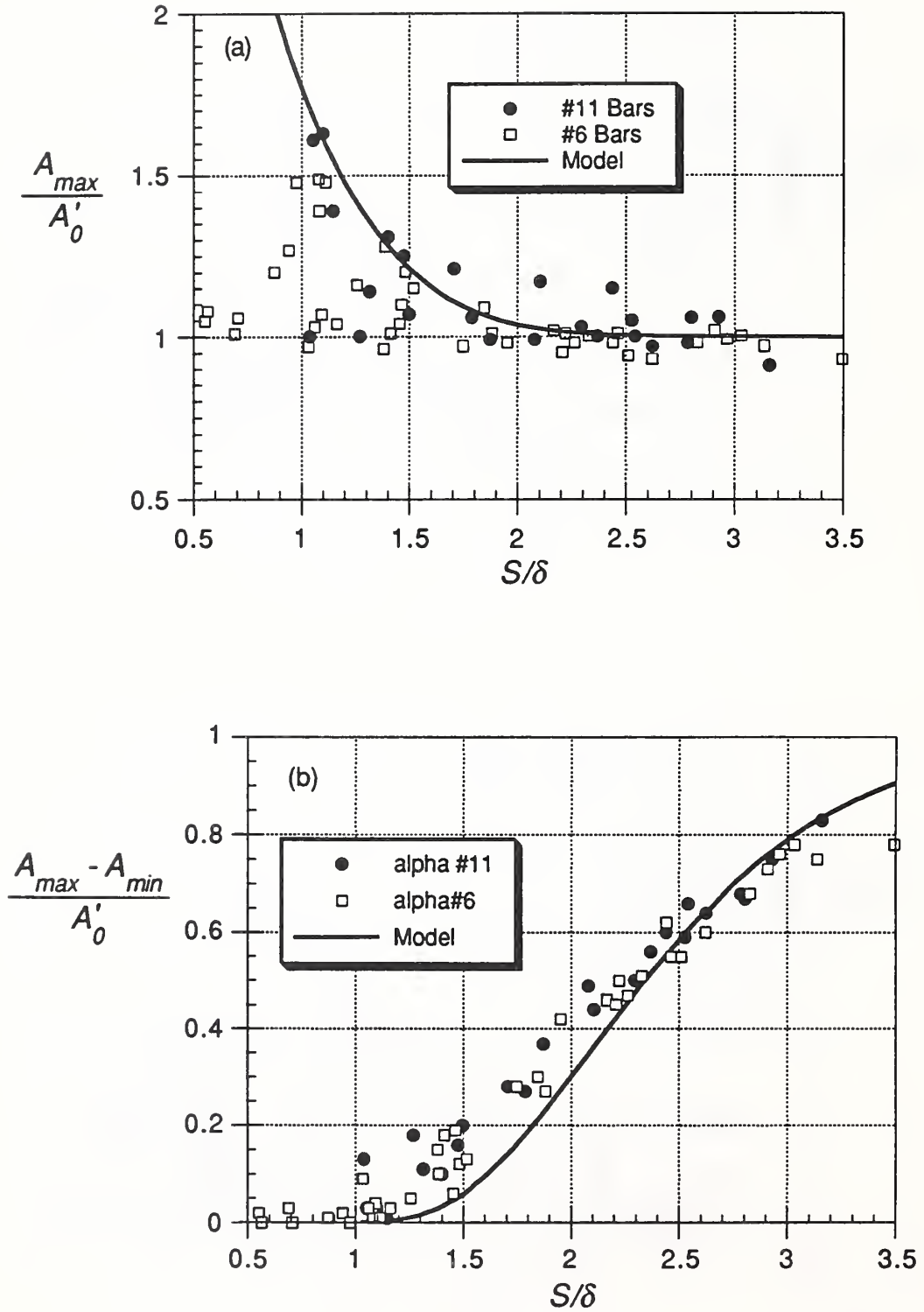


Figure 3.25 (a) Ratio of measured maximum amplitude over middle bar to single-bar amplitude for all cases; (b) ratio of range in measured amplitude to single-bar amplitude for all cases.

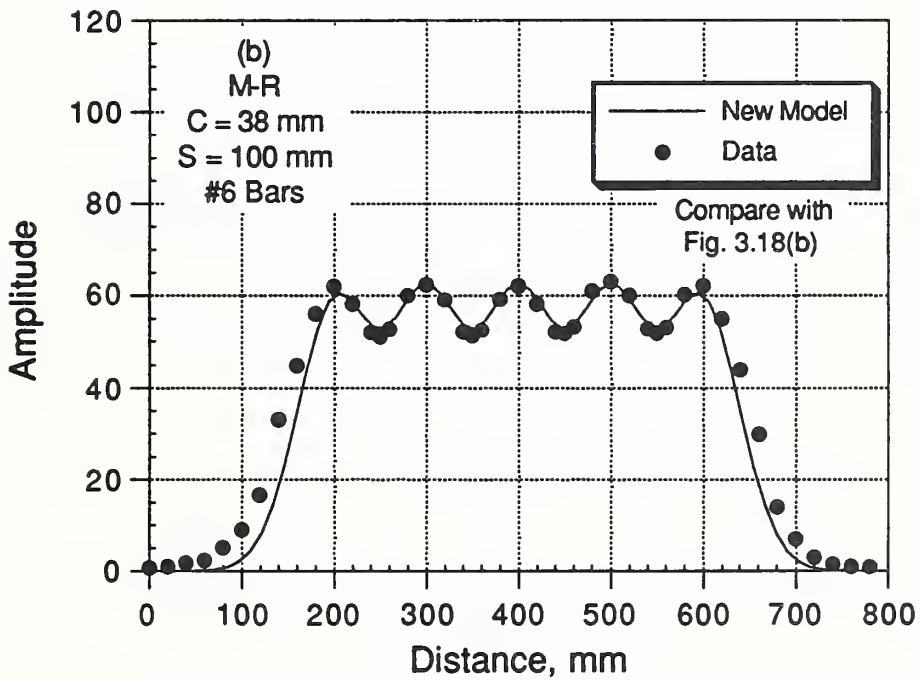
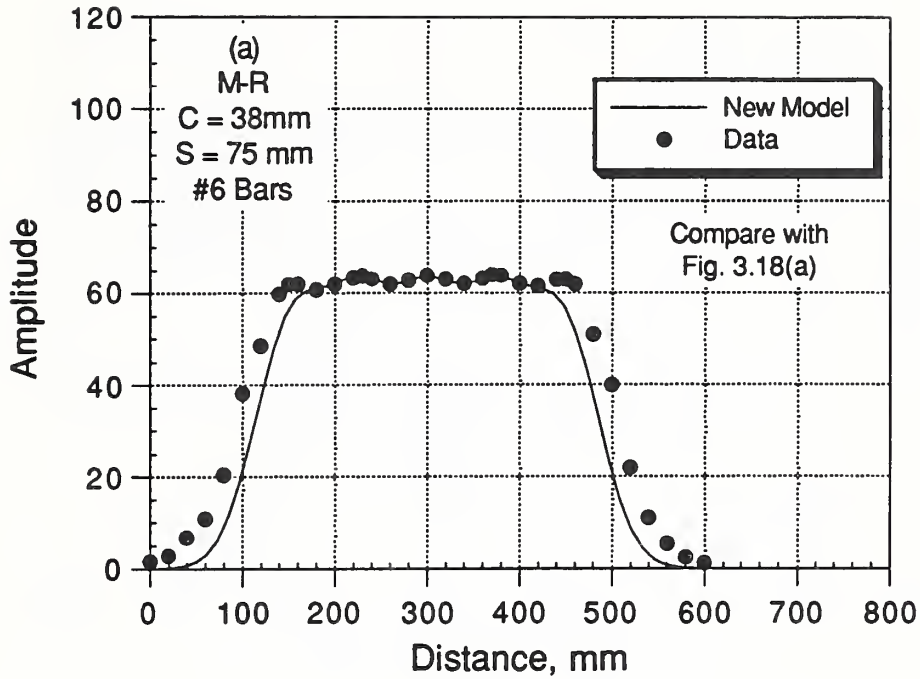


Figure 3.26 Comparison of measured amplitude for scan across the five bars using the M-R meter and the computed variation using corrected values of  $\delta$  and  $A_0$

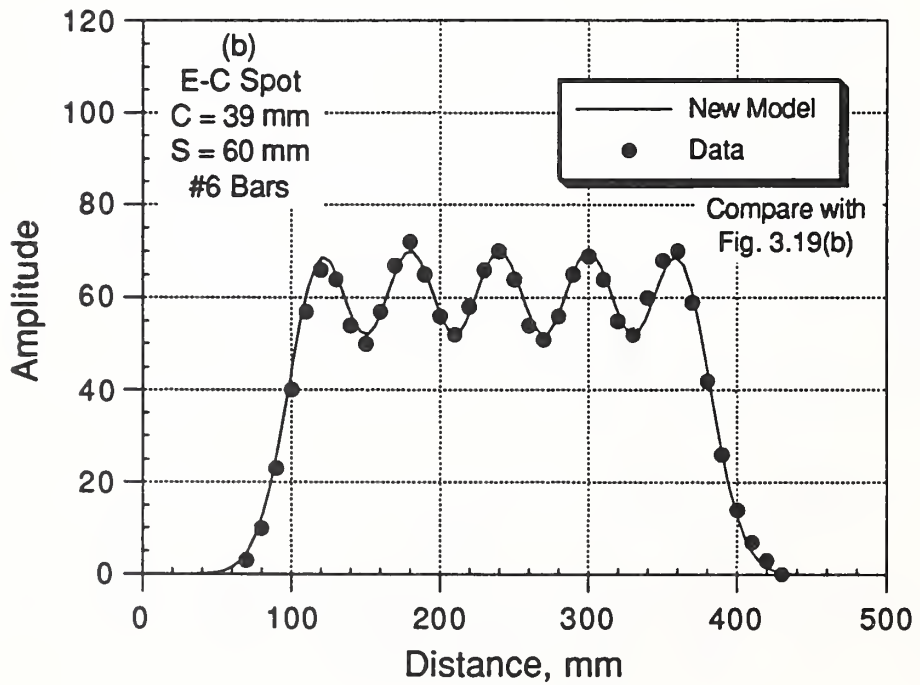
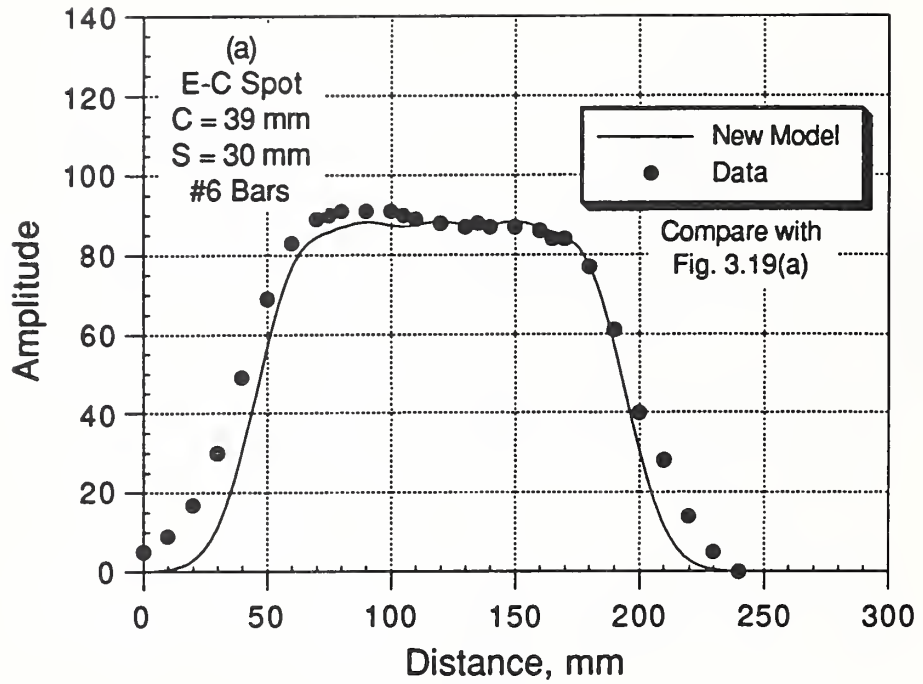


Figure 3.27 Comparison of measured amplitude for scan across the five bars using the E-C meter with spot probe and the computed variation using corrected values of  $\delta$  and  $A_0$

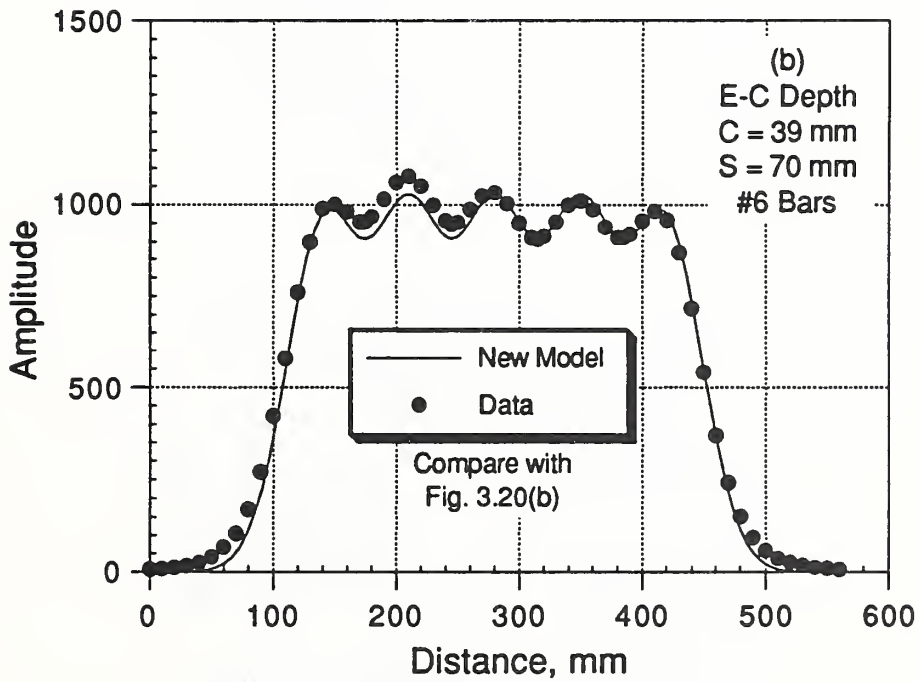
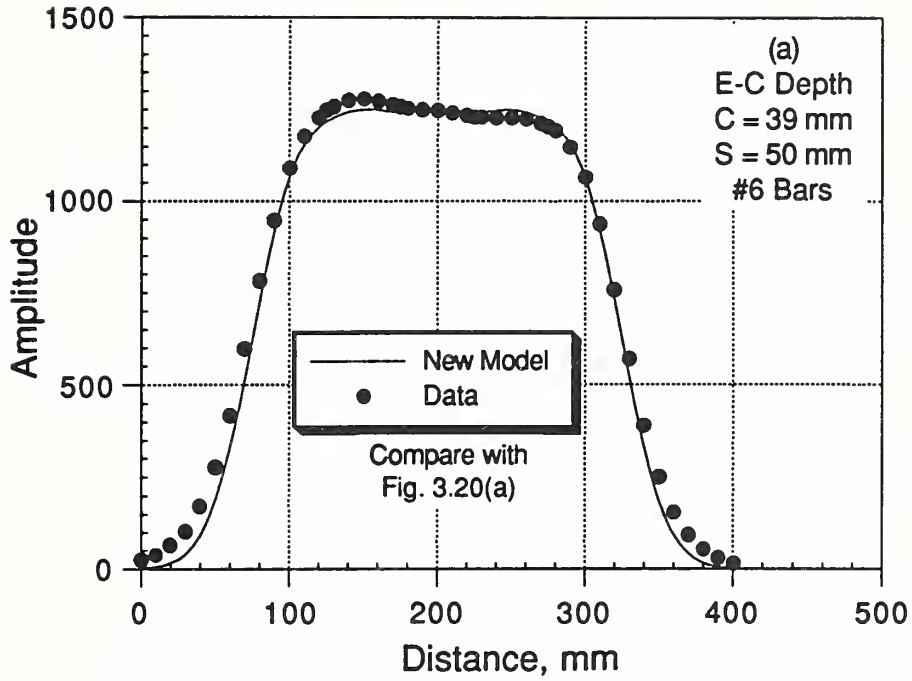


Figure 3.28 Comparison of measured amplitude for scan across the five bars using the E-C meter with depth probe and the computed variation using corrected values of  $\delta$  and  $A_0$

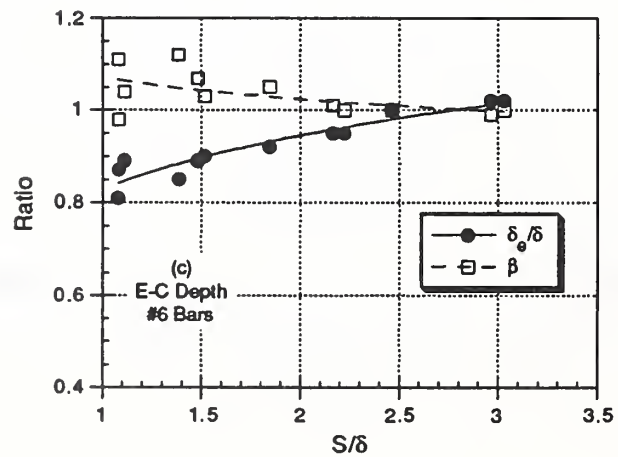
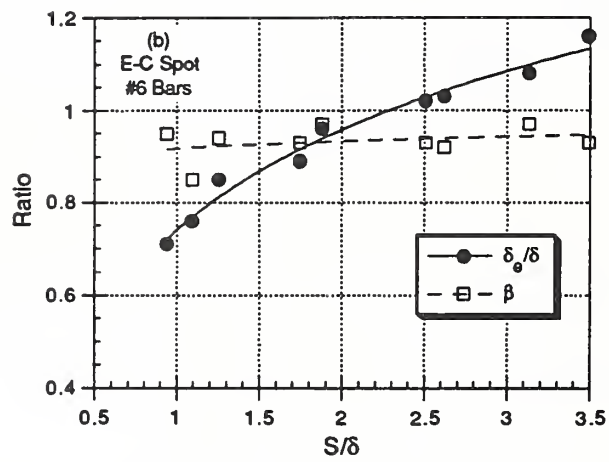
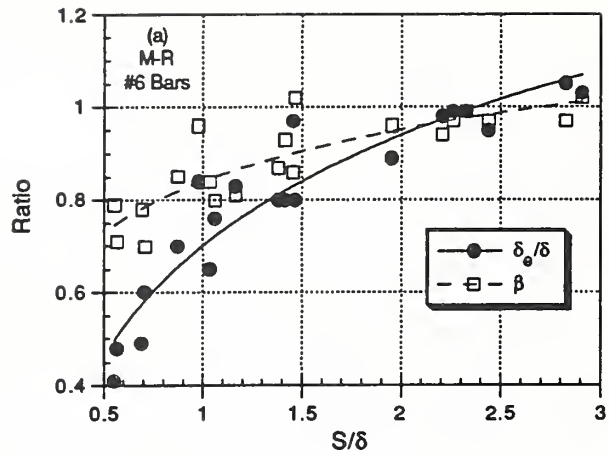


Figure 3.29 Values of  $\delta_0/\delta$  and  $\beta$  as a function of  $S/\delta$  for #6 (19 mm) bars.

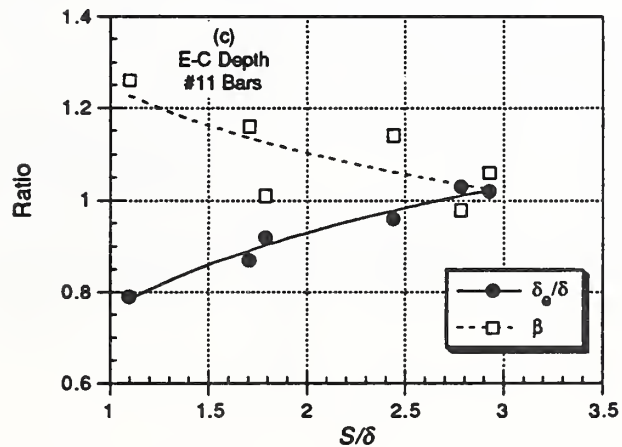
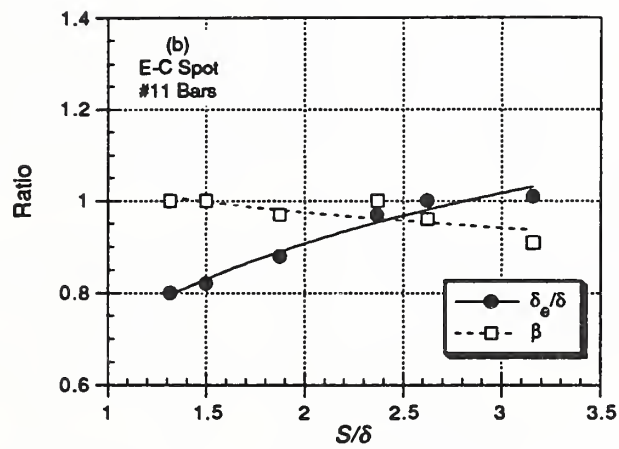
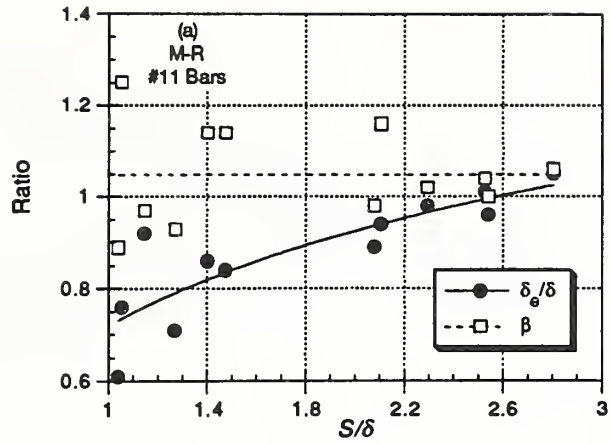


Figure 3.30 Values of  $\delta_e/\delta$  and  $\beta$  as a function of  $S/\delta$  for #11 (36 mm) bars.

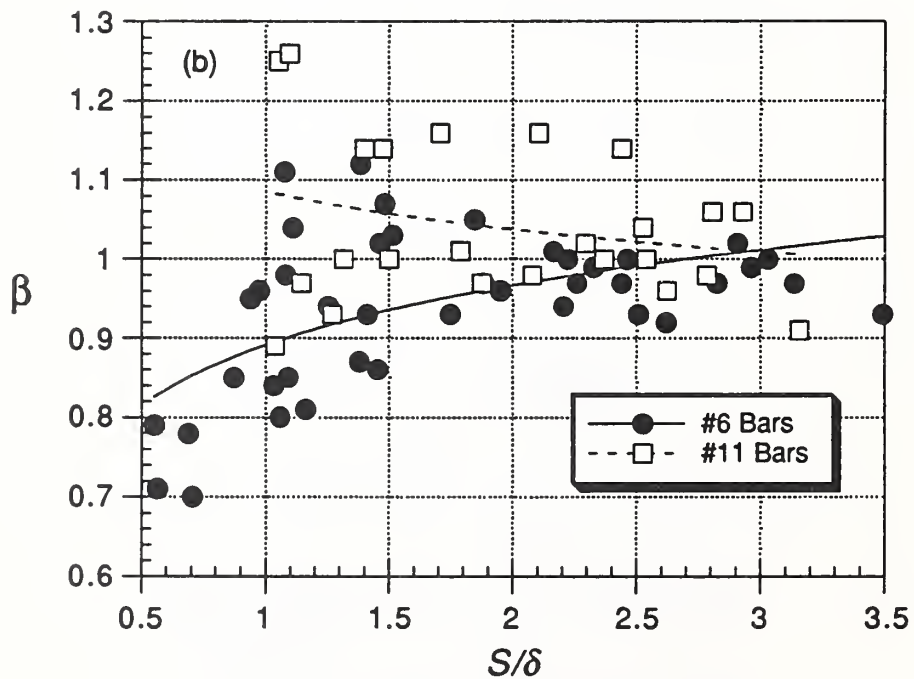
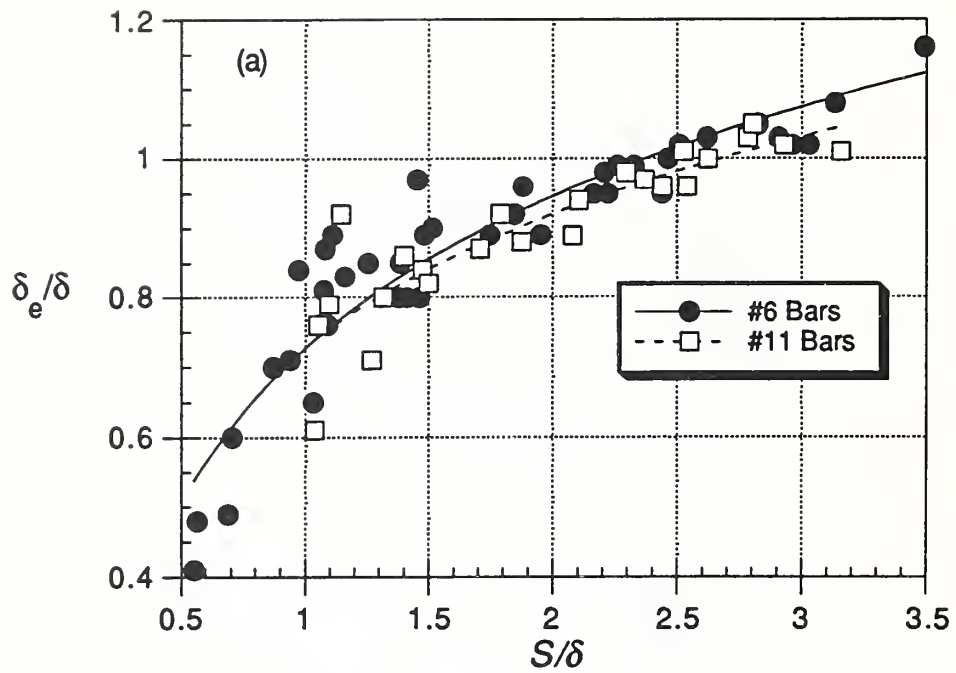


Figure 3.31 (a) Values of  $\delta_e/\delta$  and (b) values  $\beta$  as a function of  $S/\delta$  for all cases.

### 3.5 Bars in two layers

Often reinforced concrete members include steel bars in two or more layers. For example, slabs contain top and bottom reinforcement or beams may contain two layers of bars on each face. This series of tests was designed to examine whether the two types of covermeters could discern a layer of bars located directly below a top layer.

The experimental setup for this exploratory study is shown in Fig. 3.32. Three cases were considered: Case 1 was a single bar at the deeper location, Case 2 was a single bar closer to the surface, and Case 3 included both bars. Three sizes were considered: #5, #6, and #11. The cover,  $C$ , and the clear spacing,  $C_d$ , were chosen to be representative of what might be encountered in a real structure and were as follows:

Bar Size, (mm)	Cover, mm	Clear spacing, mm
#5 (16)	40	27
#6 (19)	42	27
#11 (36)	43	35

Figure 3.33 shows examples of the amplitude as a function of the horizontal offset for the M-R meter. The points labelled *Case 1 + 2* are the sums of the responses for Case 1 and Case 2, i.e., they represent the amplitude assuming the top and bottom bars do not interfere. There are two important observations: (1) the measurements for Case 3 were less than those predicted by summing the results of Case 1 and Case 2, and (2) the results for Case 3 were similar to those for Case 2.

The results from these exploratory tests are summarized in Fig. 3.34, which shows the maximum amplitudes when the search heads were directly above the bars. The lack of significant differences between the measurements for Case 2 and Case 3 leads to the conclusion that the presence of the lower bar would not be able to be detected.

The search head of the M-R meter is highly directional, but the probes for the E-C meter are not directional, i.e., the response is not affected by rotating the probes 90° with respect to the bar axis. As a final test, the M-R meter was used to test the 2-layer configuration by scanning perpendicular to the bars as shown in Fig. 3.35. The results, which are shown in Fig. 3.36, were more encouraging. In Fig. 3.36(a), it is seen that for the #6 bars there is a difference between the Case 2 and Case 3 measurements. Thus the presence of the lower bar had a measurable effect on the measured amplitude, and it might be possible to infer the presence of the lower bar if the depth of the top bar were known accurately. However, for the #11 bars, there were small differences between the Case 2 and Case 3 measurements.

Based on these exploratory studies, it is concluded that these covermeters could not be used routinely to detect the presence of two layers of bars with typical covers and clear spacings. No further studies were performed on this aspect, and this must be recognized as an inherent limitation of electromagnetic covermeters.

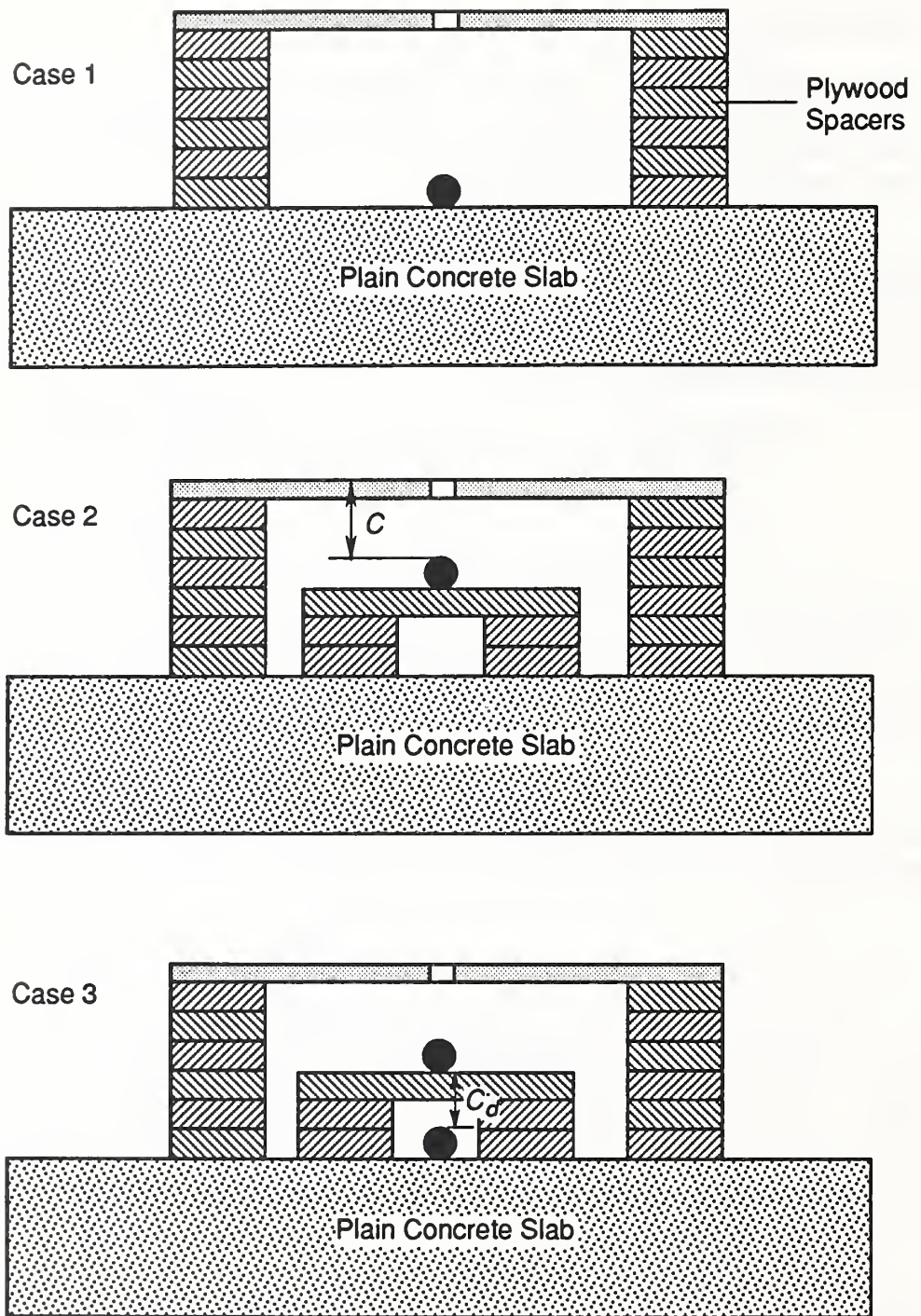


Figure 3.32 Experimental set up for 2-layer tests.

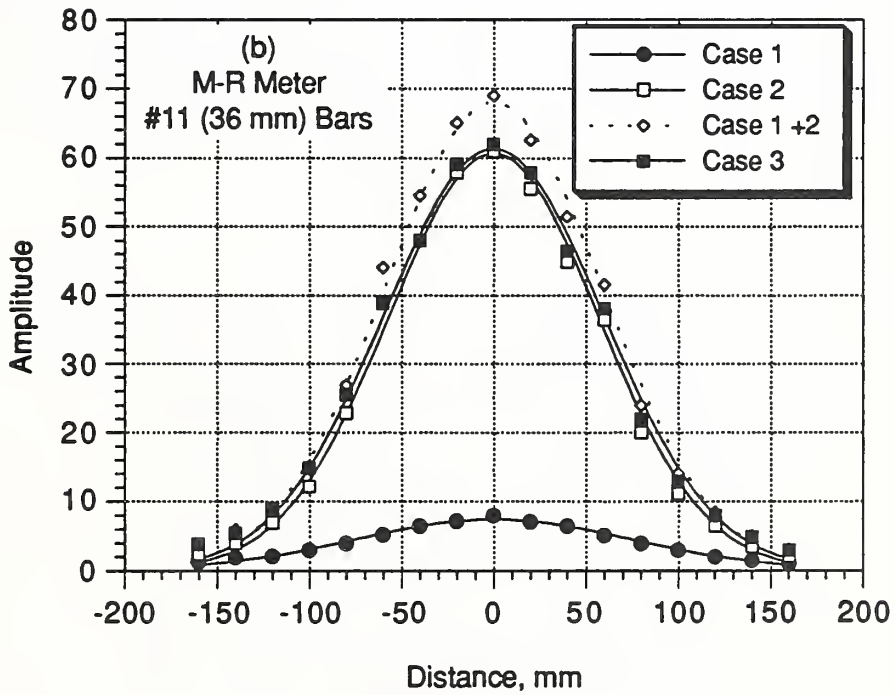
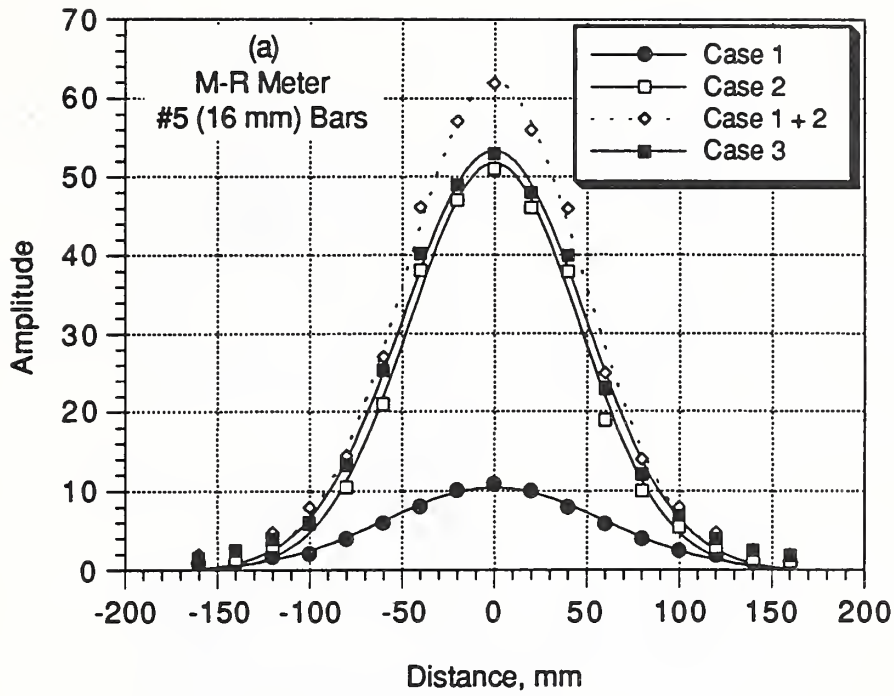


Figure 3.33 Example of results from 2-layer tests using M-R meter.

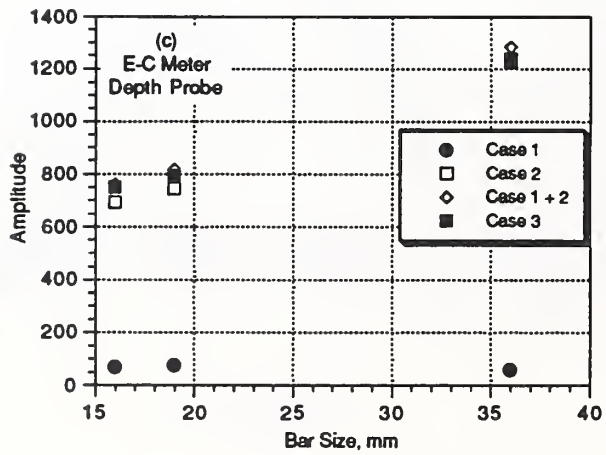
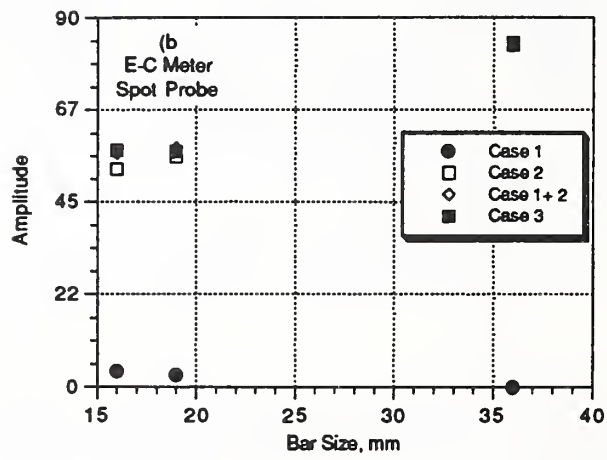
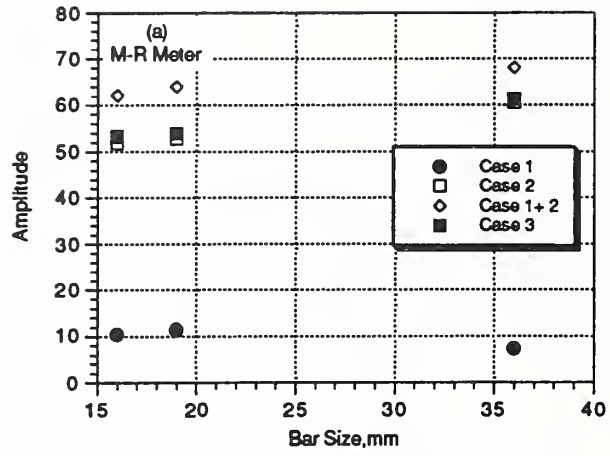


Figure 3.34 Summary of peak amplitudes in 2-layer tests for different bar sizes.

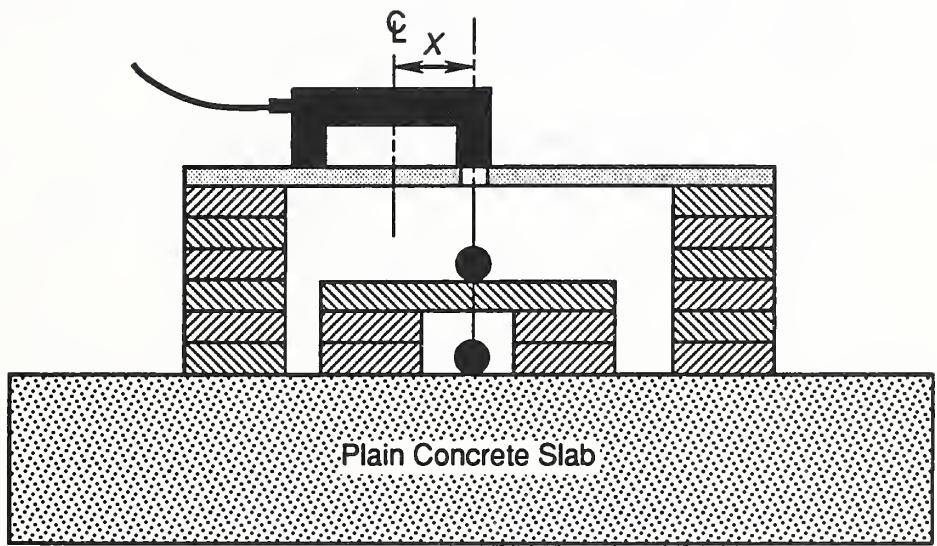


Figure 3.35 Schematic of 2-layer tests with M-R meter search head scanning perpendicular to bar axes.

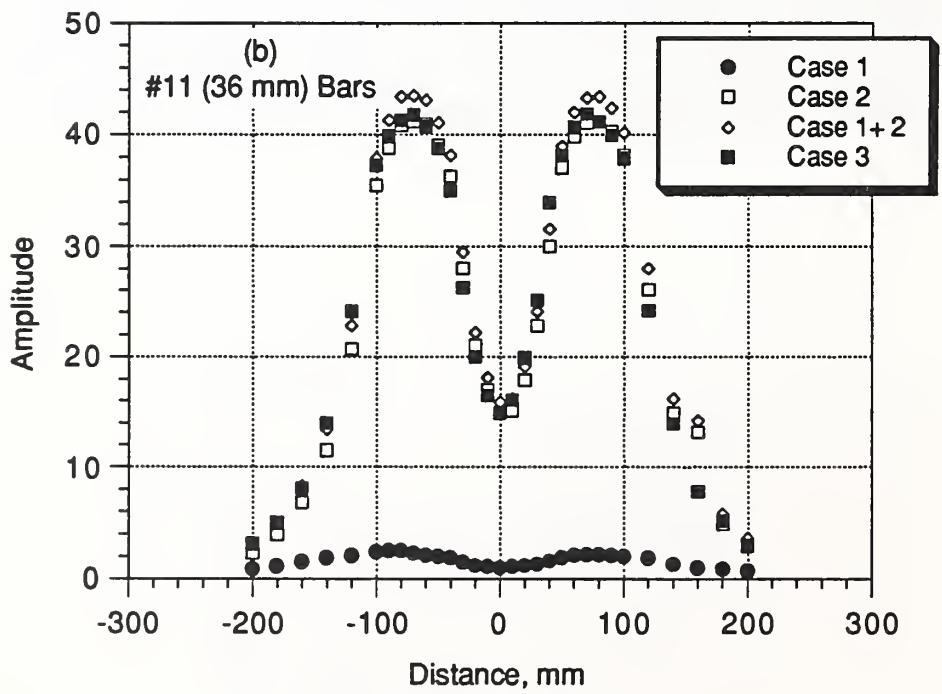
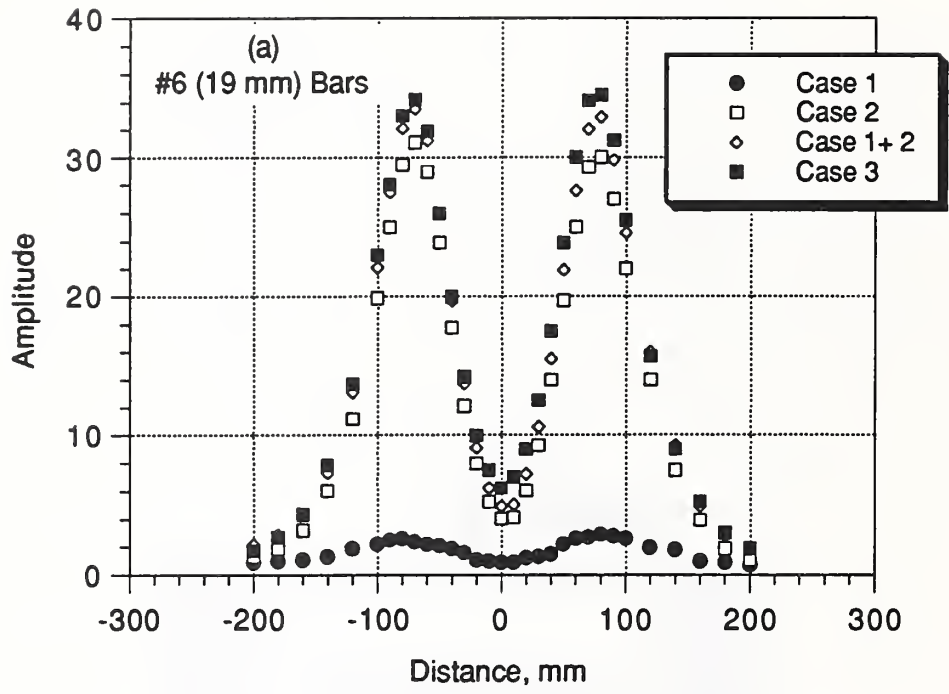


Figure 3.36 Results of perpendicular scans with M-R meter.

### 3.6 Locating ends of bars

To assess the adequacy of the reinforcement in a structure, it is sometimes necessary to locate the ends of the bars so that it can be determined whether the required development lengths exist. While it is obvious that a covermeter should be able to locate the end of a bar, it is not obvious how the response changes as the search head passes over the end. Experiments were conducted to examine how accurately the end of a single bar could be detected with the two types of covermeters.

The experimental setups are shown in Fig. 3.37. The search heads were supported horizontally by plywood resting on the plain concrete slab. Pieces of 19-mm thick plywood were placed between the search head and a single bar. The bar was supported so that its centerline coincided with the centerline of the search head. The location of the end of the bar from the search heads of the M-R and E-C meters was measured as shown in Fig. 3.37 (a) and (b), respectively. The bar sizes were: #4, #6, #8, and #11. Cover depths ranged from 19 to 95 mm. The meter reading was recorded as the bar was moved in 10 (or 20) mm increments relative to the search head.

The variations of the amplitude as function of the location of the bar are shown in Fig. 3.38 for the M-R meter. The solid vertical lines at 0 and 143 mm indicate when the end of the bar passes by the leading (first) and the trailing (second) poles of the U-shaped search head. Examination of the plots in Fig. 3.38 reveals the following:

- For the 19-mm cover, the meter amplitude begins to decrease gradually when the leading pole of the search head passes over the end of the bar. There is a sudden drop in amplitude when the trailing pole passes over the end of the bar.
- As the cover increases beyond 19 mm, the decreases in amplitude as the poles pass over the end of the bar become more gradual.

The variations in amplitude for the E-C meter are shown in Fig. 3.39. Compared with the M-R meter, they are no sudden changes in the rate of amplitude decrease, especially with increasing cover<sup>h</sup>. Based on these observations, it might be concluded that the E-C meter would be inadequate for identifying the end of a bar. However, it will be shown that this is not the case.

A close study of Figs. 3.38 and 3.39 shows that for a particular value of cover, the curves for different bar sizes have similar shapes. Hence the amplitudes were normalized by dividing by the corresponding amplitudes measured away from the end of the bar. Figure 3.40 shows the resulting relative amplitude curves for the M-R meter. Examination of these curves does not reveal a common feature which could be used to indicate the end of the bar for all values of cover. For cover up to 38 mm, the end of the bar could be identified to within 10 mm by noting the point at which the amplitude begins to decrease. For deeper bars, the M-R meter could identify the end of a bar with an accuracy of about 50 mm. In all cases, the *apparent* end of the bar would be indicated before the leading probe is directly over the actual end of the bar. Thus the apparent bar length would be longer than the actual length.

The relative amplitude curves obtained with the E-C meter are shown in Fig. 3.41. There are remarkable features to these curves. For the spot probe, the relative amplitude drops to about 0.6 when the center of the probe is directly over the end of the bar, and for the depth probe the value is about 0.55. Thus it appears that the E-C meter can be used very effectively to locate the end of

---

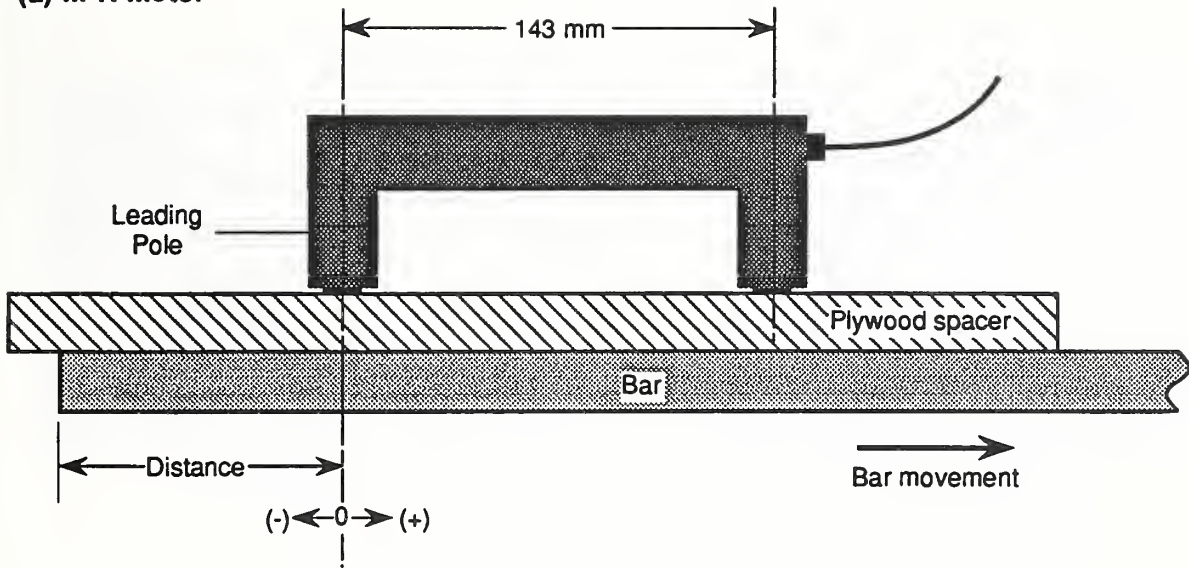
<sup>h</sup>The cyclical variation of the amplitude of the #11 (36 mm) bar for a 19-mm cover (Fig. 3.39(a)) is due to the large lugs for this size bar.

a bar. Note also in Fig. 3.41 that the curves for the different bar sizes are nearly identical in shape except when the center of the probe is approaching the end of the bar, in which case the relative amplitude is a function of the bar size.

In summary, these tests revealed that covermeters can be used to accurately determine the location of the end of a bar. The E-C meter seemed to have the most consistent behavior, and the end of the bar could be identified by noting the location where the amplitude decreases to a certain fraction of the amplitude measured away from the end of the bar. For the M-R meter, reliable indications of the end of the bar are possible only for cover less than about 40 mm. When the leading pole passes over the end of the bar, a gradual decrease in amplitude begins. Thus the user needs a plot of amplitude versus distance to establish where the end of the bar is located. For either meter, the scan must be performed along a line directly above the bar axis. Therefore, the location of the bar has to be determined accurately and the scan direction has to be precise.

These findings were for an individual bar. Time constraints did not allow testing with multiple bars. Therefore, it is not known whether the covermeters could locate the ends of a bar in the presence of congested reinforcement.

(a) M-R Meter



(b) E-C Meter

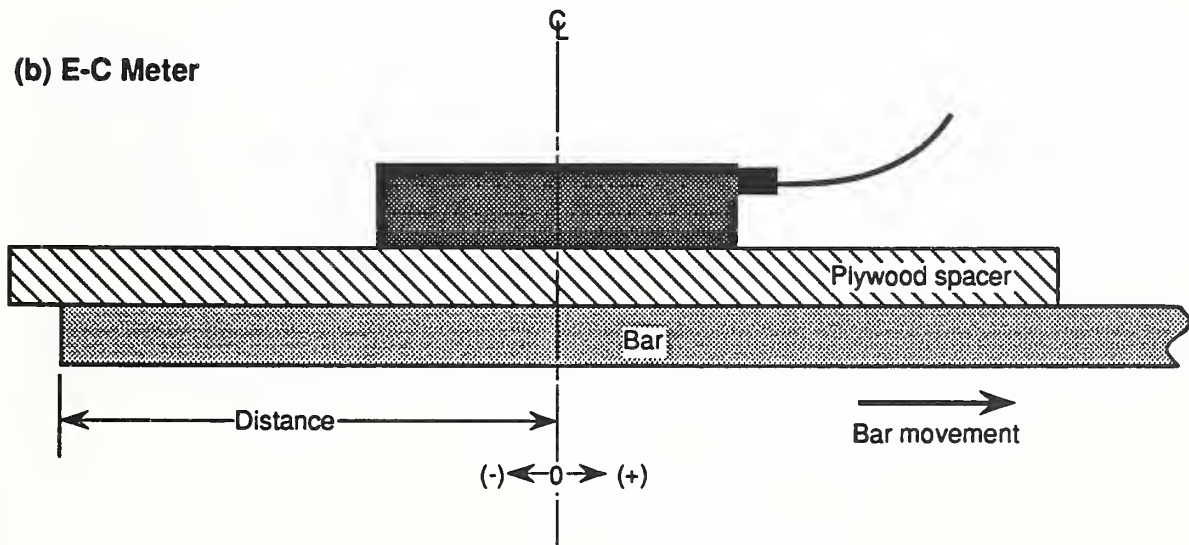


Figure 3.37 Testing configuration for tests to locate end of bars.

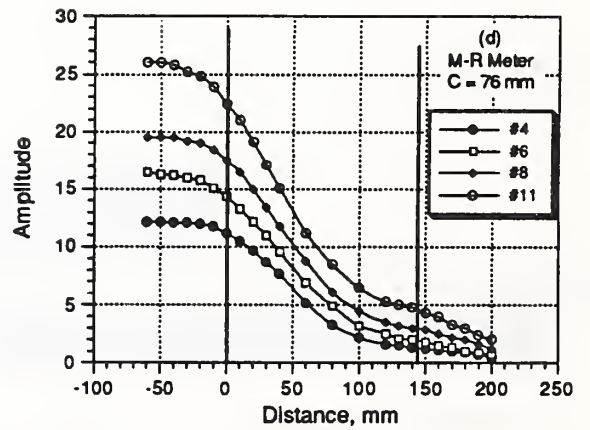
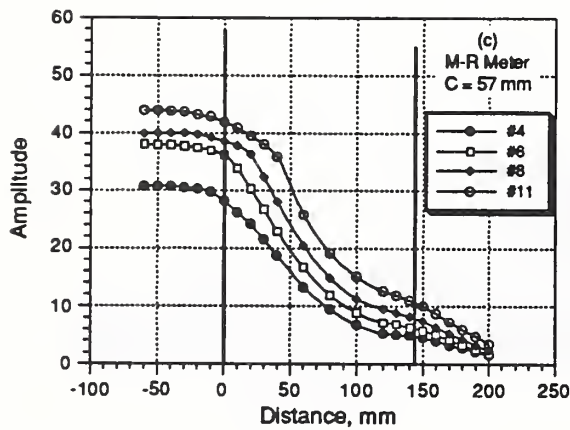
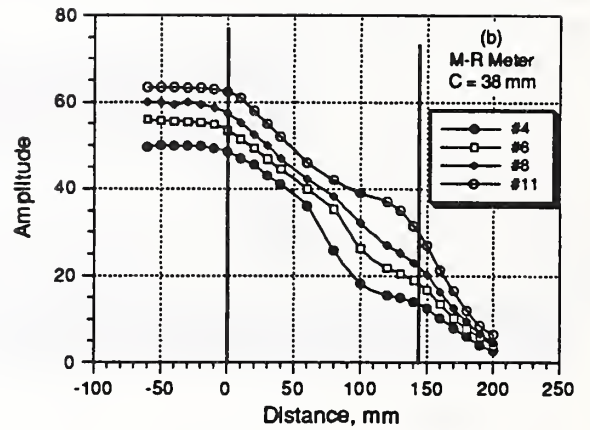
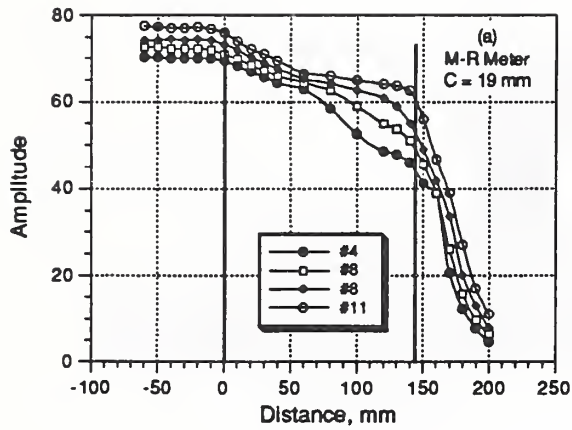


Figure 3.38 Variation of amplitude as bar is moved relative to the search head (M-R meter).

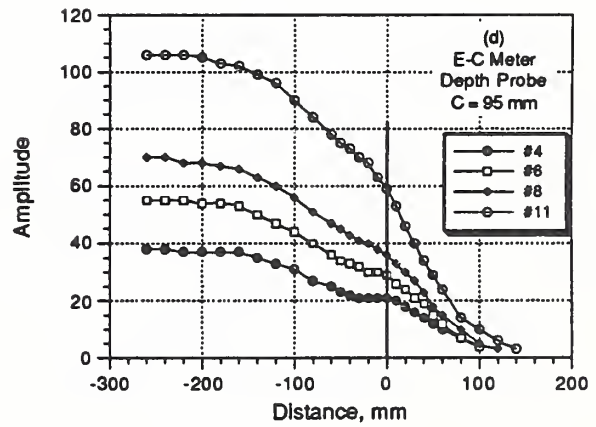
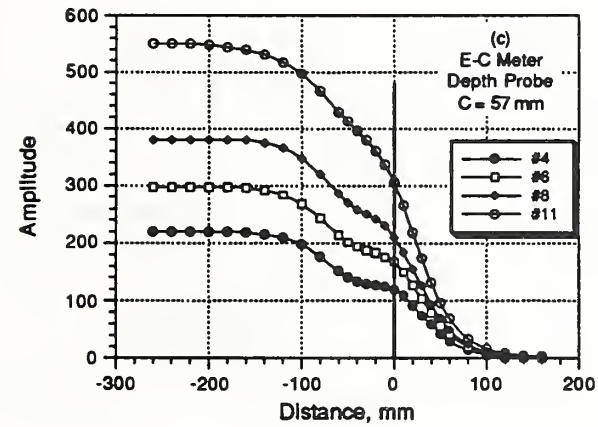
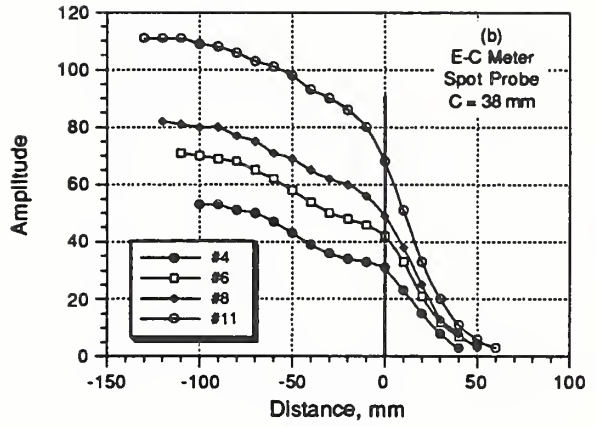
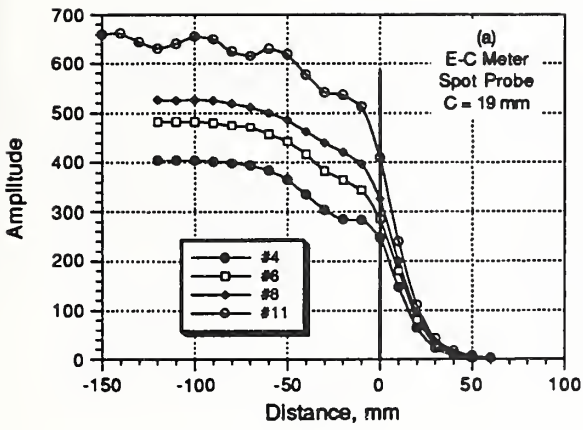


Figure 3.39 Variation of amplitude as bar is moved relative to the search head (E-C meter).

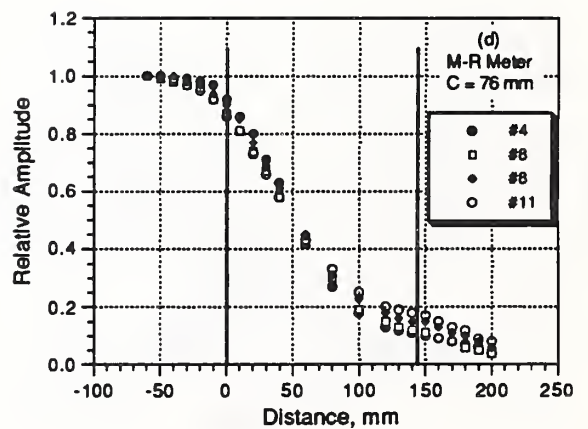
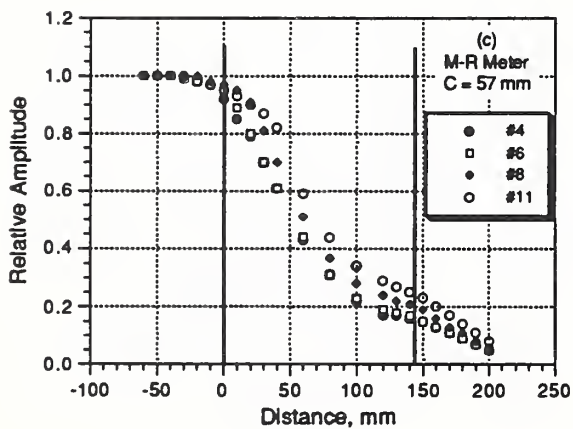
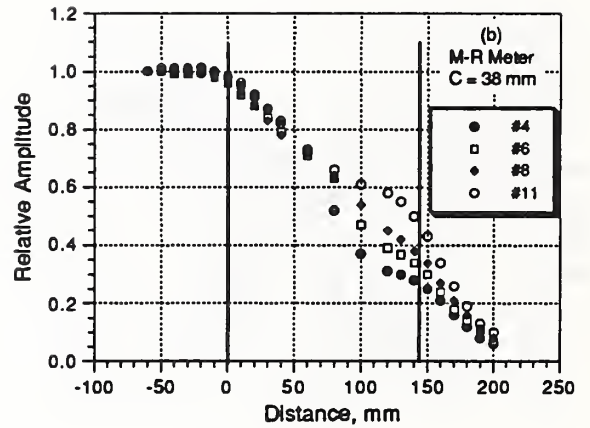
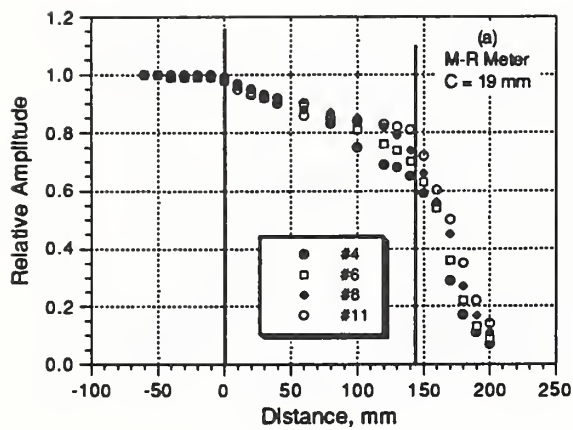


Figure 3.40 Variation of in relative amplitude as bar is moved relative to the search head (M-R meter).

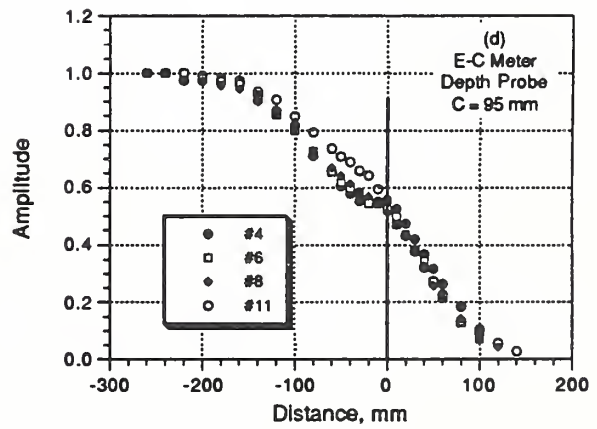
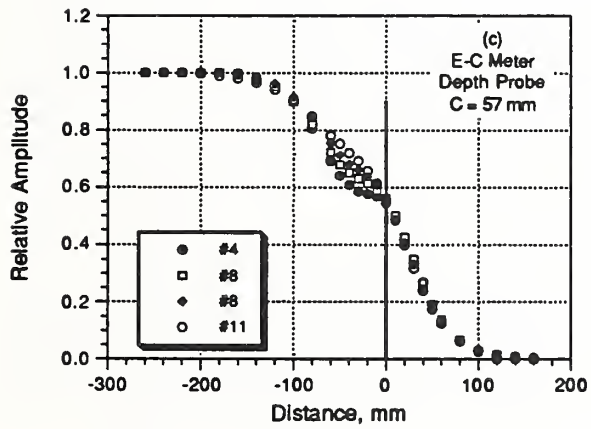
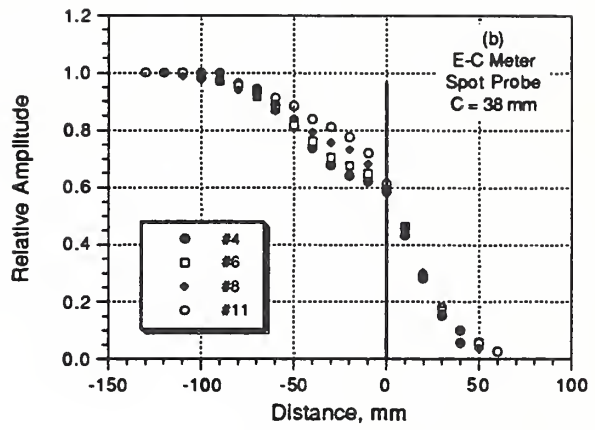
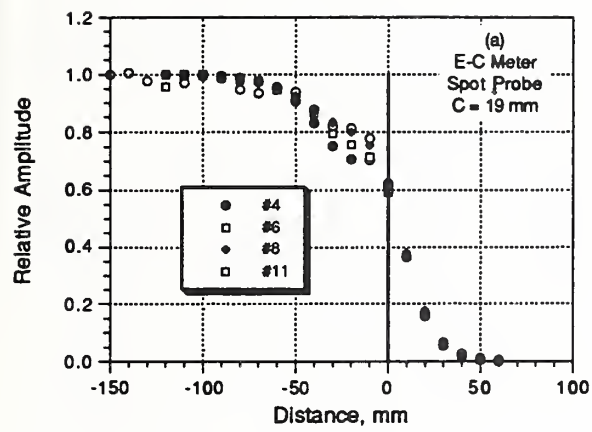


Figure 3.41 Variation of relative amplitude as bar is moved relative to the search head (E-C meter).



### 3.7 Measurement of splice length

The last series of tests investigated the capability of the two type of covermeters to determine the length of the lap splice between adjacent bars. Knowledge of the lap length is critical to determine whether reinforcement details satisfy code provisions. For these tests two lap splice configurations were used: (1) a *side-by-side* (SbS) layout in which the bars were in the same horizontal plane; and (2) an *over-under* (OU) layout in which one bar was located above the other bar. These two configurations are illustrated in Fig. 3.42. The lap lengths were 500 or 600 mm.

To examine the ability to detect the lap region, the amplitude of the meter readings were plotted as function of the position,  $X$ , along the scan line. Figure 3.43 shows the various dimensions in the test specimens. Meter readings were recorded at 10- and 20-mm spacings as shown in Fig. 3.43; the closer spacing was used in the vicinity of the bar ends. The origin of the scan position axis was taken as the point 70 mm away from the start of the lap (SoL) splice. The position of the search head was measured from this zero point. For the E-C meter, the position refers to the center of the search head and for the M-R meter it refers to the leading pole of the U-shaped head. Thus for the E-C meter, when  $X = 70$  mm, the center of the search head is directly above the start of the splice. For the M-R meter, when  $X = 70$  mm, the leading pole is over the start of the lap splice; and when  $X \approx 213$  mm, the second pole is over the start of the lap splice. (Recall from Fig. 3.37 that the distance between the poles of the M-R meter search head is about 143 mm). Other key values of  $X$  are given in the table in Fig. 3.43.

The following bar sizes were used in the lap splice tests: #3, #4, #5, #6, #11, and #14. Approximate cover depths were 19 and 38 mm. Table 3.8 lists the different cases that were investigated. For the side-by-side configuration, two scan lines were used as shown in Fig. 3.43: *Scan 1* was directly over one of the bars and *Scan 2* was directly over the line where the bars touched. Due to the large number of cases that were tested, only representative results are shown to give a general picture of the capabilities of the two covermeters. The presentation is divided into parts: (1) the results of the SbS-configuration, (2) the results of the OU-configuration, and (3) the results in the presence of adjacent parallel bars.

#### 3.7.1 *Side-by-Side (SbS) configuration*

A series of figures is used prepared to illustrate the behavior of the two covermeters. Each figure is composed of plots of meter amplitude versus distance obtained from scans over lap splices for different bar sizes. The various figures are presented without discussion, and they are followed by a summary explanation of the behavior.

The first figure, Fig. 3.44, shows the responses obtained with the M-R meter along scan line "1" for the 19-mm cover. To assist in interpretation, each graph shows the location of the lap splice in relation to the *distance value*. In all cases, the presence of the lap splice is clearly indicated by the rise in amplitude, the plateau region, and the fall in amplitude as the probe passes over the lap. Figure 3.45 shows the results when the cover is about 38-mm. Again, the presence of the lap is indicated by the presence of the *plateau* in the response.

Figures 3.46 and 3.47 show the results obtained with the E-C meter for the 19-mm and 38-cover, respectively. For the 19-mm cover, the spot probe was used for all bar sizes. For the 38-cover, the depth probe was used for the smaller bar sizes, but the spot probe had to be used for the larger

bars because of out-of-range readings with the depth probe<sup>h</sup>. These results show that the E-C meter is also able to indicate the presence of the lap. However, the responses does not have the same well-defined *plateau* regions that were present in the responses with the M-R meter. The erratic response shown in Fig. 3.46(d) is due to the large deformations on the #14 bars. Note that the data for the #14 bars with 38 mm of cover in Fig. 3.47(d) are questionable because the amplitudes are significantly lower than those obtained with the #11 bars shown in Fig. 3.47(c).

Figure 3.48 compares the responses obtained over the two scan lines. To review, scan line "1" is over the centerline of one of the bars, and scan line "2" passes over the line where the bars are in contact. As shown in Fig. 3.48, the main effect on the meter reading occurs before and after the lap. As expected, for scan "1" the amplitudes are much lower when the probe passes by the end of the lap, while for scan "2" the amplitudes are similar before and after the lap. The positions of the significant discontinuities in the patterns of the responses are not affected significantly by the location of the scan line provided that it is maintained parallel to the bar axes.

In summary, these results showed that the presence of the lap splice could be detected by either covermeter when the bars were in the side-by-side configuration. In addition, the plots of amplitude versus distance showed consistent patterns as the probes passed over the starting and ending points of the lap. The important question, however, is: How accurately can the length of the lap be determined using these meters? To answer this question, the amplitude versus distance responses for the two meters were examined more closely.

Figure 3.49(a) shows the characteristic response obtained by using the M-R meter. Four critical points are identified on the graph, and the sketch below the graph shows the corresponding locations of the search head relative to the lap. From this figure, it is seen that the *plateau* region, which indicates the presence of the lap splice, extends from the points labelled "2" and "3." Point "2" corresponds to when the trailing pole is above the start of the lap, and point "1" corresponds to when the leading pole is above the end of the lap<sup>i</sup>. By adding the length of the "plateau" region to the distance between the poles of the search head, the lap length of the splice can be determined. The pattern of the response in Fig. 3.49(a) was noted in all the other scans (results not reported here) using the M-R meter. However, the "plateau" region was not always as flat due to slight variations in the cover along the scan.

Figure 3.49(b) shows the characteristic response obtained using the E-C meter. The points "1" and "2" correspond to when the center of the search head passes over the start and the end of the lap, respectively. As the search head approaches the start of the lap, there is a rapid increase in the amplitude. When the head passes over the start of the lap there is a discontinuity in the rate of increase, and then the amplitude continues to increase until a relatively constant level is reached. As the head approaches the end of the lap, the amplitude begins to decrease, and there is another discontinuity when the head passes over the end of the lap. When the head goes beyond the lap, there is sharp decrease in the amplitude. Thus the lap length corresponds to the distance between

---

<sup>h</sup>When the signal amplitude is too large because of low cover, large bar size, or a combination of the two, the digital display of the E-C meter gives a reading of "1999". If this situation were encountered in the field, the operator could use a spacer of known thickness made of non-conductive material (wood or plastic) to reduce the strength of the signal and permit a valid measurement. This approach was not used in this testing program.

<sup>i</sup>The term "leading" and "trailing" are in reference to the direction of the scan. As the search head is scanned over a point, the leading pole is the first one to pass over that point.

the point where the amplitude stops its sharp increase and the point where it begins its rapid decrease. However, examination of Figs. 3.46 and 3.47 shows that these critical points are not always distinct on the response curves. It is more difficult to identify accurately the point corresponding to the start of the lap as the bar size increases and the cover decreases.

### 3.7.2 *Over-Under (OU) configuration*

The lap splice configuration in which one bar was directly below the other was expected to be a more difficult situation because the top bar shields the bottom bar making it more difficult to identify the end of the lower bar. Figures 3.50 and 3.51 show the results obtained using the M-R meter. The upward arrow in each plot represents the point where the trailing pole is over the start of the lap, and the downward arrow represents the point where the leading probe is over the end of the lap. It can be seen that for the #3 and #6 bars (parts (a) and (b) of Figs. 3.50 and 3.51) the positions of the arrows are in good agreement with the ends of the plateau region. On the other hand, for the #11 and #14 bars, there is no well-defined plateau in the response. The end of the lap is identified easily, but the start of the lap is not identified as easily, especially for the 19-mm cover. From these results, it is concluded that when the M-R meter is used for a lap splice in the over-under configuration, the lap length can be measured with reasonable accuracy for #6 and smaller bars. For #11 and #14 bars, the end of the lower bar cannot be easily detected. Additional tests would be needed to determine whether the lap length could be measured for bar sizes between #6 and #11, which were not measured in this study.

The performance of the E-C meter is summarized in Figs. 3.52 and 3.53. The arrows indicate the points where the center of the search head is over the start and the end of the lap. For the nominal 19-mm cover, only the response of the splice with the #3 bars (Fig. 3.52(a)) has the characteristic discontinuities that were observed for the side-by-side configuration. The same discontinuities were observed in the tests with #4 bars. For bars larger than #5, there was no characteristic discontinuity in the response when the head passed over the end of the lower bar. Hence it is concluded that for the shallow depth, the lap length can be measured only for #3 and #4 bars. For the tests with the nominal 38-mm cover and with #3 or #6 bars, the characteristics of the responses in Fig. 3.53(a) and (b) are similar to those obtained for the side-by-side configuration. Thus it would be possible to estimate the lap length for #6 and smaller bars. For the larger bar sizes there is no characteristic discontinuity in the response when the head passes over the end of the lower bar (Fig. 3.53(c) and (d)), and it is not possible to determine accurately the lap length using the discontinuities that were identified in the tests with the side-by-side configuration. However, another approach may be possible. As shown in Fig. 3.53(d), the distance between the point where the amplitude begins to increase and the point where the amplitude begins to decrease is approximately the same as the lap length. Note that this test was performed using the spot probe because the amplitude exceeded the range of the meter when the depth probe was used.

### 3.7.3 *Presence of parallel bars*

The previous results were obtained under an ideal condition, i.e., there were no interfering effects due to parallel bars. The final series of tests investigated the ability of the covermeters to measure the lap length in the presence of parallel bars. The testing configurations are shown in Fig. 3.54. Tests were conducted using #6 and #14 bars, the lap length was 600 mm, and the clear spacing varied from 25 to 90 mm. Table 3.9 summarizes the cover and clear spacings that were used. The minimum clear spacing was taken as the larger of either 25 mm or the bar diameter, in accordance with paragraph 7.6.1 of the ACI Code (ACI 318-89).

First, the results obtained for the laps with the side-by-side configuration are presented. Figures 3.55 and 3.56 show the amplitude versus distance relationships obtained by using the M-R

meter. The results for the minimum clear spacing and a larger spacing are used for comparison. Again, the arrows correspond to points where the trailing pole of the search head passes over the start of the lap and where the leading pole passes over the end of the lap. (Note that the lack of flat plateaus for some of the cases in Figs. 3.55 and 3.56 is believed to be due to variations of about  $\pm 2$  mm in the actual cover along the length of the scans.) These results should be compared with parts (b) and (d) of Figs. 3.44 and 3.45. In the presence of the parallel bars, the characteristic response of the M-R meter that was obtained without parallel bars (see Fig. 3.49(a)) is still evident. Thus the ability of the M-R meter to determine the lap length for the side-by-side configuration is not diminished by the presence of adjacent parallel bars.

The results for the side-by-side configuration obtained by using the E-C meter are shown in Figs. 3.57 and 3.58, which should be compared with parts (b) and (d) of Fig. 3.46 and 3.47. For the #6 bars, the characteristic discontinuities in the response, that were obtained without parallel bars (see Fig. 3.49(b)), are present when the search head passes over the start and the end of the lap. These discontinuities are more evident in Fig. 3.57(c) and (d) when the depth probe was used for the 38-mm cover. For the #14 bars, the start of the lap could not be easily identified for the 19-mm cover because of the effect of the deformation pattern on the meter reading. This behavior is similar to what was obtained without parallel bars as was shown previously in Fig. 3.46(d). Note that with the #14 bars, the depth probe could not be used for the 38-mm cover because of out-of-range readings. While the characteristic discontinuities that identify the limits of the lap were not present in the results with the 38-mm cover, the length of the lap could be estimated to within 30 mm by considering the distance between the point where the amplitude begins to increase as the start of the lap is approached and the point where the amplitude begins to decrease as the end of the lap is approached (see Fig. 3.58 (c) and (d)). This is the same observation that was noted with the over-under configuration in the absence of parallel bars (see Fig. 3.53(d)).

Finally, the results obtained using laps with the over-under configuration are presented. Figures 3.59 and 3.60 show the results for the M-R meter, and these should be compared with parts (b) and (d) of Figs. 3.50 and 3.51. In the absence of parallel bars (Figs. 3.50 and 3.51), it was found that the lap length for the over-under configuration was discernible for #6 bars but not with #14 bars. As shown in Fig. 3.59, for the #6 bars and a cover of 19 mm, the presence of parallel bars made it difficult to discern the start of the lap. On the other hand for the 38-mm cover, the presence of the lap was evident but the *plateau* region tended to be longer than the lap length. For the #14 bars, comparison of Fig. 3.60 with Figs. 3.50(d) and 3.51(d) shows the parallel bars did not have a major influence on the response, and it would be difficult to measure the length of the lap.

The results for the over-under configuration that were obtained by using the E-C meter are shown in Figs. 3.61 and 3.62. For the 19-mm cover, the start of the lap could not be discerned for either the #6 or #14 bars, which is the same finding as when no parallel bars were present (see Fig. 3.52(b) and (d)). For 38-mm cover and for the #6 bars, the depth probe was used and there was a discontinuity in the response when the head was over the start of lap. Thus the lap length could be measured to within about 20 mm. For the #14 bars, the spot probe had to be used for the clear spacing of 45 mm. The presence of the lap was discernable and there was a discontinuity in the response when the head passed over the start of the lap. When the depth probe was used for the clear spacing of 90 mm, the lap was discernable but the start of the lap did not correspond to a discontinuity in the response.

In summary, the results of this last series of lap splice tests showed that the presence of the parallel bars did not have a significant effect on the ability or inability to discern the presence of the

lap and to measure its length. This conclusion is based on tests in which the clear spacings were not less than the minimum values specified in the ACI Code.

#### 3.7.4 Summary

Tests were conducted to examine the ability of two types of covermeters to detect the presence of a lap splice and to determine the lap length. Two splice configurations were used. In one case, the lapped bars were placed side-by-side in a plane parallel to the free surface to be scanned, and in the other case the lapped bars were placed in a plane perpendicular to the free surface. Scans were performed along the length of the splices, and readings were recorded at regularly spaced intervals. The readings were plotted as a function of the distance along the scan line.

As expected, the extent of the lap splices were easier to measure for the side-by-side configuration than for the over-under configuration. For the M-R meter, the plots had a well defined *plateau* region corresponding to where both poles of the search head were over the lap. In this case, the length of the lap could be determined easily from the plots by measuring the length of the *plateau* and adding the distance between the poles of the search head. For the E-C meter, the responses were more complicated and it was not always possible to establish the length of the splice with certainty. The ability to measure the lap length depended on the probe that was used, the bar size and the cover. In general, as the cover decreased and/or the bar size increased, it became more difficult to measure the lap length. Under optimum conditions, the lap length could be measured based on noting the distance between two distinct discontinuities in the response, which corresponded to when the search head passed over the ends of the lapped bars.

There were two reasons why it was more difficult to determine the lap length for the over-under configuration compared with the side-by-side configuration. Firstly, the top bar shields the lower bar. Secondly, as the bar size increases, the cover for the lower bar also increases, and the effect of the lower bar on the signal diminishes when the search head passes over the lap. The ability of the M-R meter to determine the lap length was reduced as the bar size increased. The performance of the E-C meter was, again, a function of the probe, bar size, and cover. For larger bar sizes, the lap length was easier to identify with the E-C meter at the deeper cover. Thus, if shallow cover were present in the field, a spacer could be used to improve the performance.

Finally, the effects of adjacent parallel bars was investigated. The minimum clear spacing was in accordance the ACI Code provisions. For those cases where the lap splices could be discerned in the tests without parallel bars, the presence of the parallel bars did not eliminate the characteristic discontinuities in the responses that could be used to identify the limits of the lap splice. The main effect of the parallel bars was to increase the amplitude of the meter readings.

Table 3.8 Summary of tests to measure length of lap splice

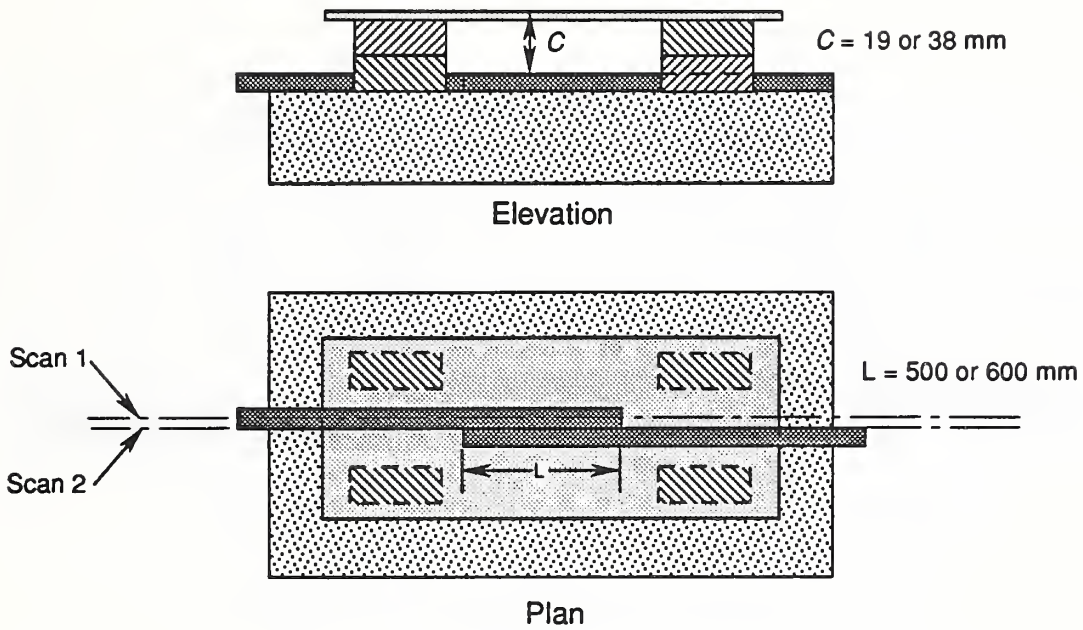
Bar (mm)	Cover (mm)	Lap Length (mm)	Testing Configuration
#3 (9)	19	500	Side-by-side
	38	500	Side-by-side
	22	500	Over-under
	38-39	500	Over-under
#4 (12)	18-20	500	Side-by-side
	38-39	500	Side-by-side
	20	500	Over-under
	39	500	Over-under
	20	600	Over-under
	38	600	Over-under
#5 (16)	20-23	600	Side-by-side
	39-41	600	Side-by-side
	19	600	Over-under
	38-40	600	Over-under
#6 (19)	19	600	Side-by-side
	39-41	600	Side-by-side
	21	600	Over-under
	38-39	600	Over-under
#11 (36)	18-20	600	Side-by-side
	38-39*	600	Side-by-side
	18-20	600	Over-under
	40-41	600	Over-under
#14 (43)	19-20	600	Side-by-side
	37-38*	600	Side-by-side
	18-20	600	Over-under
	38-39*	600	Over-under

\* Depth probe could not be used due to over ranging

Table 3.9 Summary of lap splice tests with adjacent parallel bars

Bar (mm)	Cover, mm	Clear spacing, mm
#6 (19)	19	25, 50, 75
	38	25, 75
#14 (43)	19	45, 70, 90
	38	45, 90

(a) Side-by-Side (SbS) Configuration



(b) Over-Under (OU) Configuration

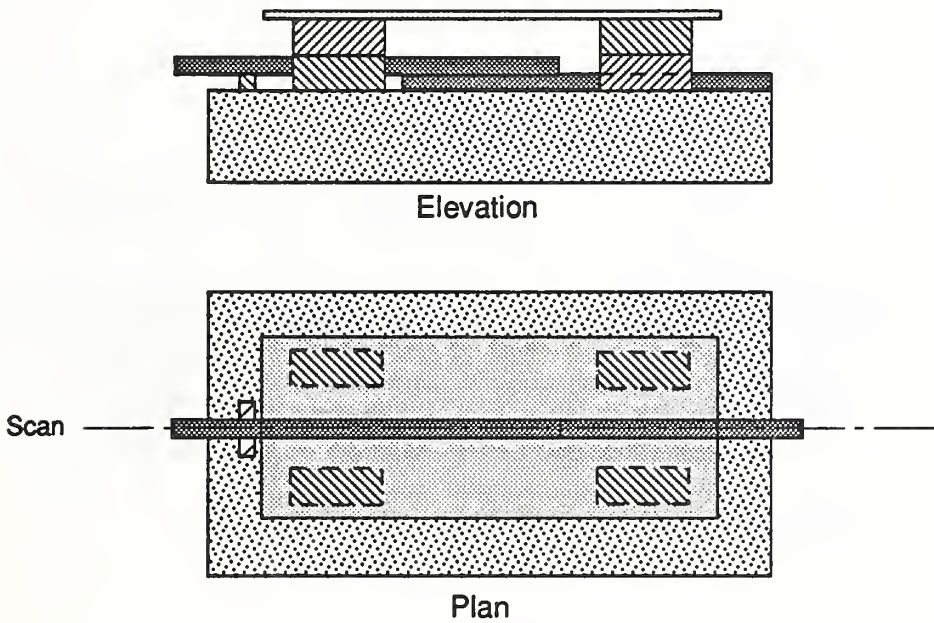
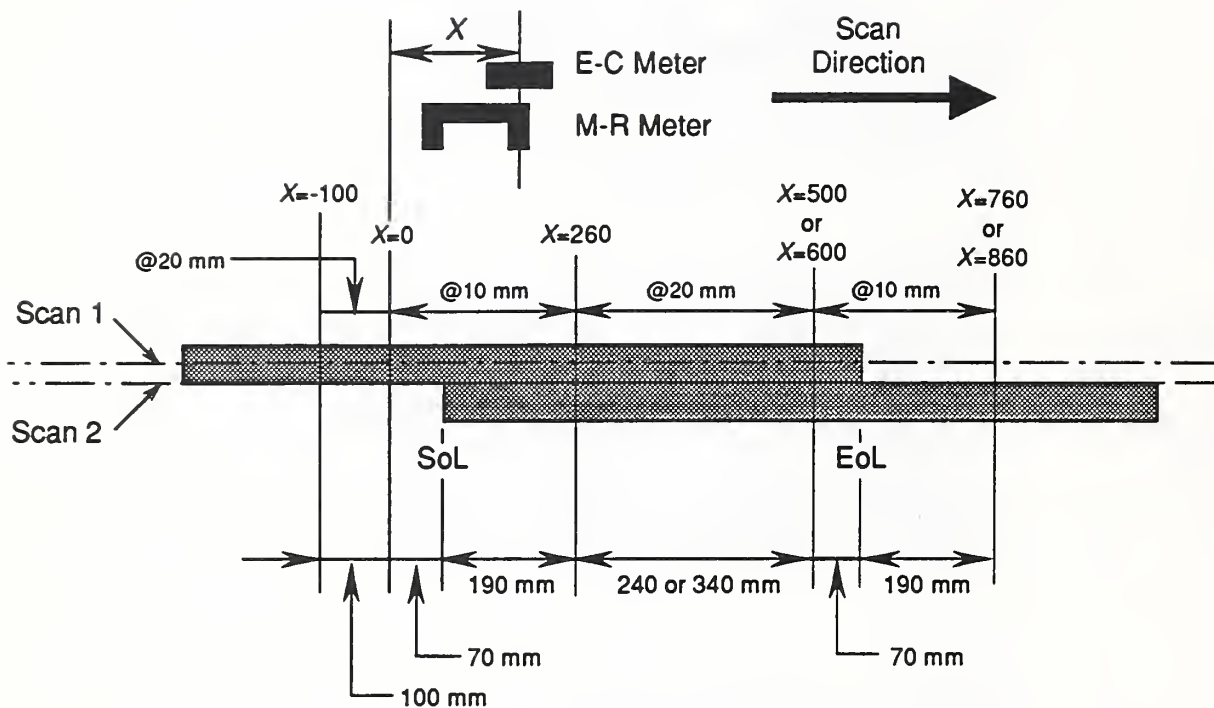


Figure 3.42 Testing configuration for lap splice tests: (a) bars placed side-by-side and (b) one bar placed above other bar.



### Key values of X

Event	L = 500 mm	L = 600 mm
E-C probe at SoL	70 mm	70 mm
E-C probe at EoL	570 mm	670 mm
M-R first pole at SoL	70 mm	70 mm
M-R second pole at SoL	213 mm	213 mm
M-R first pole at EoL	570 mm	670 mm
M-R second pole at EoL	713 mm	813 mm

SoL = Start of lap  
EoL = End of lap

Figure 3.43 Dimensions in the splice tests; the probe position is measured from the point X=0 to the center of the E-C probe or to the center of the leading pole of the M-R probe.

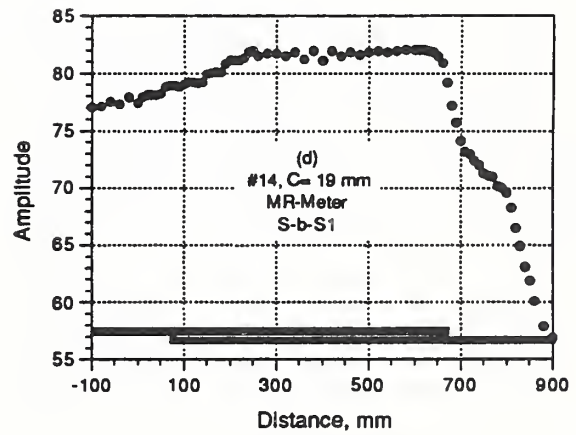
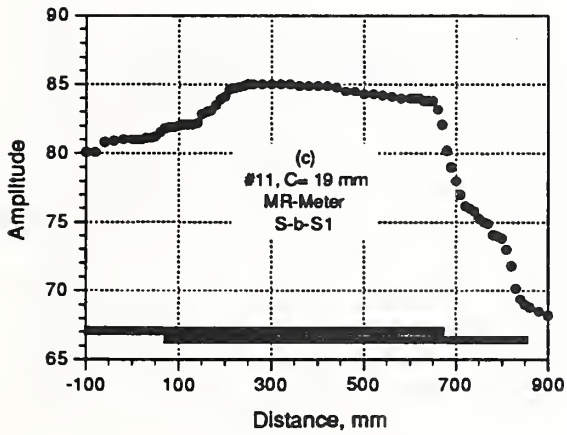
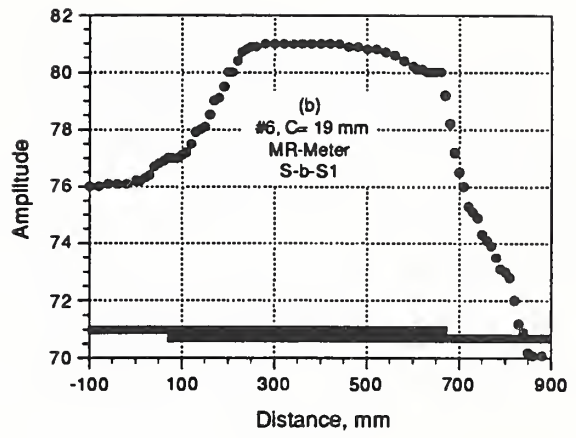
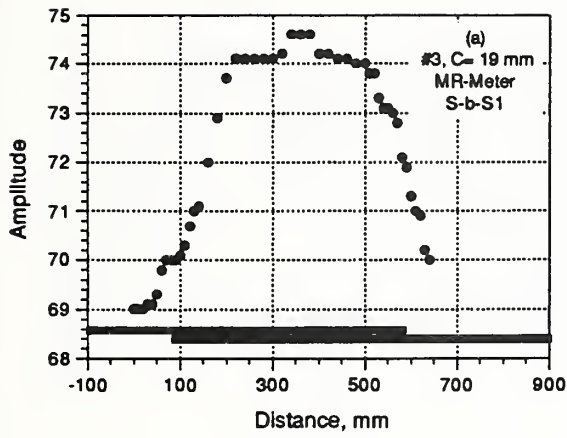


Figure 3.44 Amplitude versus distance for lap splice tests using M-R meter with 19-mm cover (side-by-side configuration, scan line "1").

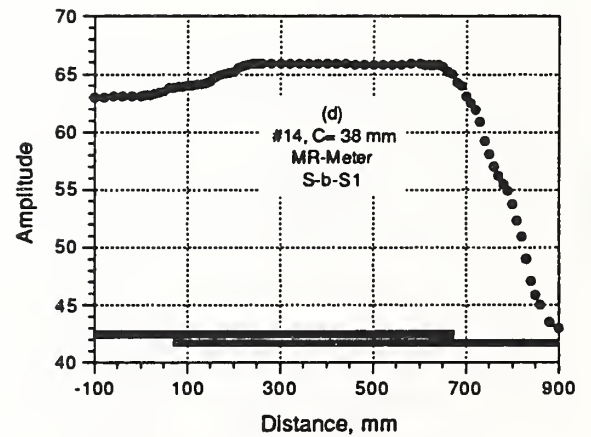
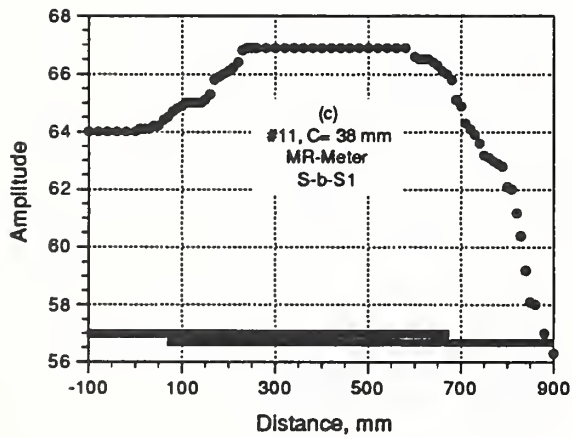
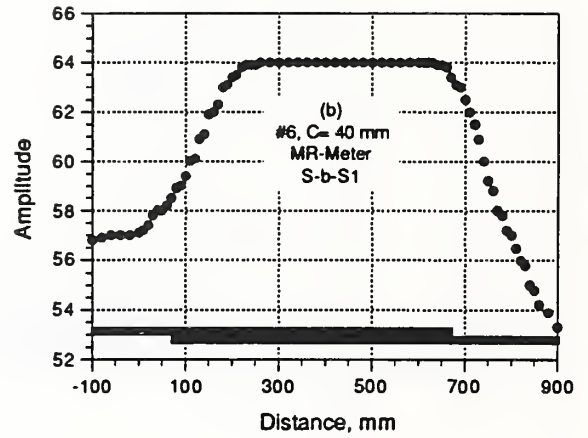
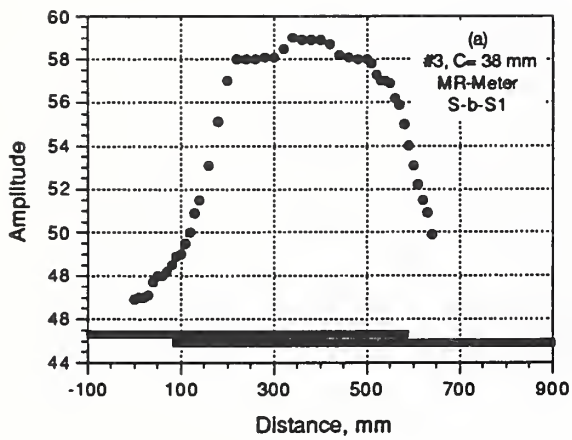


Figure 3.45 Amplitude versus distance for lap splice tests using M-R meter with 38-mm cover (side-by-side configuration, scan line "1").

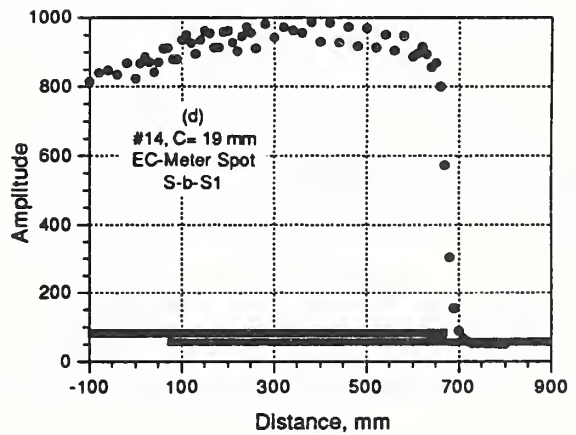
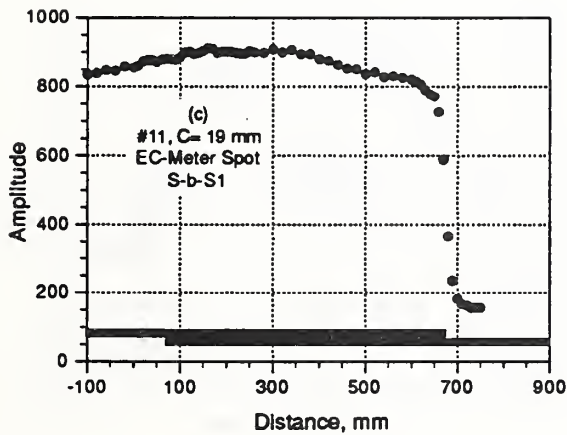
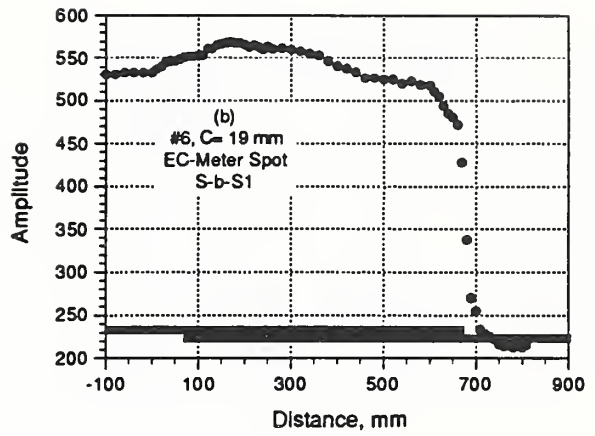
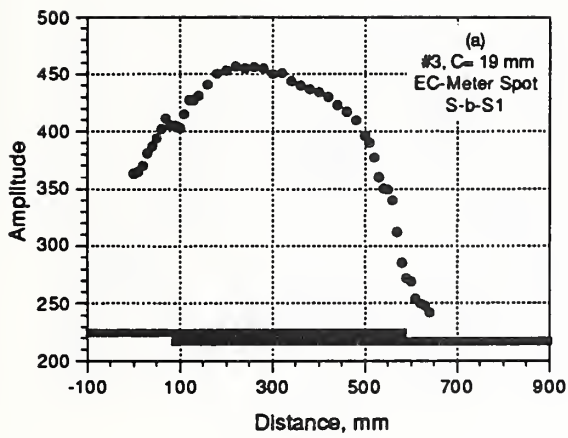


Figure 3.46 Amplitude versus distance for lap splice tests using E-C meter with 19-mm cover (side-by-side configuration, scan line "1").

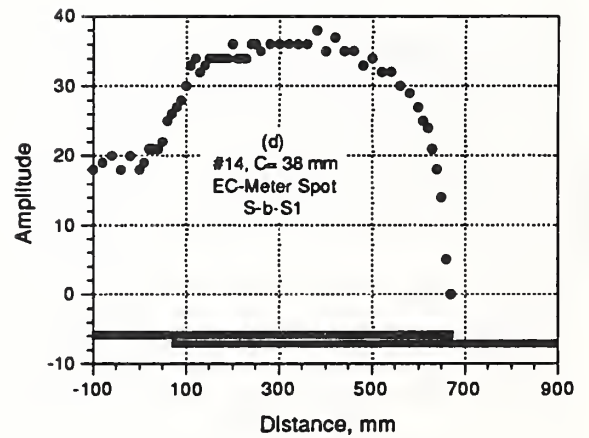
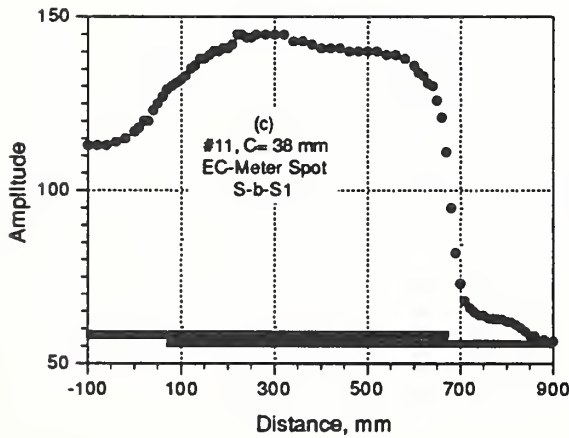
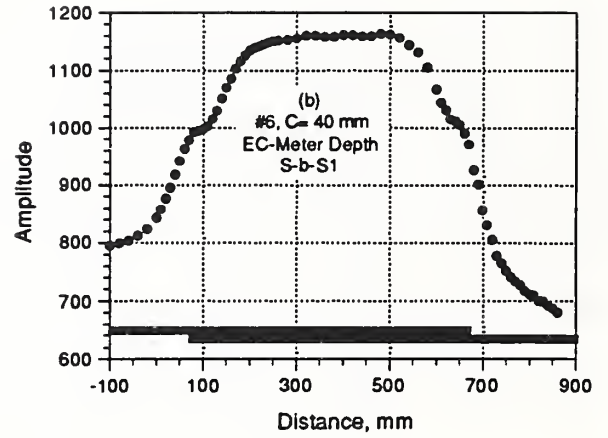
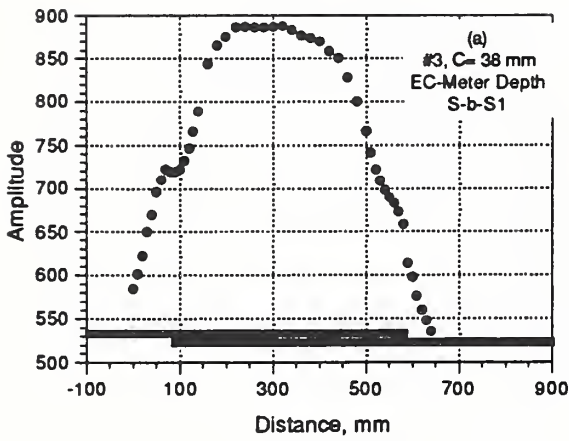


Figure 3.47 Amplitude versus distance for lap splice tests using E-C meter with 38-mm cover (side-by-side configuration, scan line "1").

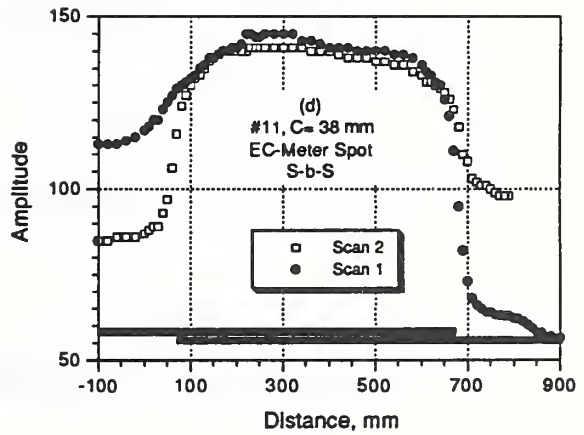
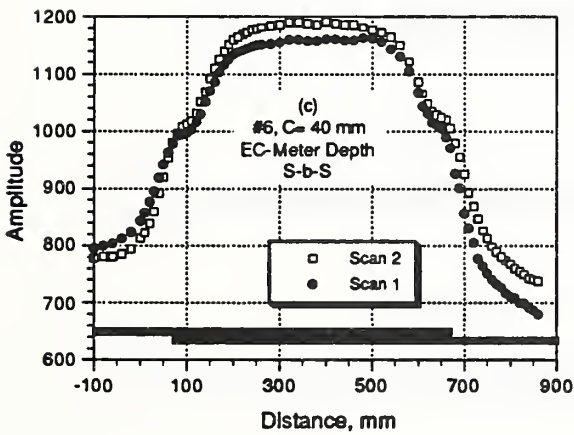
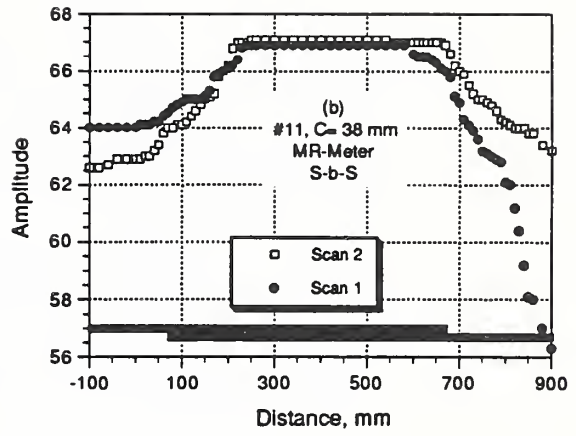
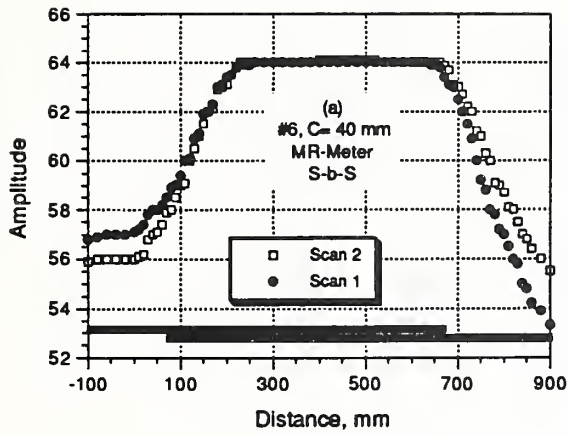


Figure 3.48 Comparison of results along scan lines "1" and "2" for the side-by-side configuration.

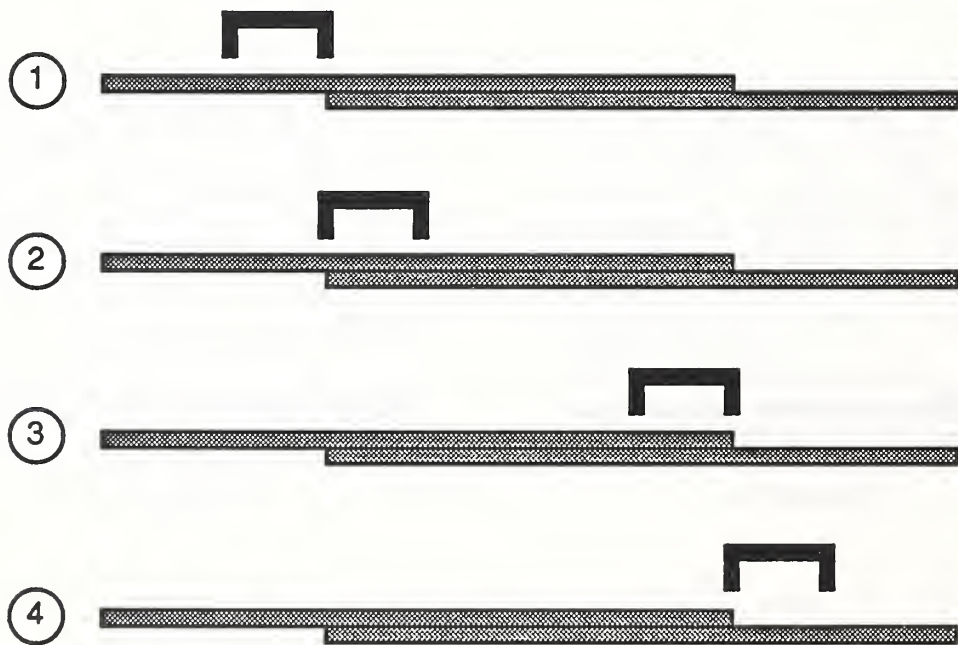
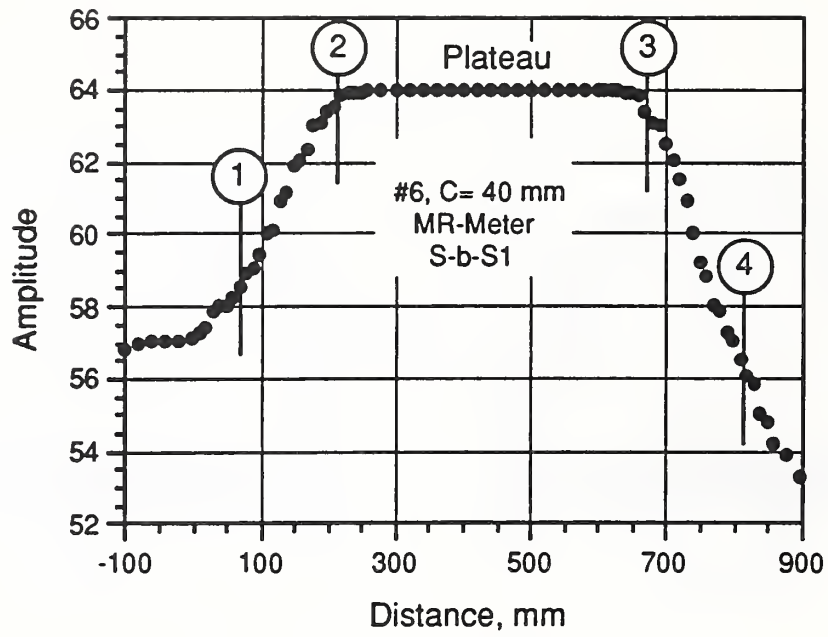


Figure 3.49(a) Summary of response using the M-R meter to determine lap length for the side-by-side configuration (scan line "1").

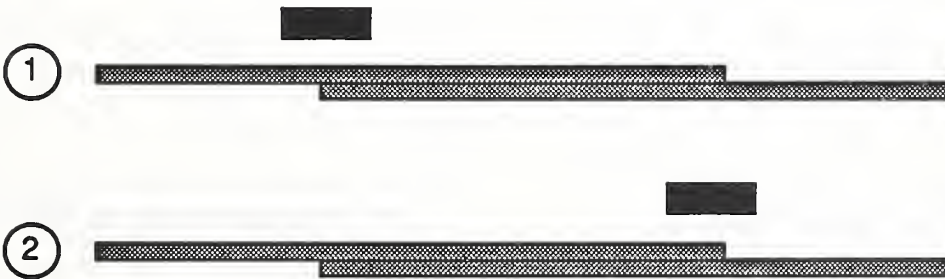
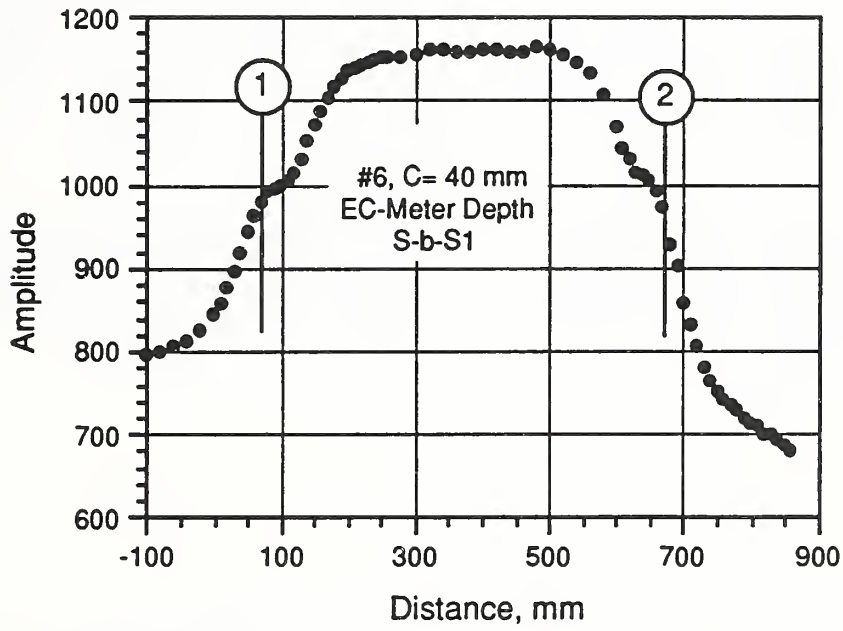


Figure 3.49(b) Summary of response using the E-C meter to determine lap length for the side-by-side configuration (scan line "1").

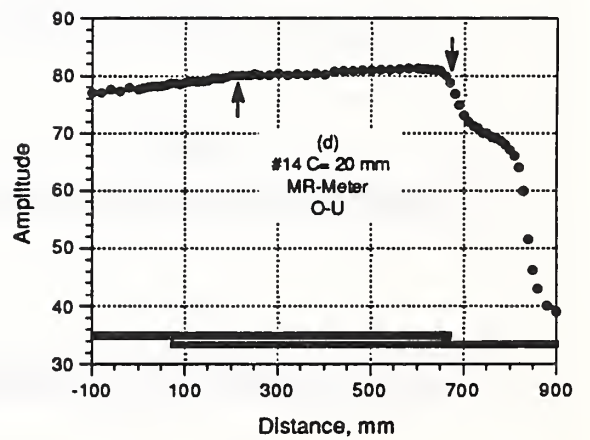
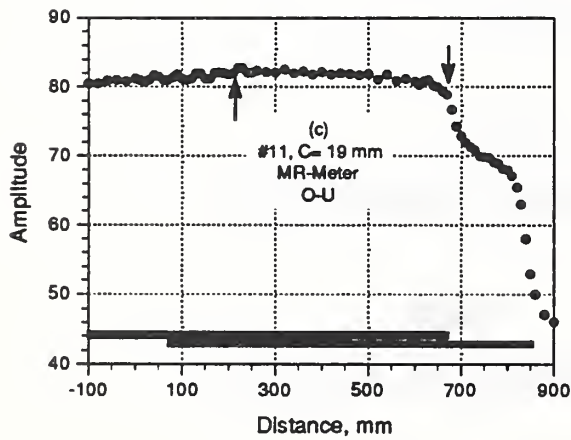
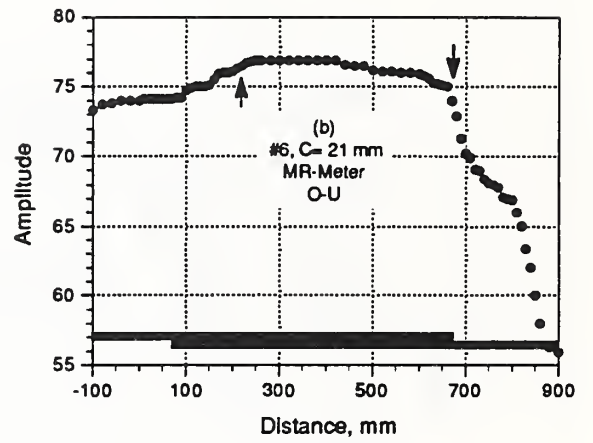
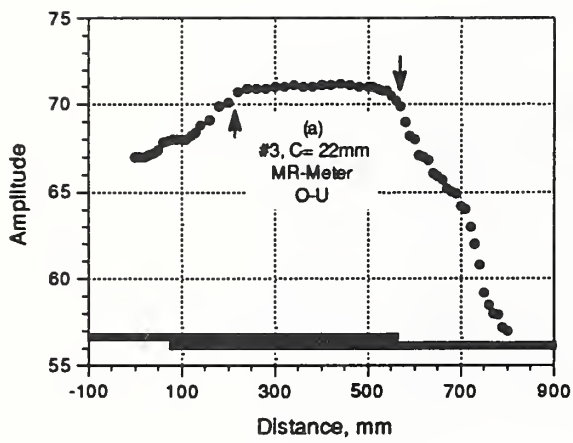


Figure 3.50 Amplitude versus distance for lap splice tests using M-R meter with nominal 19-mm cover (over-under configuration).

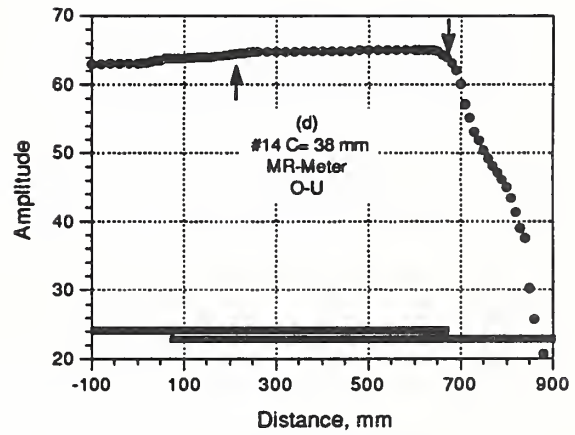
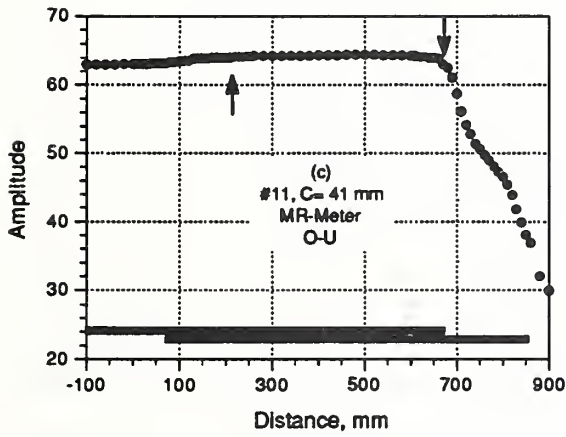
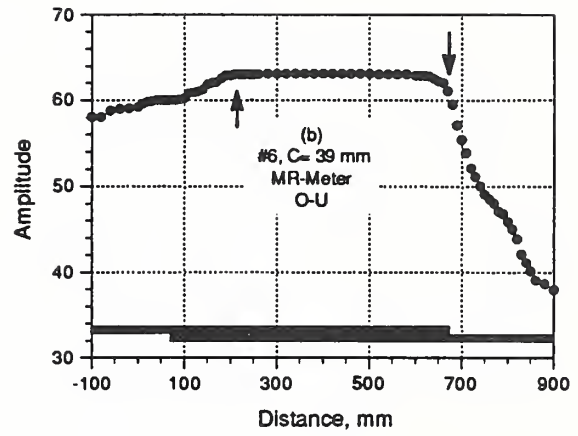
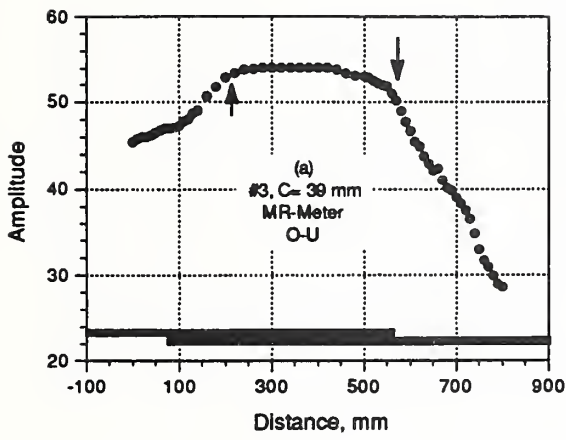


Figure 3.51 Amplitude versus distance for lap splice tests using M-R meter with nominal 38-mm cover (over-under configuration).

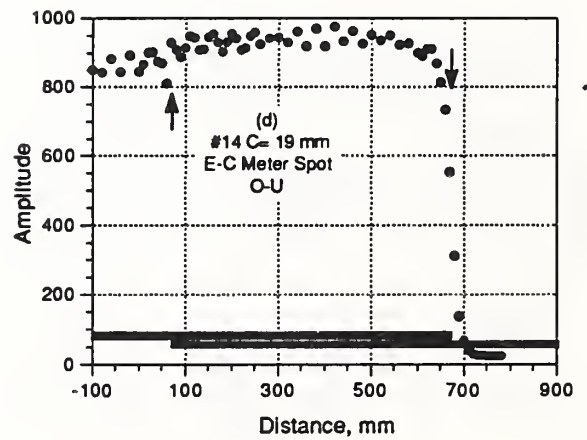
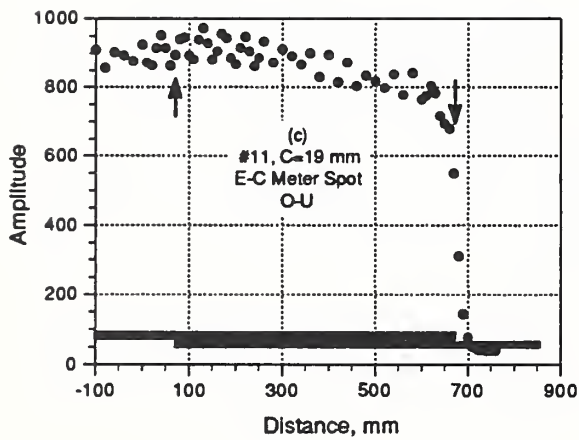
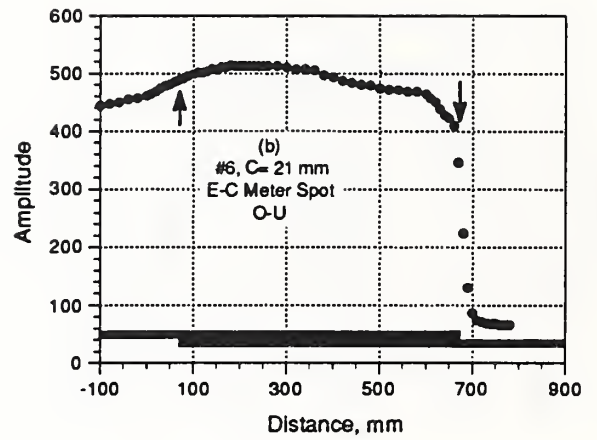
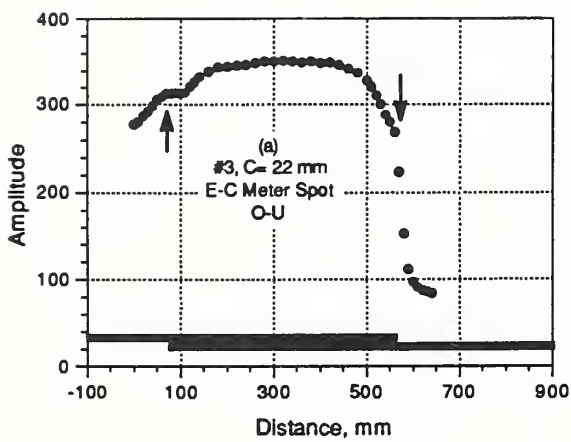


Figure 3.52 Amplitude versus distance for lap splice tests using E-C meter with nominal 19-mm cover (over-under configuration).

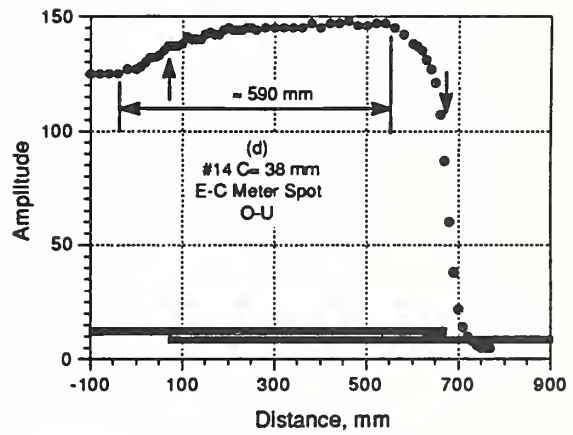
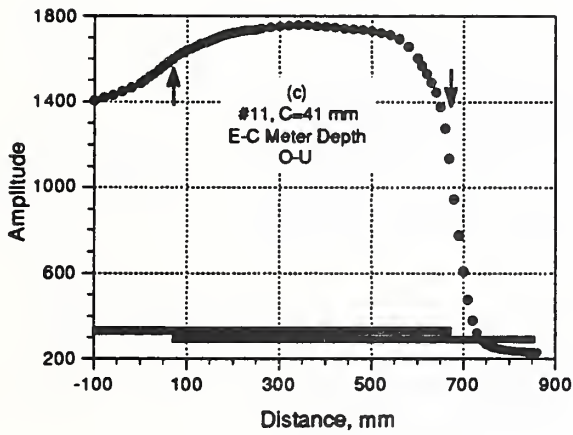
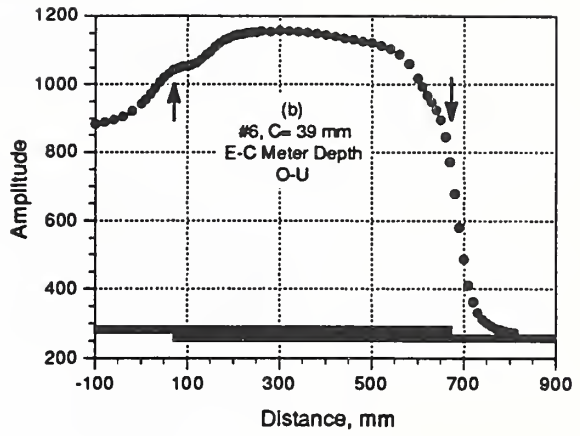
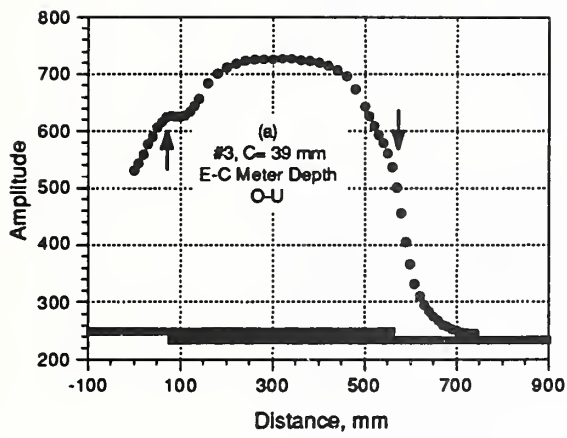
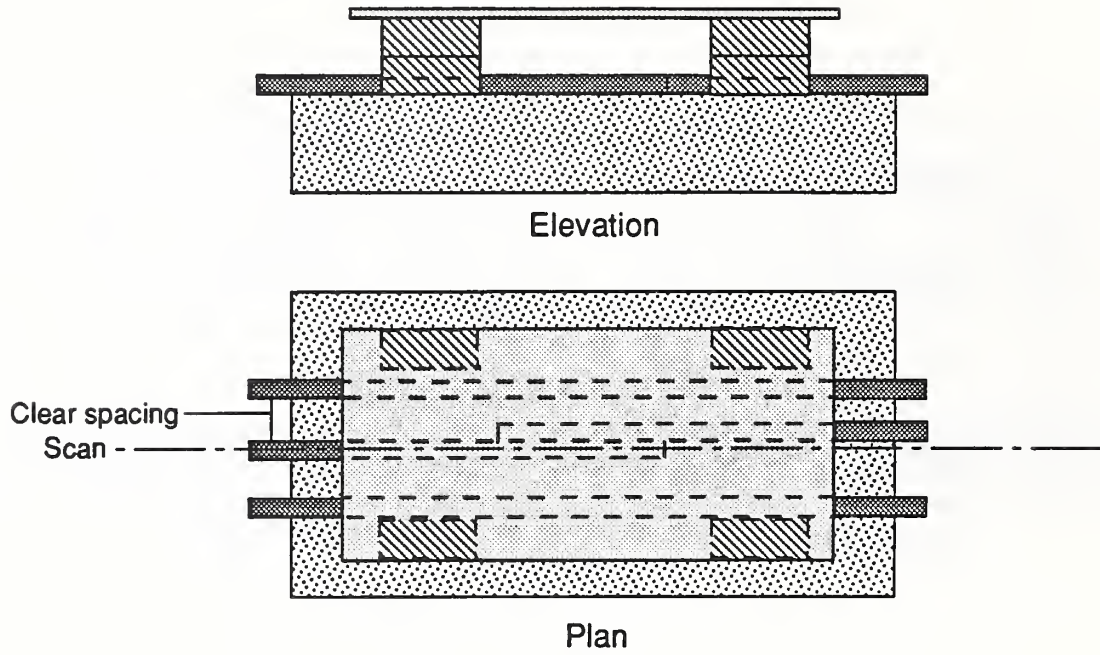


Figure 3.53 Amplitude versus distance for lap splice tests using E-C meter with nominal 38-mm cover (over-under configuration).

(a) Side-by-side configuration



(b) Over-under configuration

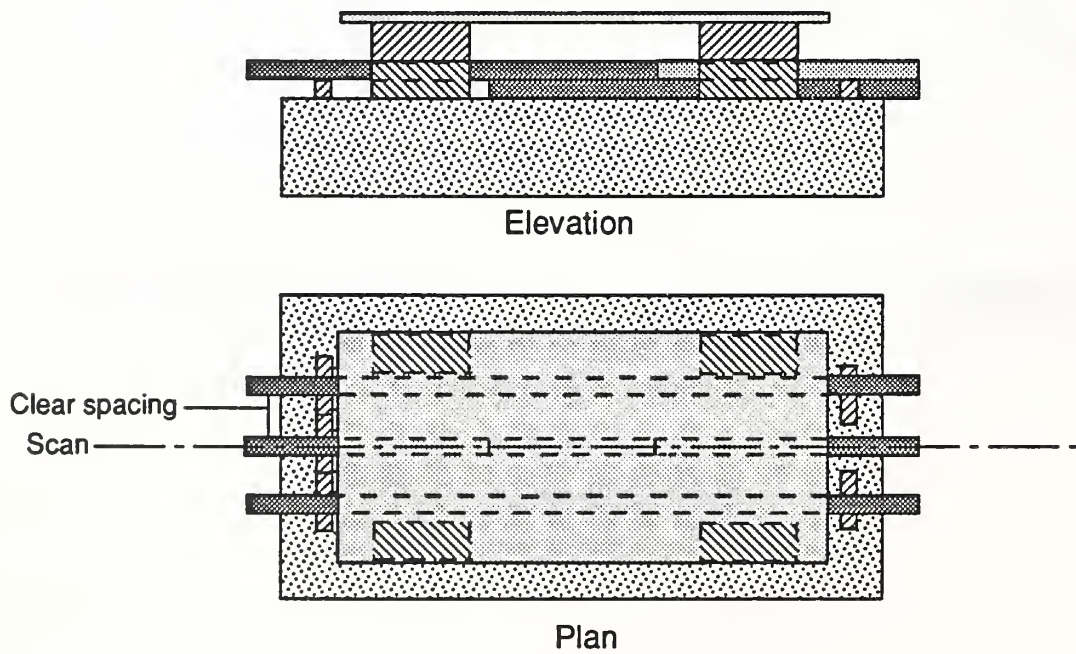


Figure 3.54 Testing configuration for lap splice tests in the presence of parallel bars: (a) side-by-side configuration and (b) over-under configuration.

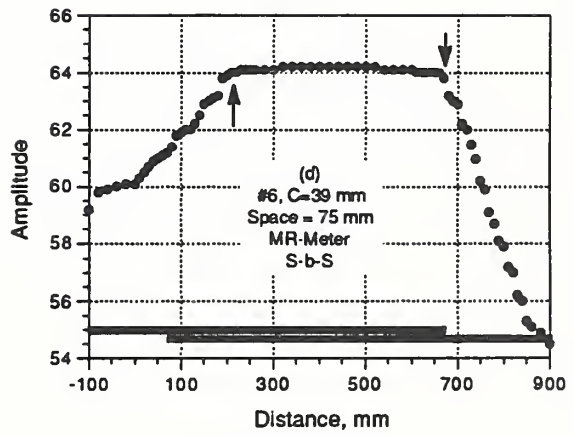
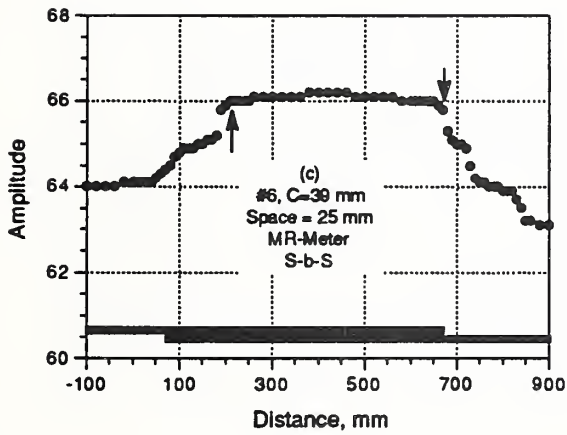
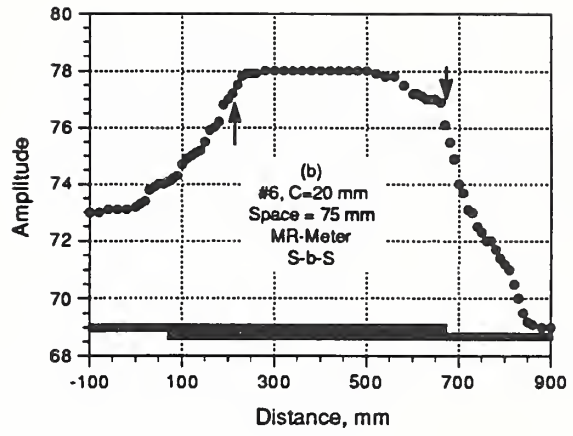
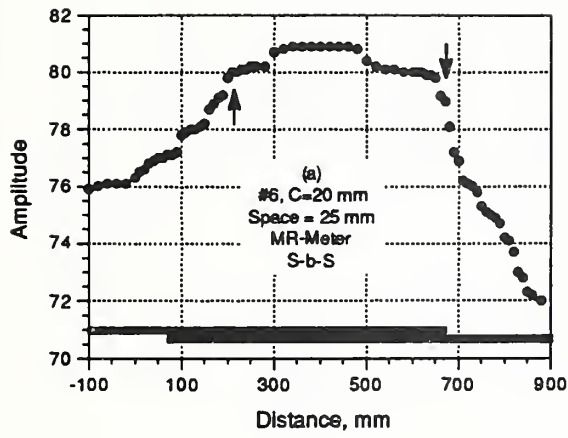


Figure 3.55 Amplitude versus distance for lap splice tests with adjacent bars present, #6 (19 mm) bars using M-R meter with the side-by-side configuration

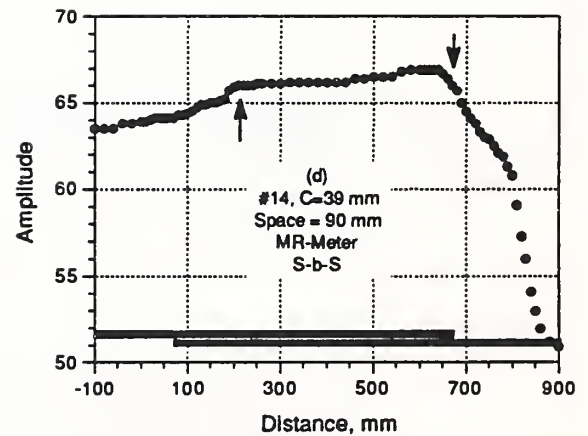
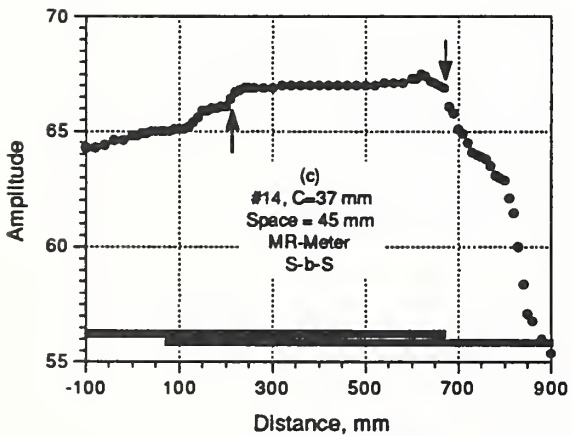
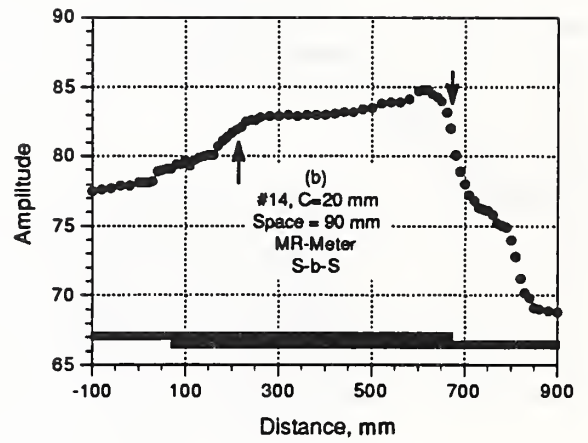
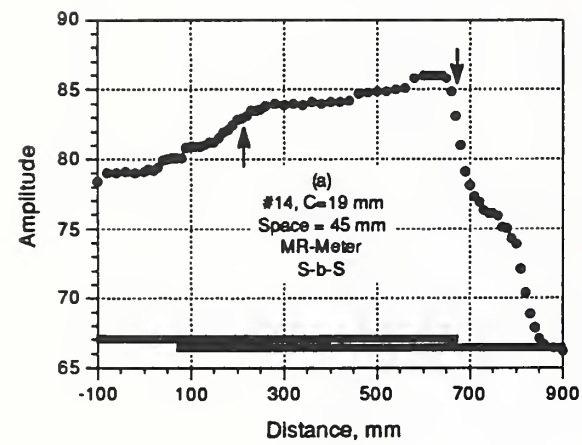


Figure 3.56 Amplitude versus distance for lap splice tests with adjacent bars present, #14 (43 mm) bars using M-R meter with the side-by-side configuration

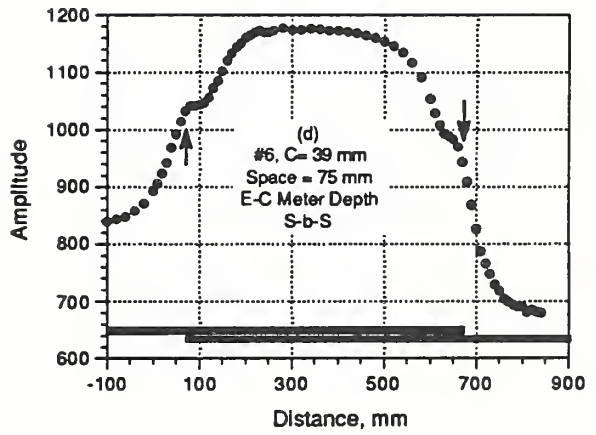
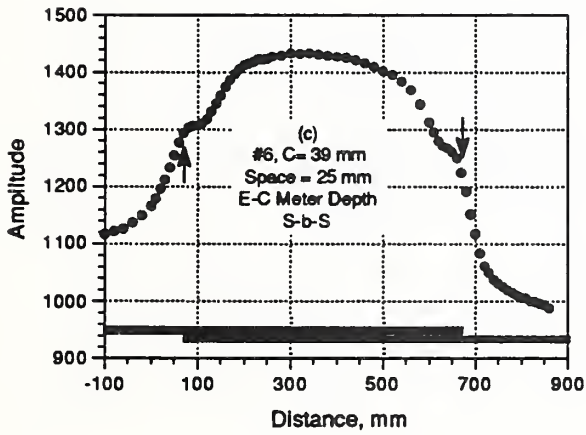
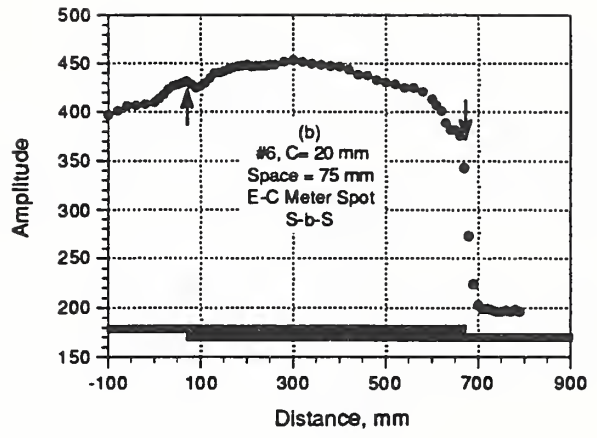
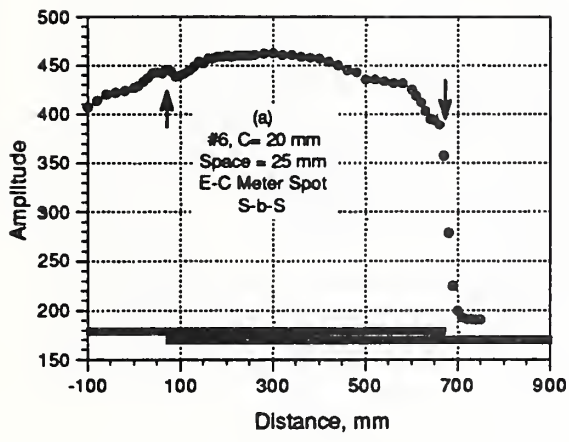


Figure 3.57 Amplitude versus distance for lap splice tests with adjacent bars present, #6 (19 mm) bars using E-C meter with the side-by-side configuration

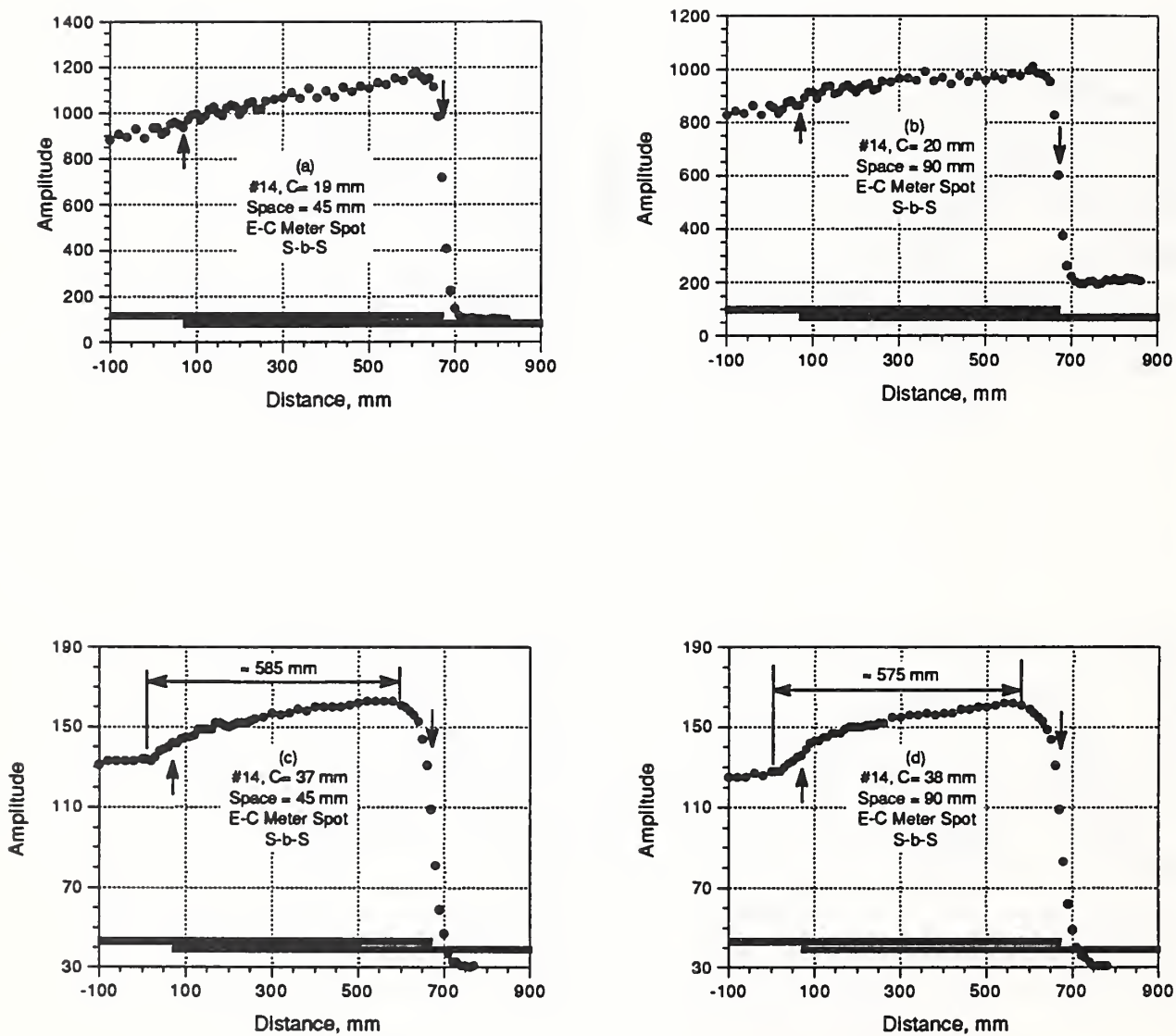


Figure 3.58 Amplitude versus distance for lap splice tests with adjacent bars present, #14 (43 mm) bars using E-C meter with the side-by-side configuration

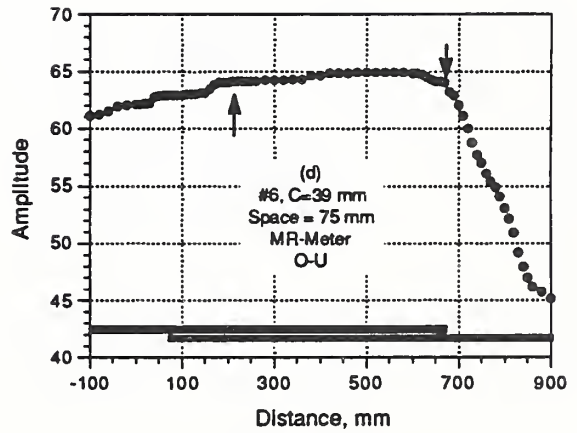
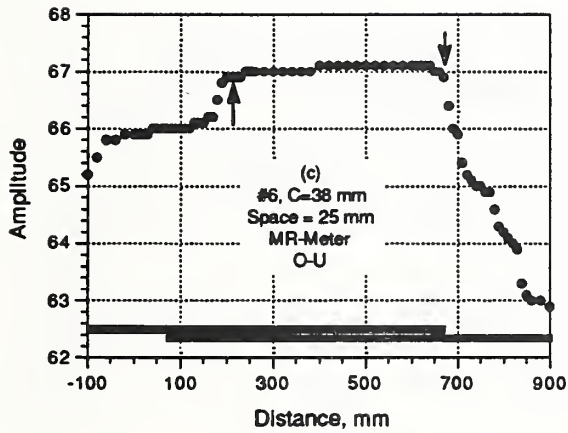
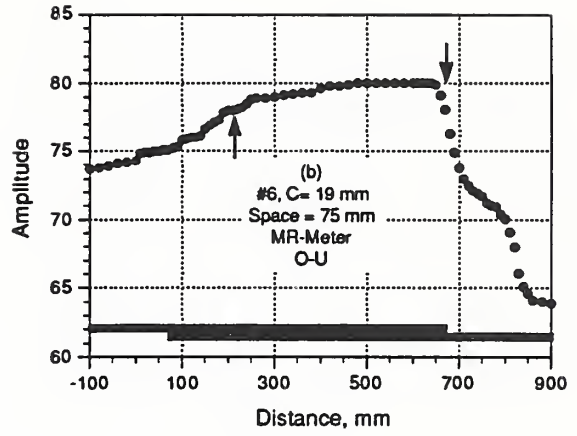
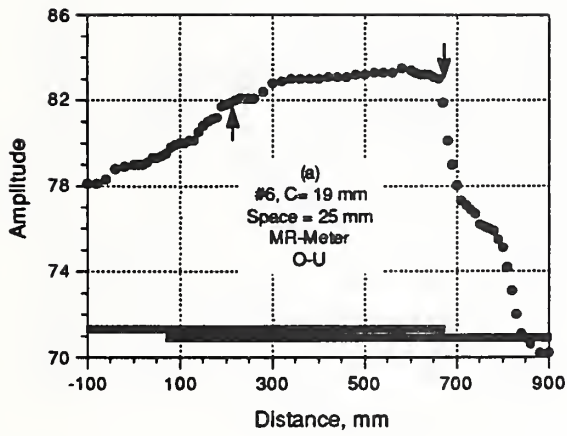


Figure 3.59 Amplitude versus distance for lap splice tests with adjacent bars present, #6 (19 mm) bars using M-R meter with the over-under configuration

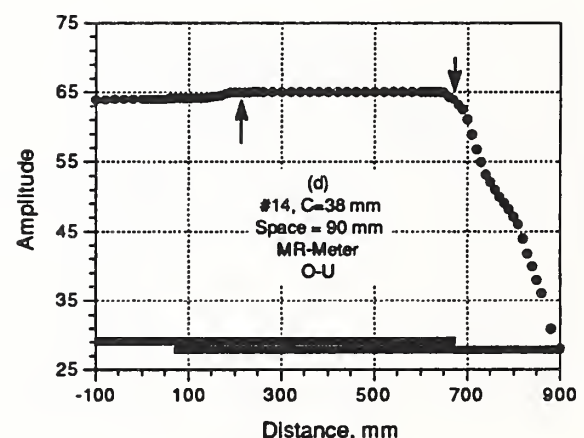
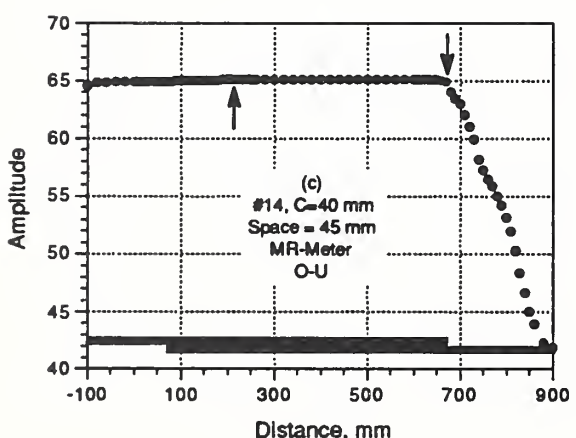
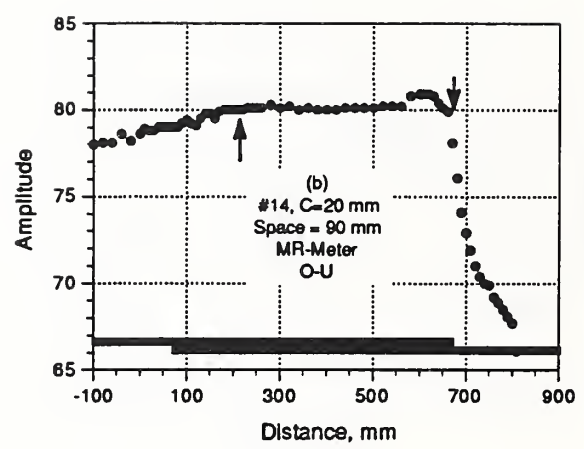
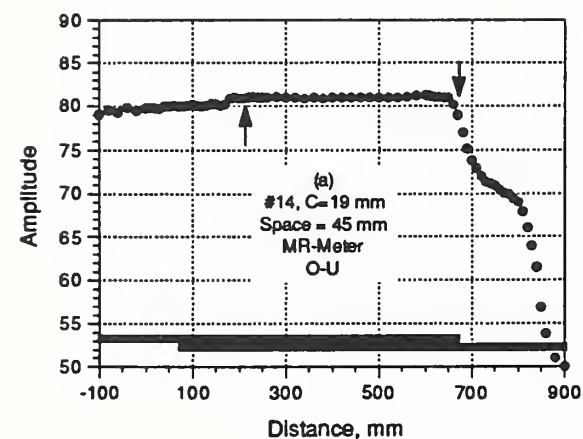


Figure 3.60 Amplitude versus distance for lap splice tests with adjacent bars present, #11 (43 mm) bars using M-R meter with the over-under configuration

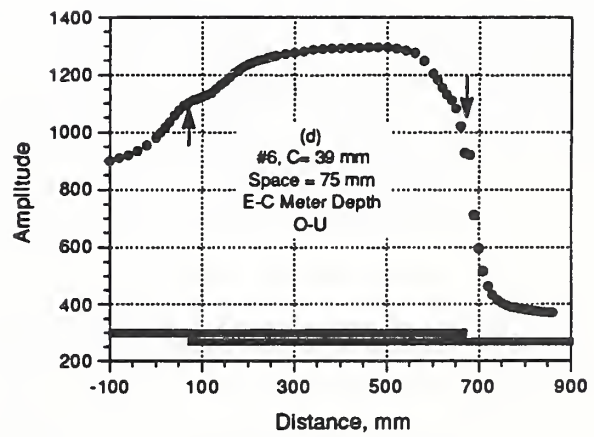
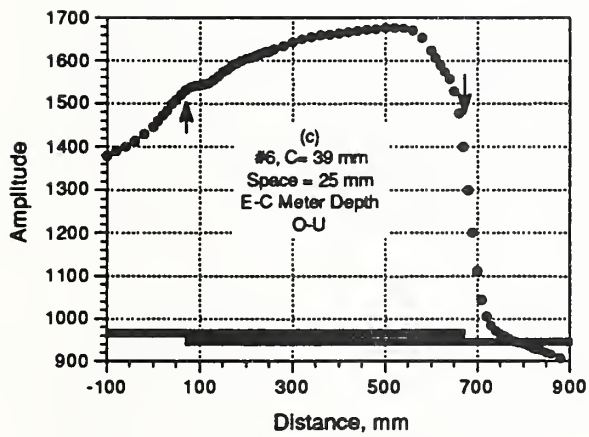
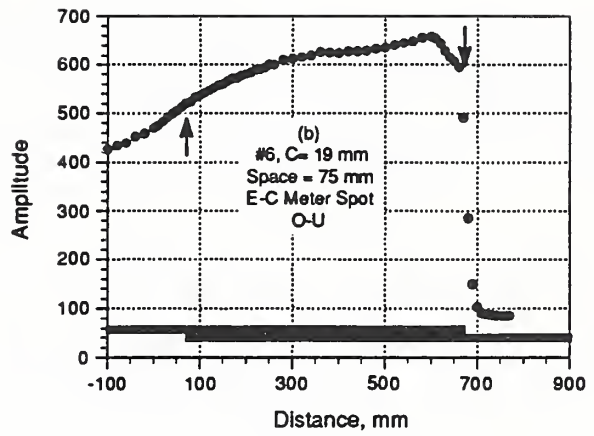
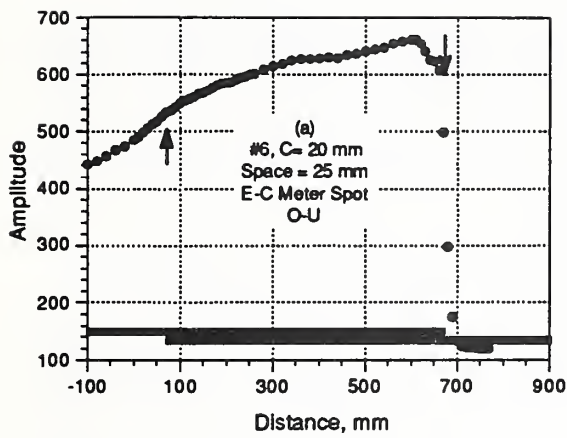


Figure 3.61 Amplitude versus distance for lap splice tests with adjacent bars present, #6 (19 mm) bars using E-C meter with the over-under configuration

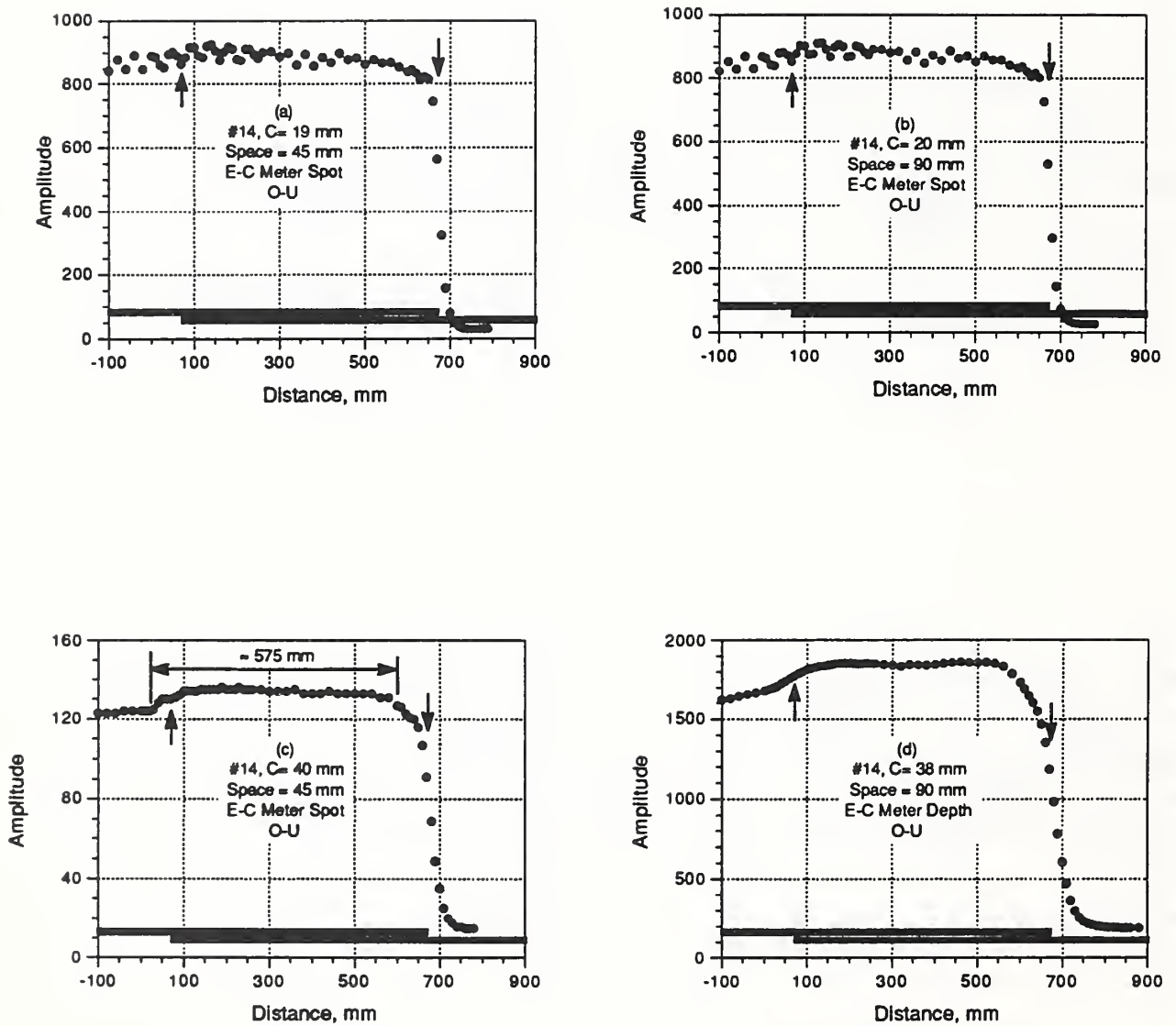


Figure 3.62 Amplitude versus distance for lap splice tests with adjacent bars present, #14 (43 mm) bars using E-C meter with the over-under configuration

## 4. SUMMARY AND RECOMMENDATIONS

### 4.1 Summary

This investigation was carried out to gain an understanding of the basic characteristics of two types of commercial covermeters. One meter is based on the magnetic reluctance principle and is identified as the M-R meter. The other meter is based on the eddy current principle and is identified as the E-C meter. Experiments were carried out to understand the responses of these instruments in the presence of individual bars and in the presence of multiple bars with various configurations. The following paragraphs summarize the results of these experiments.

#### 4.1.1 *Amplitude versus cover*

Empirical models were fitted to the amplitude versus cover data to permit a systematic analysis of the effect of bar size on the calibration curves. The models involve two parameters,  $A'$  and  $\gamma$ , where  $A'$  is an amplitude coefficient and  $\gamma$  is an indicator of the maximum penetration of the covermeter probe. Ideally, the value of  $A'$  should be strongly dependent on the bar size. However, for the two meters that were used, the values of  $A'$  for adjacent bar sizes were similar. Hence, it would be difficult to distinguish bars of similar diameters by using the amplitude-cover relationships and the spacer technique. These results show the inherent limitations of electromagnetic covermeters in discriminating between bars of slightly different sizes.

It was found that the parameters obtained for the #5, epoxy-coated bar deviated from the trends defined by the bare steel bars. It is not known whether the anomalous behavior is due to the epoxy-coating or to a difference in the metallurgical characteristics of the steel in the coated bar. The effects of epoxy coating merits further study because of the widespread use of epoxy-coated bars in highway construction. This finding also reinforces the importance of developing calibration relationships for the specific bars that are to be investigated. Failure to do so casts doubts on the reliability of the measured cover thicknesses which are obtained by using the manufacturer's calibration relationships. When calibration relationships are developed, the operator should include the ranges of bar size and cover thickness that are expected in the field. Otherwise, the operator will be forced to make extrapolations for conditions that have not been tested.

#### 4.1.2 *Amplitude versus horizontal offset*

It was found that the variation of meter reading with horizontal offset could be described by a bell-shaped, quadratic-exponential function as shown in Fig. 4.1. This function is defined by an amplitude coefficient,  $A'_0$ , and a parameter  $\delta$ , which were obtained using regression analysis. The value of  $\delta$  defines how the signal amplitude decays with the horizontal offset, and is, therefore, a measure of the extent of the influence zone of the search head. For example, when the horizontal offset equals  $1.75\delta$ , the amplitude drops to 5% of the maximum value when the search head is directly above a bar. Thus if the value of  $\delta$  were 50 mm (2 in.), the amplitude would be 5% of the maximum value for a horizontal offset of about 90 mm (3.5 in.). A smaller value of  $\delta$  indicates that the zone of influence of the search head is more focused, and would be desirable for minimizing the interfering effects of adjacent bars. For the M-R meter, the value of  $\delta$  was essentially independent of cover up to a thickness of 60 to 70 mm, and it increased approximately linearly with cover for thicknesses above these values. Larger bars resulted in larger values of  $\delta$ . For the E-C meter,  $\delta$  increased approximately linearly with cover thickness and was affected little by bar size.

#### 4.1.3 *Multiple bars*

These tests investigated the responses of the covermeters as the search heads were scanned over a set of five, evenly spaced bars lying in a plane parallel to the surface being scanned. The

objective was to determine the critical spacings between the bars below which: (1) individual bars could not be discerned and (2) the measured cover would be underestimated by using the single-bar, amplitude versus cover relationship. To guide the experiments, a simple summation model, based on the single-bar measurements of amplitude versus horizontal offset, was used to predict the responses as the search head was scanned across the five bars. Based on these *predictions*, it was postulated that:

- individual bars could not be discerned for  $S/\delta$ -values less than about 1, and
- the measured cover would be in error for  $S/\delta$ -values less than 2,

where  $S$  is the center-to-center distance between adjacent bars and  $\delta$  is the value obtained from single-bar tests as discussed in 4.1.2. Tests were performed with #6 and #11 bars to compare with the predictions.

Measurements with the M-R meter revealed the following: Individual bars could be discerned at values of  $S/\delta$  less than 1, especially for shallower cover and the larger bar size. The critical value of  $S/\delta$  above which the cover could be measured accurately depends on the cover thickness. For shallow cover (19 and 38 mm), the critical value of  $S/\delta$  was about 1; for deeper cover ( $> 77$  mm), the critical value was about 2.

The performance of the E-C meter was in better agreement with the predictions than the M-R meter. In general, individual bars could be discerned when  $S/\delta$  exceeded 1 and the cover could be accurately measured when  $S/\delta$  is greater than 2. An exception was the case when the depth probe was used with 96-mm of cover, for which error in the cover measurement occurred up to  $S/\delta$  of 3.

To explain some of the discrepancies between the predictions and the measurements, the simple model was used to calculate the effective  $\delta$ -value,  $\delta_e$ , when multiple bars are present. It was found that  $\delta_e$  decreased as  $S/\delta$  decreased below 2.5, which lead to the inference that influence zone of the search head decreased as the bar spacing was reduced.

The summation model that was used to predict the multiple-bar response is too simple to properly account for the complex interactions that occur between the multiple bars and the electromagnetic fields of the different search heads. Nevertheless, its prediction of a critical  $S/\delta$ -value of about 1 is a conservative approximation that can be used to estimate the bar spacing below which the two covermeters studied would not be able to discern individual bars. The critical  $S/\delta$ -value at which cover can be accurately measured will, apparently, depend on the specific meter, but the value of 2 predicted by the model appears to be a reasonable conservative value for the two meters studied.

In conclusion, the value of  $\delta$  obtained from single-bar tests, in which the amplitude is measured as a function of the horizontal offset for different cover depth, provides essential information for predicting the limitations of a particular covermeter in the presence of multiple parallel bars.

#### 4.1.4 *Bars in two layers*

Limited exploratory tests were conducted to assess the potential of the two types of covermeters to detect the presence of a second layer of bars located directly below a first layer. Realistic values of cover and bar spacings were used. A comparison was made between the meter reading when only the top bar was present and when top and bottom bars were present. The results showed that these covermeters could not be used routinely to detect the presence of two layers of bars in reinforced concrete elements. This is recognized as an inherent limitation of the two covermeters used in this study.

#### 4.1.5 *Locating ends of bars*

Experiments were conducted to examine how accurately the end of a single bar could be detected with the two types of covermeters. Meter amplitude was plotted as a function of position as the search head was moved along the length of the bar. Test results showed that covermeters can be used to accurately determine the location of the end of a bar. The E-C meter seemed to have the most consistent behavior, and the end of the bar could be identified by noting the location where the amplitude decreased to a certain fraction of the amplitude measured away from the end of the bar. For the M-R meter, reliable indications of the end of the bar were possible only for cover less than about 40 mm. These findings were for an individual bar, and it is not known whether the covermeters could locate the ends of a bar with similar reliability in the presence of congested reinforcement.

#### 4.1.6 *Lap Splices*

Tests were conducted to explore the ability of the two types of covermeters to detect the presence of a lap splice and to determine the lap length. Two splice configurations were used: (1) the lapped bars were in a plane parallel to the surface to be scanned (side-by-side), and (2) the lapped bars were in a plane perpendicular to the surface to be scanned (over-under). Plots of meter reading versus distance along the scan line were used to interpret the results.

The extent of the lap splices were easier to measure for the side-by-side configuration. For the M-R meter, the plots had a well defined *plateau* region corresponding to where both poles of the search head were over the lap. The length of the lap could be determined by measuring the length of the *plateau* on the plots and adding the distance between the poles of the search head. For the E-C meter, the responses were more complicated and it was not always possible to establish the length of the splice with certainty. In general, as the cover decreased or the bar size increased, it became more difficult to measure the lap length with the E-C meter. Under optimum conditions, the lap length could be measured by measuring the distance between two distinct discontinuities in the plot, which corresponded to where the search head passed over the ends of the lapped bars.

It was more difficult to determine lap length for the over-under configuration because of the shielding effect of the top bar and the deeper cover of the lower bar. The ability of the M-R meter to determine the lap length was reduced as the bar size increased. The performance of the E-C meter depended on the type of probe, bar size, and cover. For larger bar sizes and shallow cover, the lap length could not be determined with the E-C meter because of the erratic readings due to the effect of the deformation pattern on the bar. However, at the deeper cover, the lap length was discernable for the larger bars.

Finally, the effect of adjacent parallel bars was investigated. The minimum clear spacing was chosen in accordance the ACI Code provisions. For those conditions where the lap length was discernable in the absence of parallel bars, the presence of parallel bars did not obscure the characteristic discontinuities in the responses that served to identify the limits of the lap splice. Again, the side-by-side configuration resulted in more reliable measurements.

## 4.2 Recommendations

### 4.2.1 *Standards development*

In the U.S., users of covermeters must rely on the manufacturer's recommendations because there are no consensus-standards governing covermeters. Thus ASTM Committee C-9 on Concrete and Aggregates should initiate activities to develop a standard practice on the use of covermeters.

The standard practice should provide a methodology to characterize the performance of any covermeter. It should furnish procedures (such as those in BS 1881, Part 240, or as used in this study) to develop calibration relationships in the laboratory. In addition, procedures for checking the calibration in the field should also be provided. Test procedures should also address determination of the relationship between amplitude and horizontal offset. As shown in this study, this provides key information for predicting the performance of a covermeter in the presence of multiple parallel bars. Finally, the standard should include tests to establish the performance of the covermeter for other applications besides measurement of cover and bar size, such as locating the ends of bars or determining lap splice lengths as done in this study,

#### 4.2.2 *Enhancements to existing devices*

As demonstrated in this study, the capabilities of covermeters can be extended beyond the usual applications of measuring cover thickness. However, these other applications require a plot of meter amplitude as function of position along the scan line. These plots were produced by recording the meter reading at regularly spaced intervals along the scan line and entering the data into a computer. This time-consuming and tedious approach is not practical for field application. Thus manufacturers of covermeters should provide for external output of the amplified meter signal so that the data can be captured and stored on a digital data acquisition system. By combining meter reading data with the output of a distance measuring transducer, one can obtain a plot of amplitude versus location along the scan line. Such an approach was attempted by Moore (1975) who used a commercially available M-R meter connected to a strip-chart recorder. However, the instrument did not find widespread interest as it was relatively cumbersome and was only applied for cover measurements. The availability of compact, lightweight, and powerful computer-based data acquisition systems provides a better opportunity to develop a useable field system. Felhaber (1988) provides an example of how the personal computer can be used to enhance the capabilities of a covermeter. Popovics and Popovics (1992) discuss how a computer-based data acquisition system can be used to analyze multiple measurements (amplitude versus offset) to arrive at reliable estimates of bar size.

#### 4.2.3 *Development of new covermeters*

The study on amplitude versus cover revealed one of fundamental weakness of current covermeters, namely, the relative insensitivity of meter reading to changes in bars size compared with the sensitivity to changes in cover. New meter designs should be investigated which would enhance the sensitivity of the meter to the bar size. For such improved meters, a dual measurement, like the spacer technique, would probably be required to establish the bar size prior to measuring cover using the calibration relationships.

Another inherent limitation of existing covermeters is their inability to detect and measure a second, deeper layer of bars. It may be possible to employ an array of sensors and tomographic techniques to reconstruct the reinforcing bar configuration within a concrete member. Progress in this direction is being made using microwaves (Pichot and Trouillet 1990), but an excessive amount of computing power is needed to reconstruct the bar layout. Thus the *microwave camera*, as it is called, is very expensive and cannot be used in the field to obtain "real time" results.

Alternative sensing methods should be investigated. For example, in Germany, Kroggel (1986) and Dobmann, et al. (1989) have reported on the use of a magnetic field disturbance method to calculate the size and depth of an embedded bar. In this approach, a permanent magnetic field is introduced perpendicular to the embedded bar, the perturbations in this field due to the bar are measured, and the bar size and cover are calculated (Felhaber 1987). New approaches which can make use of the latest developments in sensor and computer technology should be explored.

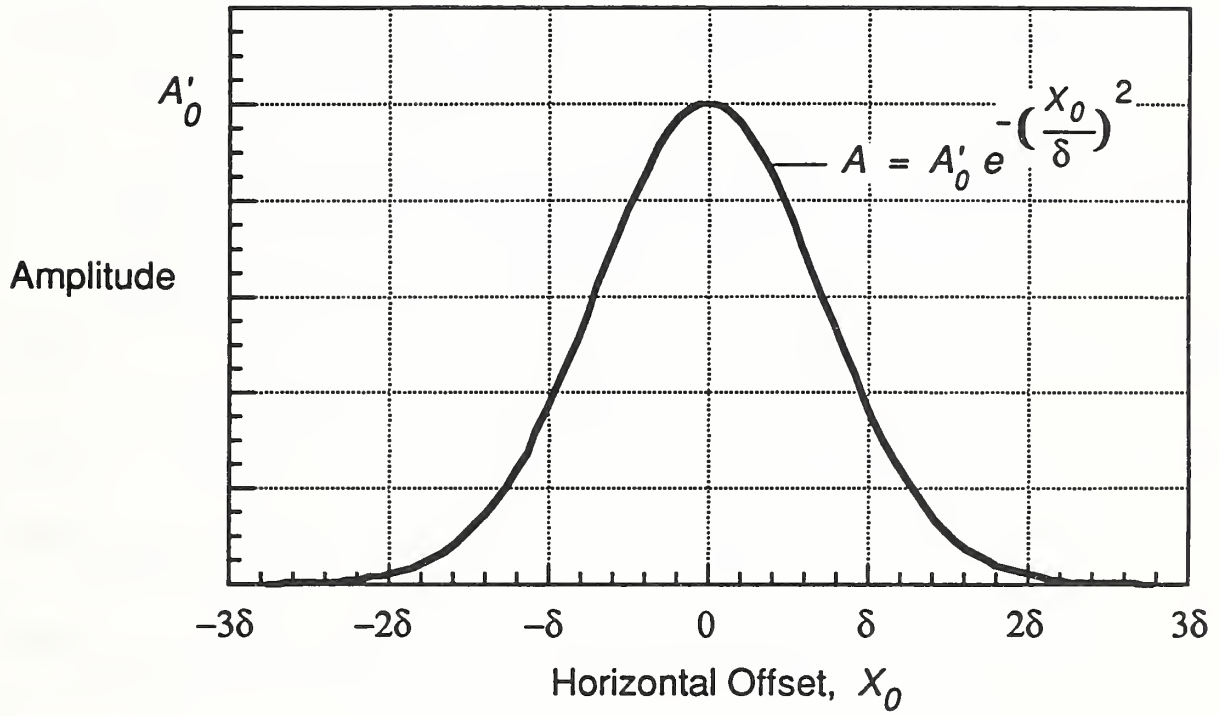


Figure 4.1 The quadratic-exponential function used to represent the variation of amplitude with horizontal offset.



## 5. REFERENCES

- ACI Committee 318, "Building Code Requirements for Reinforced Concrete," Standard 318-89, American Concrete Institute, 1989, 353 p.
- BS 1881: Part 204, "Recommendations on the Use of Electromagnetic Covermeters," British Standards Institution, London
- Bungey, J.H., Testing of Concrete in Structures, 2nd Ed., Chapman and Hall, New York, 1989.
- Das Gupta, N.C. and Tam, C.T., "Non-destructive Technique for Simultaneous Detection of Size and Cover of Embedded Reinforcement," *The British Journal of Non-Destructive Testing*, Vol. 25, No. 6, November 1983, pp. 301-304.
- Dobmann, G., Neumann, R., Schuhmacher, W. and Kroggel, O., "Nondestructive Measurement of Concrete Cover, State of the Art for the Development of a New Equipment," *Proceedings, International Conference on Monitoring, Surveillance and Predictive Maintenance of Plants and Structures*, October 15-18, 1989, Sicily, Italian Society for Nondestructive Testing and Monitoring Diagnostic, pp. 189-194.
- Felhaber, T., "Interpretation of Magnetic Data of Reinforcement in Concrete Using Hilbert Transforms," *Darmstadt Concrete*, V. 2, 1987, pp. 29-36.
- Felhaber, T., "Electromagnetic Covermeasuring Devices", *Darmstadt Concrete*, Vol. 3, 1988, 19 pp.
- Fitzgerald, A.E., Higginbotham, D.E., and Grabel, A., Basic Electrical Engineering, McGraw Hill Book Co., New York, 1967.
- Hagemaier, D.J., Fundamentals of Eddy Current Testing, Amer. Soc. for Nondestructive Testing, Inc., Columbus, OH, 1990.
- Halmshaw, R., Non-destructive Testing, Edward Arnold Publishers, Ltd., 1987.
- Kroggel, O., "Measurement of the Concrete Cover and the Size of Reinforcement Bar by Magnetic Methods," *Darmstadt Concrete*, V.1, 1986, pp. 183-190.
- Lauer, K.R., "Magnetic/Electrical Methods," Chapter 9 in Handbook on Nondestructive Testing of Concrete, V.M. Malhotra and N.J. Carino, Eds., CRC Press Inc., Boca Raton, FL, 1991, pp. 203-225.
- Malhotra, V.M., "Testing Hardened Concrete: Nondestructive Methods," American Concrete Institute Monograph No. 9, 1976.
- Moore, K.R., "Rapid Measurement of Concrete Cover on Bridge Decks," *Public Roads*, Vo. 39, No. 2, September 1975, pp. 48-52.
- Popovics, S. and Popovics, J.S., "Improved Determination of the Locations and Sizes of Steel Rebars in Concrete," *Proceedings, ACI International Conference on Evaluation and Rehabilitation of Concrete Structures and Innovations in Design*, Hong Kong, 1991, ACI SP-128, American Concrete Institute, pp. 485-495

- Pichot, C. and Trouillet, P., "Diagnosis of Reinforced Structures: An Active Microwave Imaging System," *Proceedings*, NATO Advanced Research workshop on Bridge Evaluation, Repair, and Rehabilitation, A.S. Nowak, Ed., Kluwer Academic Publishers, 1990, pp. 201-215.
- Serway, R.A., Physics for Scientists and Engineers/ with Modern Physics, Saunders College Publishing, Philadelphia, 1983.
- Shirley, D.E., "Electromagnetic Covermeters," *The British Journal of Nondestructive Testing*, Vol. 13, No. 6, November 1971, pp. 179-180.
- Smith, D. N., Etebar, K. and Wood, L. A. "The Detection of Embedded Reinforcement in Concrete - A Note", *Proceedings, International Conference on Structural Faults and Repair*, July 7-9, 1987, edited by M. C. Forde, University of 'Edinburgh.
- Tam, C. T., Lai, L. H., and Lam, P. W., "Orthogonal Detection Technique for Determination of Size and Cover of Embedded Reinforcement," *Journal of Institution of Engineers*, Malaysia, Vol. 22, June 1977, pp 6-16.

## APPENDIX 1 — Notation

$A$	=	amplitude displayed by covermeter
$A_0$	=	amplitude displayed by covermeter when the search head is directly above a reinforcing bar and aligned with longitudinal bar axis
$A'_0$	=	amplitude coefficient in relationship of amplitude versus horizontal offset, amplitude when $X_0=0$ , obtained from regression analysis
$A'$	=	amplitude coefficient in relationship of amplitude versus cover, obtained from regression analysis
$A_m$	=	area of magnetic circuit
$A_{max}$	=	maximum amplitude measured with search head directly above the middle bar in the five-bar arrangement used in this study
$A_{min}$	=	amplitude measured with search head midway between the middle bar and the adjacent bar in the five-bar arrangement used in this study
$A_r$	=	relative or normalized amplitude, amplitude divided by $A'_0$
$A_3$	=	theoretical amplitude when search head is directly over the middle (#3) bar in the five-bar arrangement used in this study
$A_{2.3}$	=	theoretical amplitude when search head is midway the middle bar and one of the adjacent bars in the five-bar arrangement used in this study
$B$	=	flux density, magnetic flux lines per unit area
$C$	=	cover over reinforcing bar
$i$	=	index corresponding to each of the bars in the five-bar arrangement used in this study
$L$	=	length of magnetic circuit
$S$	=	center-to-center spacing of multiple parallel bars
$X$	=	position of search head along the scan line
$X_0$	=	horizontal offset between axis of reinforcing bar and axis of search head
$\alpha$	=	$(A_{max} - A_{min})/A'_0$ , and indicator of whether individual bars are discernable
$\beta$	=	correction factor applied to $A'_0$ to obtain agreement between predicted and measured amplitude over middle bar of five-bar arrangement used in this study
$\gamma$	=	coefficient obtained by fitting equation to amplitude versus cover data, indicative of the penetration depth of the covermeter
$\delta$	=	regression constant obtained by fitting quadratic exponential equation to amplitude versus horizontal offset data, indicative of width of influence zone of the covermeter
$\delta_e$	=	effective value of $\delta$ so that measured value of $\alpha$ agrees with prediction based upon the summation model used in this study
$\mathcal{F}$	=	magnetomotive force, the magnetic flux-producing ability of a coil, analogous to electromotive force in an electrical circuit
$\Phi$	=	magnetic flux, the group of magnetic lines flowing between the poles of a magnet
$R$	=	reluctance of a magnetic circuit
$\mu$	=	magnetic permeability

## APPENDIX 2 — Annotated Bibliography

Weber, W.G., Grey, R.L. and Cady, P.D., "Rapid Measurement of Concrete Pavement Thickness and Reinforcement Location - Field Evaluation of Nondestructive Systems," *NCHRP Report 168*, National Research Council, 1976, 63 pp.

This research project was initiated to develop alternatives to the current method of determining pavement thickness and reinforcement location by coring. A major finding of the study was that "a stable, accurate, and dependable device exists for determining the location and depth of reinforcement steel in pavements." A commercial covermeter based on the magnetic reluctance principle was evaluated. Based on rigorous statistical analysis of data from laboratory testing on slabs, the following results were obtained:

- (i) The factors which had a significant effect on the readings for reinforcement depth were surface condition, bar size, bar spacing, numbers of layers of bars, and interaction between bar size and surface condition.
- (ii) There was a significant difference between bar depth as measured by the covermeter and core results, with the mean difference being a function of the depth.
- (iii) The covermeter could not detect the depth of the lower layer of two layers of reinforcing bars; only the depth of the top layer could be detected. Similarly, the lower level of two levels of steel mesh could not be detected.
- (iv) The covermeter had "excellent accuracy" in determining the horizontal positions (spacing) of reinforcing bars.
- (iv) The mean standard deviation for the depth of reinforcing bars and depth of mesh were 0.159 and 0.337 in. (4.0 and 8.6 mm), respectively. The mean standard deviation for the horizontal spacing of reinforcing bars was 0.358 inch (9.1 mm).
- (v) The operator effects were not a significant source of variability for bar depth and spacing measurements, but were a significant source of variability when measuring mesh depth.

An acceptance specification was proposed: "Non-destructive apparatus employed for determining the depth of reinforcement must have been proven capable of determining the depth with a standard deviation of less than 1/2 in. (13 mm). The apparatus must be capable of determining depth of reinforcement from 0 to 5 in. (130 mm). The apparatus must be proven stable and the results repeatable to 1/8 in. (3 mm) over a temperature range 40 to 120 °F (5 to 50 °C)."

Tam, C. T., Lai, L. H., and Lam, P. W., "Orthogonal Detection Technique for Determination of Size and Cover of Embedded Reinforcement," *Journal of Institution of Engineers Malaysia*, Vol. 22, June 1977.

An alternative technique to the so-called "spacer technique" is presented to determine both the size and cover when neither are known. In the traditional spacer technique, multiple measurements with spacers blocks are taken with the axis of the search head aligned with the longitudinal axis of the bar. The "orthogonal" technique differs from the traditional method in that readings are taken in both the parallel and perpendicular directions relative to the longitudinal axis of the reinforcing bar. Multiple measurements in the two directions and calibration charts are used to simultaneously solve for both the cover and the bar size. It is claimed that the orthogonal technique is more accurate than the conventional spacer method. This technique would only be applicable to covermeters which have a directional search head, i.e., one for which

the response is a maximum when the search head axis is aligned with the longitudinal axis of the bar.

The authors also discuss the influence of parallel and perpendicular bars on the accuracy of cover measurements based on calibration curves obtained from single-bar tests. It is mentioned that the critical spacing of parallel and perpendicular bars (spacing below which interference occurs) will depend on the specific instrument. The influence of bar length is also presented. Bar length is important for detecting ties and stirrups, where the size of the bar is small and the length of a side is short. With 6-mm diameter bars, parallel readings were affected when the length was less than 300 mm, whereas perpendicular readings were not affected even down to 150 mm.

Within the limitations of the equipment, geometry, and materials investigated, the authors concluded:

- The covermeter investigated "can be used to estimate both cover and bar size fairly accurately".
- For better accuracy, it is essential that calibration charts be based on actual materials used in the structure.
- "In the hands of a skilled operator having a thorough understanding of the basic principles involved and a clear picture of the influence of various factors, the covermeter is a useful instrument for the determination of position, cover and size of reinforcement embedded in concrete."

Ahlsen, U. and Bellander U., "Estimation of Location and Diameter of Quantity of Reinforcement in In-situ Structures," *Proceedings*, RILEM Conference on Quality Control of Concrete Structures, June 1979, Stockholm, Vol. 1, pp. 201-207.

Reports on a study using a new electromagnetic covermeter with four mutually independent magnetic fields at the legs of the search head. Two fields, one in each leg, are strong with a penetration range of 100 to 120 mm and two are weaker with a penetration range of 60 to 70 mm. The sensing technique involves measurements associated with these four fields which are used to compute two values. These values are, in theory, related to a given bar diameter at a given cover. The performance of this meter was compared with that of a conventional covermeter, having only one magnetic field between the two legs. One-way and two-way reinforcing patterns were investigated.

For 16-mm bars at a 10-mm cover, both covermeters appeared to estimate cover similarly and acceptably, in the case of both one way and two way dense reinforcement patterns. With a cover of 60 mm and for 16-mm diameter bars and with a dense one-way reinforcement pattern, the new meter estimated cover much better than the conventional meter; the conventional meter was significantly in error for bar spacings of less than 75 mm. In contrast, the new meter estimated cover well over the entire range of bar spacings. With a cover of 60 mm for 16-mm main bars at 50 mm spacing with 16-mm bars in the orthogonal direction below the main bars, the new meter also performed much better than the conventional meter. The conventional meter was significantly in error over the entire range of orthogonal bar spacings (up to 200 mm). In contrast, the new meter performed fairly well (underestimated cover by less than 5 mm) over the entire range of orthogonal bar spacings.

With one-way reinforcement and for bar spacings of 125 mm or more, the new meter was able to estimate bar diameters. The results showed that better measuring accuracy was obtained at cover depths of less than 70 mm.

The effect of the concrete and the grade of the reinforcement was shown to be insignificant. Limited field tests showed that measurements can be carried out with similar

accuracy as in the laboratory. However, in the field, the meter required frequent and time-consuming calibration work, particularly due to temperature changes.

Snell, L.M., Wallace N., and Rutledge R.B., "Locating Reinforcement in Concrete," *Concrete International: Design and Construction*, V. 8, No. 4, April 1986, pp. 19-23.

A statistical methodology is presented for interpreting the results of a covermeter survey. Equations are presented for establishing probability statements about the cover or spacing of the reinforcement based on limited measurements. For the particular covermeter used, it is assumed that the cover depth is a linear function of the meter reading. For the particular instrument, it was stated that cover versus meter reading relationships (straight lines) were relatively insensitive to bar diameter. Examples of probability statements with regard to cover and bar spacing are given for two cases: (i) compliance with specifications and for (ii) structures without specifications. There needs to be a compromise between the precision of tolerance probabilities and the cost of sampling. A sampling size of around 30 is suggested as a good compromise. The importance of a random sampling plan is emphasized.

Smith, A.P., "Underwater Nondestructive Testing of Concrete: An Evaluation of Techniques," NCEL TN-1747, Naval Civil Engineering Laboratory, Port Hueneme, CA, Feb. 1986, 64 pp.

A commercial covermeter based upon the magnetic reluctance principle was modified for use underwater. In the evaluation, the importance of initial zeroing of the instrument was studied. It was shown that the effect of the initial zeroing was insignificant when a large amplitude signal was measured, such as would occur with shallow large bars. When the signal was low (deep bars), the effect of incorrect initial zeroing was very significant. Laboratory evaluations demonstrated that the modified covermeter functioned under water the same as it did in the dry. Field studies highlighted the difficulties in estimating cover when the bar spacing is below a critical value. In such cases the measured cover will be lower than the actual cover.

Kroggel, O., "Measurement of the Concrete Cover and the Size of Reinforcement Bar by Magnetic Methods," *Darmstadt Concrete*, V.1, 1986, pp. 183-1990.

Discusses an approach whereby a static magnetic field is applied to the concrete containing embedded reinforcement and the distribution of the field along the concrete surface is measured. The presence of a reinforcing bar gives rise to a leakage flux which distorts the applied field. The measured field distribution between the poles of the applied field can be used to calculate the diameter and depth of the bar.

Felhaber, T., "Interpretation of Magnetic Data of Reinforcement in Concrete Using Hilbert Transforms," *Darmstadt Concrete*, V. 2, 1987, pp. 29-36.

Discusses the mathematical approach to analyze the leakage flux field produced by a bar in the presence of static magnetic field, when the applied field is inclined at an angle to the concrete surface. Equations are given for estimating the bar diameter and cover. Additional

work is needed to develop digital-based analysis methods, and to investigate the effect of a second reinforcing bar within the measurement region.

Dixon, D. "Analysis of Cover Data," in ACI SP-101, Computer Use for Statistical Analysis of Concrete Test Data, Balaguru, P. and Ramakrishnan, V., eds., American Concrete Institute, 1987, pp. 47-63.

A linear correlation model was used to represent the relationship between covermeter readings and measurements of the actual cover for 345 field measurements. The cover varied from 25 mm to over 75 mm, and the reinforcing bars were 25-mm in diameter. An analysis was performed of the variation of the data from the best-fit line. It was found that as the cover increased, the variation between the estimated cover and the true cover increased. However, this difference was not statistically significant. Confidence intervals for the estimated depth for a particular covermeter reading were established. For example, the confidence interval for an individual estimate at the 90% level was found to be about plus or minus 8 mm.

Smith, D.N., Etebar, K. and Wood, L.A. "The Detection of Embedded Reinforcement in Concrete - A Note", *Proceedings*, International Conference on Structural Faults and Repair", July 7-9, 1987, University of London, M. C. Forde, Ed., Engineering Technics Press

Studied the performance of two commercial covermeters. The influence of the spacing of parallel bars of the same diameter was investigated. For example, for one meter and with a 57-mm cover, the effect of parallel bars became noticeable when the spacing was reduced to less than about 200 mm.

The effect of transverse reinforcement was also investigated. The following variables were investigated:

Main bar diameter: 16, 20, 25, and 32 mm

Main bar spacing: 100 and 200 mm

Transverse bar diameter: 16 and 20 mm

Transverse bar spacing: 150 and 300 mm

Calibration curves (meter reading versus cover) were developed for which the diameter and spacing of the main reinforcement was varied and 16-mm transverse bars were present at a 150-mm spacing. It was found that the calibration curves for the 16- and 20-mm bars were close together and indistinguishable when measurement error is included. Increasing the transverse bar spacing from 150 to 300-mm had no significant effect on the meter readings. The applicability of the spacer technique in the presence of transverse reinforcement was also studied. The calibration curves supplied by the manufacturer and those obtained from the orthogonal bar configurations were used. It was concluded that: "Both instruments investigated were able to locate the main reinforcing bars of an orthotropic mesh. However, neither was able to produce the unique result required by an engineer in the estimation of bar diameter and cover. This lack of sensitivity demonstrated under laboratory conditions, could be expected to be compounded under the rigors of field work."

Felhaber, T., "Electromagnetic Covermeasuring Devices", *Darmstadt Concrete*, Vol. 3, 1988, 19 pp.

Six covermeters were evaluated to establish the accuracy of the indicated cover. One bar placed within a test box was used as the test specimen. The deviation between the actual and the measured values of cover were plotted as a function bar size for covers of 10, 25 and 40 mm. Bar diameters ranged from 5 to 28 mm. Two devices (one was a magnetic the other was an eddy-current device) were found to be more accurate than the others. These two devices were also tested for error in cover when the bar size is unknown and the instruments were set for a 12-mm bar diameter. The sensing probe of one of these devices was not stable with time and required repeated calibration, due to temperature variations of the probe over time. In contrast, the other instrument was stable for a long period. It was concluded that most of the covermeters investigated did not give reliable measurement of cover, but all of them were able to locate bars in concrete. In addition, there is discussion of a laboratory scanning technique, in which the depth of cover and the location of the sensing probe were recorded continuously using a digital data acquisition system in a personal computer. The recorded data were used to generate computer images of reinforcing bar locations.

Sohni, M. "Case Study on Durability," *Darmstadt Concrete*, V. 3, 1988, pp. 199-208.

The cover over the reinforcement in an existing building was investigated. Two covermeters were used. One had a 30 mm diameter measuring head, which allowed measurement of dense reinforcement with high accuracy (maximum deviation of  $\pm 2$  mm in the range of 10 to 40 mm cover). The disadvantages were frequent calibration when the bar diameter or the range of measurement changed and the measurement of unknown diameters required a "higher effort". The other covermeter had detector dimensions of 200 x 130 x 50 mm and was not suitable for measuring dense reinforcement. There were two measurement ranges, 0 to 30 mm and greater than 30 mm. The maximum deviation between actual and measured cover was less than  $\pm 2$  mm. Based on 674 measurements of prefabricated slabs, the average concrete cover was 15.0 mm and the standard deviation was 4.8 mm. The cover measurements followed a Gaussian distribution.

Dobmann, G., Neumann, R., Schuhmacher, W. and Kroggel, O., "Nondestructive Measurement of Concrete Cover, State of the Art for the Development of a New Equipment," *Proceedings, International Conference on Monitoring, Surveillance and Predictive Maintenance of Plants and Structures, October 15-18, 1989, Sicily, Italian Society for Nondestructive Testing and Monitoring Diagnostic*, pp. 189-194.

When the bar diameter is unknown, commercial covermeters are reported to result in errors on the order of 30 % between the measured and actual cover depth. The technique, based on measuring the surface magnetic field distribution between the poles of a static magnetic field, is discussed. The component of the magnetic field normal to the concrete surface is measured as a function of the location between the poles. The poles are oriented perpendicular to the reinforcing bar. The magnetic field between the poles intersects the bar and gives rise to a leakage flux which is measured. The leakage field is a function of the applied field, the size of the bar and the depth of the bar. The orientation of the bar is established beforehand with an ordinary covermeter with a directional search head. By measuring the variation of the magnetic field between the poles, the depth and size of the bar are calculated. Laboratory results showed good accuracy.

Kobayashi, S. and Kawano, H., "Covermeter Development in Japan and Study of Improving Electromagnetic Induction Method," *Proceedings, RILEM Workshop on Testing During Concrete Construction, Mainz 5-7, 1990*, H.W. Reinhardt, Ed., Chapman and Hall, pp. 396-403.

Discusses use of X-ray method to determine size and cover of reinforcing bars in a slab-like structure by means of multiple exposures using different source locations. Also discusses a new technique for establishing the diameter of reinforcing bars based on electromagnetic induction. Commercial covermeters will usually only measure the changes in the voltage of the sensing coil due to a reinforcing bar. The new approach is based on measuring the difference in the phase angle between the applied voltage to the primary coil and the voltage induced in the sensing coil. It is shown that this phase angle is a function of the diameter of the reinforcement. Thus by first measuring the phase angle, the bar diameter is established and then the cover can be measured based upon the ordinary calibration curves. Another approach to determine the diameter and cover of a bar is to measure the amplitude of the signal as the search head is scanned over the bar. From the plot of signal voltage versus distance from the centerline of the bar, one determines the distance required for the signal to drop to one-half its maximum value. From the maximum amplitude and this distance, the diameter and cover can be estimated based upon a previously established calibration chart. Additional work is recommended to improve the precision and to accommodate closely spaced bars and the presence of transverse bars.

Felhaber, T. and Kroggel, O., "NDE Techniques to Examine Concrete Cover," *Darmstadt Concrete*, V. 6, 1991, pp. 137-144.

Presents an overview of methods to determine the cover and diameter of steel reinforcement in concrete. An electromagnetic bore-hole probe was developed to determine whether multiple layers of reinforcement exist. Ground probing radar offers the potential of greater penetration than electromagnetic covermeters, but no information is possible on the diameter of the bars. The accuracy of cover measurements with electromagnetic-type covermeters is due to a combination of factors: (1) the characteristics of the instrument, (2) the arrangement of the reinforcing bars in the structure, and (3) the qualification of the personnel making the measurements.

Measurements of reinforcement are of two types: (1) point measurements to establish conditions at specific locations and (2) measurements at many sites to establish the statistical distribution of the cover in an entire structure. For the first type, an instrument should be used that is optimal for the conditions in terms of depth sensitivity and horizontal spatial resolution. For the second type, consideration must be given to those factors that contribute to the variability of measurements so that the true variability of the cover can be established.





